Dynamics of a Neuronal Triad During the Extinction of Fear Memories

Miguel Fernandes
Master Degree in Mathematics
Department of Mathematics, Faculty of Sciences of the University of Porto
2022

Supervisor
Isabel Salgado Labouriau, Department of Mathematics,
Faculty of Sciences of the University of Porto

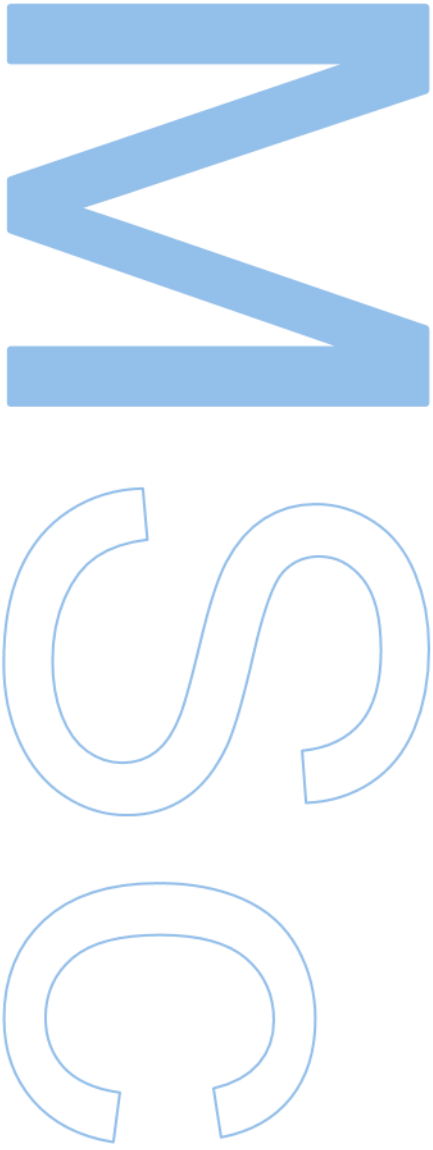


U.PORTO
FACULDADE DE CIÊNCIAS
UNIVERSIDADE DO PORTO

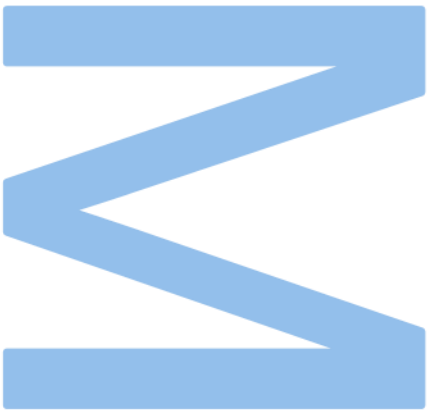

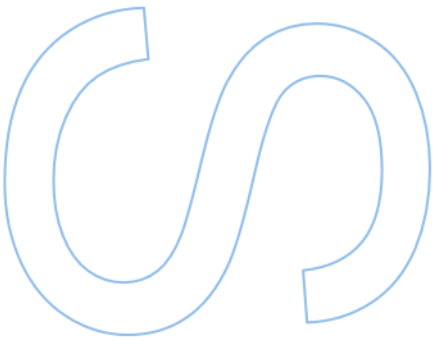

Declaração de Honra

Eu, Miguel Ângelo Simão Fernandes, inscrito(a) no Mestrado em Matemática da Faculdade de Ciências da Universidade do Porto declaro, nos termos do disposto na alínea a) do artigo 14.º do Código Ético de Conduta Académica da U.Porto, que o conteúdo da presente dissertação reflete as perspetivas, o trabalho de investigação e as minhas interpretações no momento da sua entrega.

Ao entregar esta dissertação, declaro, ainda, que a mesma é resultado do meu próprio trabalho de investigação e contém contributos que não foram utilizados previamente noutros trabalhos apresentados a esta ou outra instituição.

Mais declaro que todas as referências a outros autores respeitam escrupulosamente as regras da atribuição, encontrando-se devidamente citadas no corpo do texto e identificadas na secção de referências bibliográficas. Não são divulgados na presente dissertação quaisquer conteúdos cuja reprodução esteja vedada por direitos de autor.

Tenho consciência de que a prática de plágio e auto-plágio constitui um ilícito académico.

Miguel Ângelo Simão Fernandes

Braga, 30 de Setembro de 2022

The writing of this thesis was motivated by our mathematical intuition in explaining the etiology of anxiety-derived conditions.

The authors appreciate that the reader avoid any sort of bias while consulting this text.

I. Abstract

This dissertation treats the analysis of a well-known model in the range of neurosciences, the Wilson-Cowan system. In particular, an application of this model to a neuronal triad is performed using certain computational tools. A detailed description of the results and a subjective discussion follows the presentation of the simulations.

II. Resumo

Esta dissertação trata da análise de um modelo bem conhecido no campo das neurociências, o sistema de Wilson-Cowan. Em particular, uma aplicação deste modelo a um tríade neuronal é concebida através de determinadas ferramentas computacionais. Uma descrição detalhada dos resultados e uma discussão subjetiva seguem a apresentação das simulações.

Contents

I. Abstract 3
II. Resumo 4
III. Introduction 6
IV. The Wilson-Cowan Model 9
V. General Analysis of the Wilson-Cowan Model: Equilibrium Points and Respective Stability 13
VI. Bifurcation Analysis of the Wilson-Cowan Model 20
VI.1. Saddle-node bifurcation 20
VI.2. Pitchfork bifurcation 24
VI.3. Hopf bifurcation 28
VI.4. Bogdanov-Takens bifurcation 39
VII. Bifurcation diagrams 40
VII.1. Hysteresis 41
VIII. Emotional Regulation in the context of Psychiatry 44
VIII.1. Rhythmic activity of fear mechanisms 45
IX. Modelling the mPFC-amygdala-hippocampus triad 48
IX.1. The model 48
IX.2. Periodic solutions 49
IX.3. Simulation 52
IX.3.1. Bifurcation of periodic solutions 55
IX.3.2. How the oscillatory dynamics and surrounding behaviours will be interpreted in this context? 56
IX.3.3. Simulation diagrams 61
X. Results 72
XI. Discussion 77
XII. Future Directions 81
XIII. Appendix 82
XIII.1. A special case: Obsessive-compulsive disorder 82
References 84

III. Introduction

This dissertation is an attempt to explain certain neurobiological phenomena using mathematical tools, either analytical or numerical, the latter drawing essentially on the softwares *Mathematica* and *Matlab*.

Neurobiology and psychiatry are inevitably connected with each other. This dyadic interaction is based on certain factors that support the brain's development, namely the individual's genetic load and the enviromental experiences. In fact, these contextual/physiological components interact mutually to shape one's behaviour.
Inspired by such relations, we aim to exemplify how a specific neuronal mechanism may be a cause of a psychophysiological condition. This could, eventually, provide clues for a successful treatment.

The above scientific areas are not isolated from other fields. The link between Mathematics and all that biological/medical issue is subject of the *dynamical neurosciences*, the study of mathematical models of connections between excitable tissues. This interregional communication is intimately related with the phenomenon of *plasticity*, once explained by Hebb [22] with the statement *"When an axon of cell A is near enough to excite a cell B and repeatedly or persistently takes part in firing it, some growth process or metabolic change takes place in one or both cells such that A's efficiency, as one of the cells firing B, is increased"*. As a matter of fact, the concept of plasticity is broadly applied in the range of neurosciences and comprehends many neuronal processes, including synaptic strengthening and dendritic arborization. Regarding these two examples, only the first will be extensively explored in this text, as the second would in principle require a space-time framework.

This text is split up into two main parts. The first, comprising sections IV to VII, treats the Wilson Cowan Model [53], a system of two ordinary differential equations (the independent variable is the time) modelling the interaction of two interconnected excitable tissues (groups of neurons). Each group of cells has a connection to the other group and a feedback connection. This is a particular instance of a pure activator-inhibitor system [38], where one group of cells has a self-inhibitory connection and also inhibits the second group, whereas the other group has excitatory connections to itself and to the first group. We explore some of the rich dynamics of this model, including the asymptotic behaviour of the system around its equilibria and the types of bifurcation occuring under the variation of certain connection strengths or external inputs.
Although the number of equilibria of the system is variable, our initial study is mostly based on the presence of three equilibrium points, as

this scenario associates to opposite states of activity [20] (down and up states).
In terms of bifurcations, we deduce that the perturbation of some connection strengths (the number depends on the codimension of the bifurcation) is apt to make the system undergo certain topological transitions. These transitions include the appearance of equilibrium points and the emergence of limit cycles, as well as of homoclinic orbits. In this context, both analytical and numerical computations are performed, the latter making use of bifurcation diagrams.
Most of the constructions in this first part are based in methods adopted by the authors, so that previous literature concerning the dynamical analysis of the Wilson-Cowan model was pratically neglected.

The growing investment in the explanation of the processes underpinning the brain's ability to regulate emotions [7, 8] encouraged the development of the second part of the dissertation, which consists in the modelling and subsequent analysis of a neuronal triad.
In section VIII, a short description of the neurobiological/medical facts concerning the targeted neuronal circuit precedes the rigorous exposition of the goal of the study.
That introductory concept is then used to present, in section IX, a modification of the Wilson Cowan Model that describes the interaction of three different structures in the brain, giving rise to a system of three ordinary differential equations. We will be concerned primarily with the dynamics of oscillatory type, when it arises via Hopf bifurcation. In particular, our focus will target stable oscillations, given their biological relevance (unstable oscillations are not fisically observable). This is based on some innovative purposes: we regard the meaningful eletrical switches in a certain neuronal area as originating from a mechanism of depotentiation/strengthening of synapses, which in turn occur in parallel with the generation of neural waves. Such waves are based on periodic solutions[1] which are forced via Hopf bifurcations.

Most results are numerical and are exhibited in IX.3.3., being subsequently described and properly discussed. This discussion regards two aspects: the first based on how the period and amplitude of the oscillations vary with the selected connection strengths; the second on the extention of the oscillatory dynamics and the levels of activity to which the system converges as the periodic solutions cease. We then attempt to establish a bridge between the encountered evidence and the possible neurobiological mechanisms that may underlie it, either originating from previous findings or our own intuition.

[1] Along this text, we refer to *periodic solutions* in the strict sense, in a way that they are represented by curves that oscillate between distinct extrema (i.e. we ignore the trivial periodicity of equilibrium points).

As suggested by the title above, the neuropsychological background of the simulations is the phenomenon of extinction of fear memories, whose assumptions determine all the initial setting for the computational work.

We finally make a description of obsessive-compulsive disorder (OCD) [45], as an anxiety pathology. In fact, apart from the incompleteness of its etiology, this condition belongs to our main interests in the range of neurosciences. In particular, we are especially attracted by the functional role of the cingulate cortex [33] in the symptomatic development of the disease, as well as in general emotional processes.

IV. The Wilson-Cowan Model

Eccles et al. state in [11] that "*the same chemical transmitter is released from all the synaptic terminals of a neurone*". This idea is known as the Dale's Principle and suggests that an individual neuron in a population is either excitatory or inhibitory: in the first (resp. second) case, if when the cell fires, it promotes the increase (resp. decrease) in the voltage potential of the postsynaptic cells that it synapses onto.
This form of neuronal communication translates into a synaptic strength, which is formally defined as the (average) probabilistic amount of current or voltage excursion produced in the postsynaptic neuron by an action potential originating from the presynaptic neuron [39]. At a single synapse, this quantity, say a, results from the multiplication of two variables: the probability (P) of the presynaptic action potential causing the release of a neurotransmitter and the current or voltage jump ($\triangle V$) caused postsynaptically (in absolute value), in the presence of the neurotransmitter. Symbolically, this is written as

$$a = P \times |\triangle V| \,. \tag{1}$$

In particular, a is always a non-negative quantity and $a \leq |\triangle V|$. Along this text, we will always regard the connectivities between neurons or populations of neurons as depending on those variables.

We hereafter consider two neuronal populations, one excitatory and the other inhibitory[2], with average firing rates U_e and U_i, respectively. The *average firing rate* of a neuron is defined as the number of fires of that neuron per unit of time. Therefore, extending this notion to a group of neurons, $U_{e,i}$ represent the level of activity of the respective population.
We intend to study how the interaction between the opposite populations affects their activities. This can be achieved by analysing the *Firing Rate Model*, introduced by Harris in [20], but originally derived by Wilson and Cowan [53]. For this reason, the model is also known as the *Wilson-Cowan model*, denomination that we use from now on.

The two-dimensional Wilson-Cowan model is here represented by the coupled system of nonlinear differential equations

$$\begin{cases} U_e' = -U_e + F_e(a_{ee}U_e - a_{ei}U_i - \beta_e) =: h_1(U_e, U_i) \\ U_i' = -U_i + F_i(a_{ie}U_e - a_{ii}U_i - \beta_i) =: h_2(U_e, U_i) \end{cases}, \tag{2}$$

where $' = d/dt$ and the constants $a_{jk} \in \mathbb{R}$, with $j, k \in \{e, i\}$, refer to the connection strengths between the neuronal populations, as depicted in the diagram of Figure 1. The signs of the constants a_{jk} in (2) have to do with the fact that we deal with a pure excitatory-inhibitory system.

[2]The explanation above about the eletrical effect of a single neuron is here extended to a set/population of neurons.

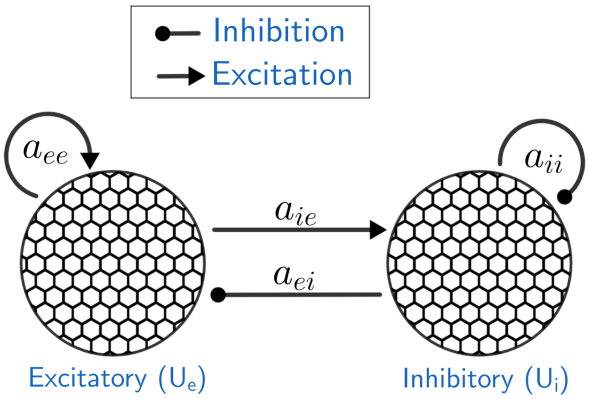

FIGURE 1. Diagram depicting the possible interactions existing inside and between the excitatory (left) and inhibitory (right) neuronal populations, giving an interpretation for the constants a_{jk} of system (2). In particular, we observe that the U_e-population has a self-excitation (a_{ee}) and excites the U_i-population (a_{ie}). The latter, in turn, has a self-inhibition (a_{ii}) and inhibits the U_e-population (a_{ei}). This describes a pure excitatory-inhibitory system.

The values of $U_{e,i}$ may actually be negative, meaning that the activity of the network is inferior to that of the background (Borisyuk et al., [3]). We ignore this hypothesis and restrict all of our analysis to the first quadrant of the plane U_eU_i.
The constants β_e and β_i of the model, which refer to external inputs (those that do not result from the natural neuronal functioning), will eventually be set to zero.
Lastly, the function $F_{e,i}$, which we refer to as the *Firing Rate Function*, is defined as the logistic sigmoid[3] [36]:

$$F_{e,i}(x) = \frac{1}{1 + e^{-\alpha_{e,i}x + \delta_{e,i}}}, \forall x \in \mathbb{R} \tag{3}$$

where $\alpha_{e,i} \in \mathbb{R}^+$ and $\delta_{e,i} \in \mathbb{R}_0^+$ (the former controls the value of the maximum slope of the sigmoid, while the latter is associated with the position of this slope, which is given by $\delta_{e,i}/\alpha_{e,i}$). Graphically, this sigmoid yields a curve that ranges increasingly from 0 to 1. As the value of $\alpha_{e,i}$ is changed, the graph of (3) displays a different steepness - see Figure 2.
The fact that F_{ei} is monotonically bounded between $y = 0$ and $y = 1$ gives a contextual meaning to these asymptotes: while $y = 0$ reflects

[3]Other functions, with the same features, are commonly found in the literature.

the neuronal deactivation, with the firing rate decaying to near-zero values (hyperpolarization), the line $y = 1$ corresponds to the neuronal activation, with the firing rate converging to top levels of activity, i.e. near-one values (depolarization) - this observation is suggested in Figure 2.

More generally, sigmoid curves are S-shaped curves whose simplicity and specific properties justify their well-known applications in population models, for instance, predator-prey models (see Gonzalez-Olivares et. al. [18]).

For further purposes, we will denote by $\mathcal{A}$ the following matrix:

$$\mathcal{A} := \begin{pmatrix} a_{ee} & -a_{ei} \\ a_{ie} & -a_{ii} \end{pmatrix}, \tag{4}$$

which collects the signed connection strengths a_{jk} in system (2).
In some situations, we will not only invoke the condition $\det \mathcal{A} = 0$, but also take it as an assumption for certain analytical procedures. Incidentally, that condition carries an interisting interpretation, being regarded as a balancing effect inside the network. For if $\det \mathcal{A} = 0$, then $a_{ee}a_{ii} = a_{ie}a_{ei}$, or equivalently

$$\frac{a_{ee}}{a_{ie}} = \frac{a_{ei}}{a_{ii}}, \tag{5}$$

as long as $a_{ie,ii} \neq 0$. For example, if $a_{ee}/a_{ie} > 1$, then $a_{ee} > a_{ie}$ and $a_{ei} > a_{ii}$, meaning that the input of the excitatory (resp. inhibitory) population is higher than (resp. is lower than) the respective output. This relation translates into a balanced intercommunication between the populations, with the inhibitory population favoring the inhibition of the opposite cluster, when this latter benefits self-excitation, rather than the forward-excitation (see Figure 3).

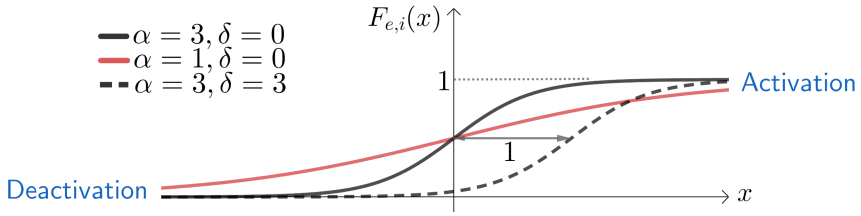

FIGURE 2. Representation of three sigmoids defined by (3) and corresponding to the pairs $(\alpha_{e,i}, \delta_{e,i}) = (3, 0)$ (black solid curve), $(1, 0)$ (red solid curve) and $(3, 3)$ (black dashed curve). The horizontal asymptotes $y = 0$ and $y = 1$ are associated with, respectively, the deactivation and activation of the neuronal populations.

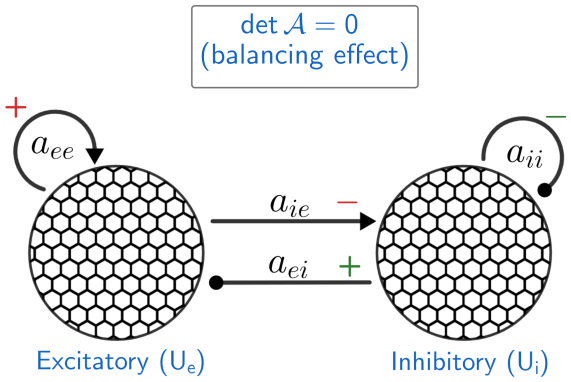

FIGURE 3. Balancing effect of the dyadic interaction between the neuronal populations, associated to the condition $\det \mathcal{A} = 0$, with $\mathcal{A}$ as in (4). The $+$ and $-$ signs, with the same colour, yield the relative comparison between connection strengths emerging from the same population (the red, resp. green, colour for those connections originating from the excitatory, resp. inhibitory, population).

V. General Analysis of the Wilson-Cowan Model: Equilibrium Points and Respective Stability

Unless otherwise explicitly stated, in what follows we take $\alpha_{e,i} = 1$ and $\delta_{e,i} = 0$. System (2) is then recast into

$$\begin{cases} U_e' = -U_e + F(a_{ee}U_e - a_{ei}U_i - \beta_e) = h_1(U_e, U_i) \\ U_i' = -U_i + F(a_{ie}U_e - a_{ii}U_i - \beta_i) = h_2(U_e, U_i) \end{cases}, \tag{6}$$

where F is the sigmoid (red curve in Figure 2)

$$F(x) = \frac{1}{1 + e^{-x}}, \forall x \in \mathbb{R} \tag{7}$$

and whose inverse reads

$$F^{-1}(x) = -\log\left(\frac{1}{x} - 1\right) = \log\left(\frac{x}{1-x}\right), \forall x \in]0, 1[\,. \tag{8}$$

As a starting point, we are interested in finding the equilibrium points of system (6), i.e. those points (U_e, U_i) of the phase space for which the vector field $(h_1(U_e, U_i), h_2(U_e, U_i))$ vanishes. In our context, the equilibrium points refer to the levels of activity of the excitatory/inhibitory populations that will remain indefinitely in time. Their abundance in the phase portrait depends on the constants a_{jk}, $j, k \in \{e, i\}$, as we will then explore.

Due to the range of the curve $y = F(x)$ in (7), all the equilibrium points lie in the square $Q_1 =]0, 1[^2$ of the phase space (first quadrant). More specifically, every square of the form $Q_A =]0, A[^2$, with $A \geq 1$, is positively invariant (orbits starting, for $t = t_0$, at a certain point of Q_A remain in this set for all $t > t_0$). To see this, it suffices to notice that both U_i' and U_e' are negative along the lines $U_i = A$ and $U_e = A$, respectively, and that both are positive on the lines of the form $U_e = B \leq 0$ and $U_i = B \leq 0$. As a consequence, all the orbits of system (6) are attracted to the square Q_1. In particular, this encourages us to restrict the dynamics to the square Q_1, instead of the first quadrant itself.

In order to find the equilibria of (6), we study the nullclines $U_j' = 0$, with $j \in \{e, i\}$, given by

$$\begin{aligned} U_i = \varphi(U_e) &:= -\frac{1}{a_{ei}}\left[F^{-1}(U_e) - a_{ee}U_e + \beta_e\right] = \\ &= \frac{1}{a_{ei}}\left[\ln\left(\frac{1}{U_e} - 1\right) + a_{ee}U_e - \beta_e\right] \qquad (U_e\text{-nullcline}), \end{aligned} \tag{9}$$

defined for $0 < U_e < 1$, and

$$U_e = \psi(U_i) := \frac{1}{a_{ie}} \left[F^{-1}(U_i) + a_{ii}U_i + \beta_i\right] = \tag{10}$$
$$= \frac{1}{a_{ie}} \left[\ln\left(\frac{U_i}{1-U_i}\right) + a_{ii}U_i + \beta_i\right] \qquad (U_i\text{-nullcline}),$$

with analogous domain, provided $a_{ei}, a_{ie} \neq 0$.
The derivatives of both $\varphi(U_e)$ and $\psi(U_i)$ are, respectively,

$$\varphi'(U_e) = \frac{1}{a_{ei}} \left(\frac{1}{U_e(U_e-1)} + a_{ee}\right), \tag{11}$$

and

$$\psi'(U_i) = \frac{1}{a_{ie}} \left(\frac{1}{U_i(1-U_i)} + a_{ii}\right). \tag{12}$$

From (9) and (11) it follows that:

(a) The U_e-nullcline has a particular asymptotic behaviour:

$$U_i \xrightarrow[U_e \to 0^+]{} +\infty$$

and

$$U_i \xrightarrow[U_e \to 1^-]{} -\infty;$$

(b) For $a_{ee} < 4$, $\varphi'(U_e)$ is negative and the graph $U_i = \varphi(U_e)$ is strictly decreasing; if $a_{ee} = 4$, the nullcline remains with the same behaviour, but with a critical point whose U_e-coordinate is equal to $1/2$; lastly, for $a_{ee} > 4$, that critical point separates into two extrema, one maximum and one minimum, between which the nullcline increases. These minimum and maximum points have the respective U_e-coordinates

$$U_e^m = \frac{2}{a_{ee}+k} \qquad \text{and} \qquad U_e^M = \frac{2}{a_{ee}-k},$$

for $k = \sqrt{a_{ee}(a_{ee}-4)}$, and do not necessarily lie in Q_1. Outside the interval $\left[U_e^m, U_e^M\right]$, the curve has a monotone behaviour according to its asymptotes.
We conclude that the constant a_{ee} determines completely the variation of the U_e-nullcline.

In an analogous manner, we see that:

(c) The asymptotic behaviour of the U_i-nullcline is

$$U_e \xrightarrow[U_i \to 1^-]{} +\infty$$

and

$$U_e \xrightarrow[U_i \to 0^+]{} -\infty;$$

(d) The sigmoidal shape of the U_i-nullcline is independent of the choice of the constants $a_{ie,ii}$ and β_i, in constrast to the U_e-nullcline that has a different behaviour in function of a_{ee}.

The deductions above make us conclude that system (6) exhibits unconditionally at least one equilibrium point in Q_1. In particular, if the constant a_{ee} is ≤ 4, the system (6) will exhibit exactly one equilibrium point, being the intersection of two strictly monotone curves.
When we have the existence of more than one equilibrium point, a special case arises, as described in [20]. In fact, a set of three equilibria contains different states of activity: the down state (E_d), the saddle state (E_s) and the up state (E_u), sorted according to the respective U_e-coordinate - see Figure 4 (left). These classifications allude to states of more or less activity in the network (the down state encodes lower levels of eletrical activity, while the up state encodes higher levels of neuronal firing).
The scenario comprising three equilibria is nonetheless conditioned by the monotocity of the U_e-nullcline. For example, a sufficient condition for the existence of three equilibrium points is given by

$$(13) \qquad \begin{cases} \varphi(U_e^m) < 0 \\ \varphi(U_e^M) > 1 \end{cases} \qquad \text{or} \qquad \begin{cases} U_e^m > (\psi \circ \varphi)(U_e^m) \\ U_e^M < (\psi \circ \varphi)(U_e^M) \end{cases} .$$

This condition, when applied, works particularly well for the deduction of the equilibria stability, as we will see further.

When $\beta_i \neq 0$, more than three equilibria can also be observed. This is due to the horizontal displacement that is promoted on the U_i-nullcline. An example exhibiting five equilibrium points is depicted in Figure 4 (right).
As commented by Ermentrout in [12], there will generically be an odd number of equilibria in system (6). An even amount, say $2n$, is perturbed to either $2n-1$ or $2n+1$ equilibrium states. In section VI, we will treat this transition with more detail.

Once the equilibria are properly identified, it is essential to study their stability, that is, the behaviour of the system in a neighborhood of those points. We first compute the Jacobian matrix of the vector field $(h_1(U_e, U_i), h_2(U_e, U_i))$ in (6):

$$(14) \quad J(U_e, U_i) = \begin{pmatrix} a_{ee}F'(b_e(U_e, U_i)) - 1 & -a_{ei}F'(b_e(U_e, U_i)) \\ \\ a_{ie}F'(b_i(U_e, U_i)) & -1 - a_{ii}F'(b_i(U_e, U_i)) \end{pmatrix},$$

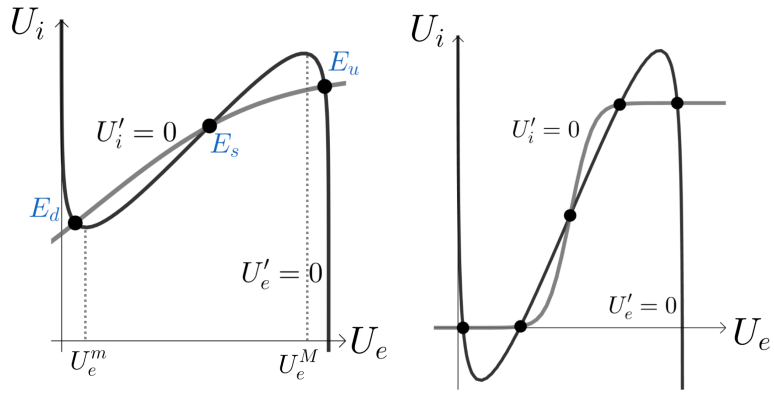

FIGURE 4. System (6) exhibiting three equilibria (left Figure), for $\beta_j = 0$, and five equilibria (right Figure), for $\beta_j \neq 0$ (more specifically, $\beta_i \neq 0$). Relatively to the first case, the three states of activity are suggested (up E_u, down E_d and saddle state E_s).

where $b_j(U_e, U_i) := a_{je}U_e - a_{ji}U_i - \beta_j$, for $j \in \{e, i\}$. We observe that J has in advance three entries with well-defined sign, while the entry $a_{ee}F'(b_e) - 1$ may assume both signs; in particular, it is negative if $a_{ee} < 4$.

Let (U_e^*, U_i^*) be an equilibrium of (6). Given the identity

$$F'(x) = e^{-x}F^2(x) = F(x) - F^2(x) \qquad \forall x \in \mathbb{R},$$

the matrix $J(U_e^*, U_i^*)$ is recast into

$$J(U_e^*, U_i^*) = \begin{pmatrix} a_{ee}p(U_e^*) - 1 & -a_{ei}p(U_e^*) \\ a_{ie}p(U_i^*) & -1 - a_{ii}p(U_i^*) \end{pmatrix}, \tag{15}$$

provided p is the degree two polynomial $p(x) := x - x^2$.
With this simplification, we write below the expressions for both the determinant and trace of the linearization $J(U_e^*, U_i^*)$, respectively denoted by $\operatorname{tr} J(U_e^*, U_i^*)$ and $\det J(U_e^*, U_i^*)$:

$$\operatorname{tr} J(U_e^*, U_i^*) = -2 + a_{ee}p(U_e^*) - a_{ii}p(U_i^*)$$

and

$$\det J(U_e^*, U_i^*) = -\operatorname{tr} J(U_e^*, U_i^*) + \det \mathcal{A}\, p(U_e^*)p(U_i^*) - 1,$$

where $\mathcal{A}$ is the matrix in (4). Specifically, supposing that $\det \mathcal{A} = 0$ (or, equivalently, that $a_{ee}a_{ii} = a_{ie}a_{ei}$), then the equilibrium point (U_e^*, U_i^*) is asymptotically stable if $\operatorname{tr} J(U_e^*, U_i^*) < -1$.

Non-hyperbolicity of the equilibrium (U_e^*, U_i^*) reads[4]

$$(\operatorname{tr} J(U_e^*, U_i^*) = 0 \wedge \det J(U_e^*, U_i^*) > 0) \vee \det J(U_e^*, U_i^*) = 0. \tag{16}$$

[4]That condition is specific of a two-dimensional phase space.

The first argument of the above disjunction regards those equilibria (U_e^*, U_i^*) for which the eigenvalues of the matrix (15) lie properly in the imaginary axis of the complex plane. These equilibria naturally associate to a type of bifurcation, the Hopf bifurcation, as we will see.

When system (6) has a unique equilibrium point it is necessarily asymptotically stable provided there are no periodic orbits, by the Poincaré-Bendixson Theorem [51]. In fact, as observed above, all the orbits converge to the square $Q_1 =]0,1[^2$, a bounded set. As a special case, for $a_{ee} \leq 4$, the unique equilibrium is always asymptotically stable, because the divergence of the vector field (h_1, h_2) is globally negative. If the nullclines of (6) satisfy condition (13), then three equilibria arise in the phase portrait. Necessarily, two of those, namely the down and up states, lie in the descending branches of the U_e-nullcline, so that the determinant of the linearization at such points gets positive and the trace negative. For our purposes[5], the saddle state (point E_s) is the state at which the U_e-nullcline has a greater slope than the U_i-nullcline and simple computations show that the determinant of the linearization is negative and hence E_s is a saddle point. This approach of using geometrical tools to deduce the equilibria stability is also used by Harris in [20].
The following example enables us to be more clear about the above assertions.

Example V.0.1. Fixing, for example, $a_{ee} = 12$, $a_{ei} = 9$, $a_{ie} = 3$, $a_{ii} = 1$ and $\beta_j = 0$, condition (13) is satisfied and thus system (6) admits exactly three equilibrium points, as represented in the Figure 5. In particular, the equilibria E_d (down state) and E_u (up state) live in the rectangles

$$E_d \in]0, U_e^m[\times]\varphi(U_e^m), \varphi(U_e^M)[, \qquad E_u \in]U_e^M, 1[\times]\varphi(U_e^m), \varphi(U_e^M)[,$$

where $U_e^m = 2/(12 + \sqrt{96})$ and $U_e^M = 2/(12 - \sqrt{96})$, that is, they lie in the decreasing branches of the U_e-nullcline. This way

$$\left.\frac{d\varphi}{dU_e}\right|_{E_d,E_u} = \left.\frac{a_{ee}F'(b_e) - 1}{a_{ei}F'(b_e)}\right|_{E_d,E_u} < 0 \Rightarrow a_{ee}F'(b_e) - 1 < 0, \tag{17}$$

so that the first entries of the matrices $J(E_d)$ and $J(E_u)$, defined according to (15), are negative.

On the other hand, when it comes to the intermediate equilibrium E_s, we need to relate the local slopes of the nullclines, which are both strictly increasing in a neighborhood of such equilibrium. In this case, the steepness of the U_e-nullcline at E_s exceeds that of the U_i-nullcline

[5] In fact, the nullclines may have a tangent contact at E_s.

and hence

$$\left.\frac{d\varphi}{dU_e}\right|_{E_s} > \left.\frac{d\psi^{-1}}{dU_e}\right|_{E_s} \Rightarrow \frac{a_{ee}F'(b_e)-1}{a_{ei}F'(b_e)} > \frac{a_{ie}F'(b_i)}{1+a_{ii}F'(b_i)}. \tag{18}$$

This construction allows us to infer about the stability of our equilibria:

- Both E_d and E_u are asymptotically stable since, by condition (17), it reads:

  $$\operatorname{tr} J\Big|_{E_d,E_u} < 0 \qquad \text{and} \qquad \det J\Big|_{E_d,E_u} > 0.$$

  Furthermore, one has

  $$\Delta(J) := \operatorname{tr}^2 J - 4\det J\Big|_{E_d,E_u} < 0,$$

  so that neighborhood orbits spiral towards E_d and E_u. Systems exhibiting double states (including periodic orbits) of stability are usually referred to as *bistable* [14], being frequent in neuronal models. As a matter of fact, when the equilibria are stable they will correspond to the observable states of the neuronal populations, as opposed to transient behaviour;
- In what concerns the equilibrium E_s, we easily see from implication (18) above that $\det J(E_s) < 0$. Therefore E_s is a saddle point.

  More specifically, $J(E_s)$ has two real eigenvalues with opposite signs, say λ_+ and λ_-. The eigenvector v_- corresponding to the negative eigenvalue λ_- is given by $v_- = (1+p(E_s^2)+\lambda_-, 3p(E_s^2))$, where E_s^2 is the second coordinate of E_s.

  Given the different behavior of the vector field (h_1, h_2) on both sides of the stable eigenspace $\{v_-\}$, we can say that this subspace acts as a threshold for the system. More specifically, the stable eigenspace works as a boundary for the basins of attraction of the up and down states (see Figure 6).

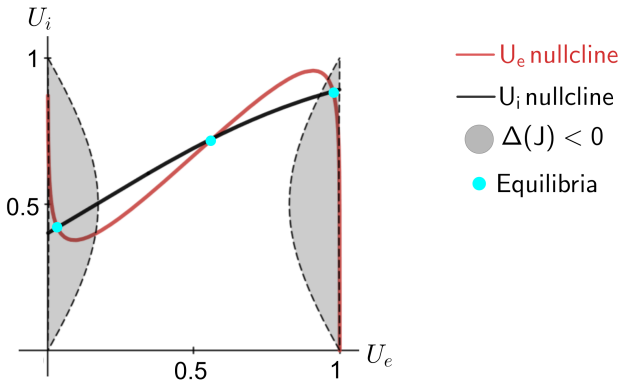

FIGURE 5. Nullclines of (6), for $a_{ee} = 12$, $a_{ei} = 9$, $a_{ie} = 3$, $a_{ii} = 1$ and $\beta_j = 0$. The red and black curves are the graphs of $U_i = \varphi(U_e)$ and $U_e = \psi(U_i)$, respectively.

We represent below the phase portrait of system (6) for the selected connection strengths in the Example V.0.1. We particularly care about the representation of the orbits that converge to the down and up states, as well as the threshold of the system, which is symbolically defined as the stable eigenspace of the saddle point (dashed blue line).

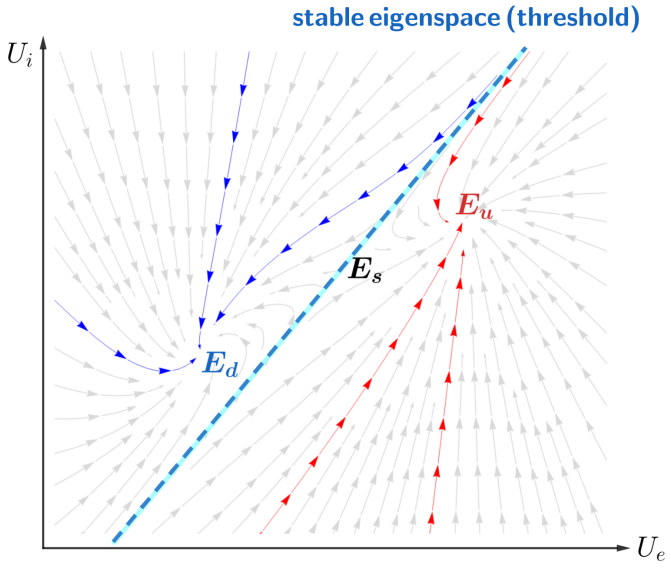

FIGURE 6. Phase portrait of system (6), for $a_{ee} = 12$, $a_{ei} = 9$, $a_{ie} = 3$, $a_{ii} = 1$ and $\beta_j = 0$. The red (resp. blue) trajectories are orbits converging to E_u (resp. E_d).

VI. Bifurcation Analysis of the Wilson-Cowan Model

Bifurcations result from the appearance of a topologically nonequivalent system under the variation of some parameters.

As observed by Borisyuk et al. [3], a variety of phase portraits and bifurcations of system (6) result from the manipulation of properly chosen parameters in the set $\{a_{jk}, \beta_j\}$.
In what follows, we deduce some of those bifurcations and their implications in the general configuration of the system.
In particular, since, as we have commented above, the system can assume multiple equilibria, we naturally start with those bifurcations that reflect the change in the number of equilibrium points.

Let $\mu \in \{a_{jk}, \beta_j\}$. We say that system (6) is of *μ-type* (μ-system, for short), if μ is a parameter of the system and all the remaining constants are held fixed. If the parameter μ is fixed at some value, say $\mu = \mu^*$, we refer to the μ-system with this substitution as the μ^*-system.

VI.1. **Saddle-node bifurcation.** Briefly, a *saddle-node (or fold) bifurcation* [29, 42, 51] (codimension one local bifurcation), say with parameter μ, arises when two equilibria (in the one dimensional case, necessarily one equilibrium is stable and the other is unstable), present for $\mu < \mu_1$, collide at $\mu = \mu_1$, forming a saddle-node point. This point then disappears as we keep increasing μ. We use the scheme below to represent this transition:

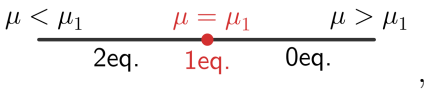

,

provided $\mu = \mu_1$ is the bifurcation value.
Graphically, the saddle-node bifurcation corresponds to a tangency of the nullclines. Reversing the orientation of the parameter μ, we find the transition

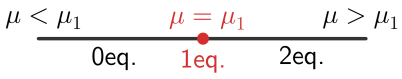

also called a saddle-node bifurcation.

A possible way (probably the easiest) of making system (6) go through a saddle-node bifurcation is by fixing the U_i-nullcline and promoting a vertical displacement of the non-monotone U_e-nullcline (without changing its configuration), so that we need $a_{ee} > 4$. This displacement can be achieved considering β_e as a parameter.
We recall that our system has unconditionally one equilibrium point.

In the case three equilibria are present, the fold bifurcation happens when two equilibria come together at a saddle-node, away from the third equilibrium that is not affected.

In what follows we look for points of saddle-node bifurcation (*limit points*) of the β_e-system (6).
Up to β_e, limit points are tangent contacts of the nullclines, thus satisfying the necessary condition

$$\varphi'(U_e)\psi'(U_i) = 1. \tag{19}$$

This equation defines a curve, on the plane U_eU_i, given by

$$U_i - U_i^2 = \frac{1 + a_{ee}U_e(U_e - 1)}{\det \mathcal{A} U_e(U_e - 1) - a_{ii}},$$

for the matrix $\mathcal{A}$ in (4). If $\det \mathcal{A} = 0$, this curve reduces to the conic

$$\mathcal{C} = \left\{ (U_e, U_i) : \frac{a_{ee}}{k a_{ii}} \left(U_e - \frac{1}{2} \right)^2 - \frac{1}{k} \left(U_i - \frac{1}{2} \right)^2 = 1 \right\},$$

with

$$k = \frac{a_{ee} - a_{ii} - 4}{4a_{ii}}.$$

Thus, if one sets $a_{ee} > a_{ii} + 4$, the conic covers all the U_i-axis and it necessarily meets the nullcline $U_e = \psi(U_i)$ at two points with $U_e \in]0, 1[$. Observe that the vertices of the conic are, in this case, given by

$$\left(\pm \sqrt{\frac{k a_{ii}}{a_{ee}}} + \frac{1}{2}, \frac{1}{2} \right),$$

which always lie in the square Q_1, under condition $a_{ee} > a_{ii} + 4$.
An intersection between $\mathcal{C}$ and $U_e = \psi(U_i)$ will also be an equilibrium of (6) if it additionally satisfies $U_i = \varphi(U_e)$. This may be achieved by varying β_e to move vertically the U_e-nullcline. The matching β_e values are then the bifurcation values of the β_e-system for a fold bifurcation.

Considering the above observations, we deduce that a sufficient condition for the β_e-system (6) to undergo a saddle-node bifurcation is given by

$$\begin{cases} \det \mathcal{A} = 0 \\ a_{ee} > a_{ii} + 4 \end{cases}. \tag{20}$$

This is nonetheless a sharp way of ensuring the bifurcation (the conic $\mathcal{C}$ may intersect the U_i-nullcline, even if the second inequality above does not hold). As in the Example below, the transition is as well observed in cases that do not verify the second inequality.

Under condition (20), equation (19) admits two solutions, say (U_e^1, U_i^1) and (U_e^2, U_i^2), satisfying $U_e^{1,2} = \psi(U_i^{1,2})$. The bifurcation values of the β_e-system, $\beta_e = \beta_e^{1,2}$, are then given by

$$\beta_e^{1,2} = \ln\left(\frac{1}{U_e^{1,2}} - 1\right) + a_{ee}U_e^{1,2} - a_{ei}U_i^{1,2}$$

and we have the transitions

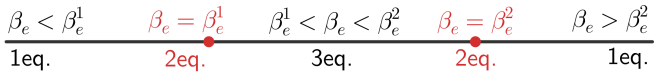

,

assuming that $\beta_e^1 < \beta_e^2$.

Example VI.1.1. We set $a_{ee} = 8$, $a_{ei} = 4$, $a_{ie} = 10$, $a_{ii} = 5$ and $\beta_i = 0$, so that $a_{ee}a_{ii} = a_{ie}a_{ei}$. In particular, we have $\det \mathcal{A} = 0$, but $a_{ee} < a_{ii} + 4$. The resulting β_e-system is given by

$$\left\{ \begin{array}{l} U_e' = -U_e + F(8U_e - 4U_i - \beta_e) \\ U_i' = -U_i + F(10U_e - 5U_i) \end{array} \right. . \tag{21}$$

The U_i-nullcline and the conic $\mathcal{C}$ intersect at two points, yielding the β_e bifurcation values

$$\beta_e^1 \approx 0.938 \qquad \text{and} \qquad \beta_e^2 \approx 1.177.$$

These bifurcation values are such that:

(1) for $\beta_e < \beta_e^1$, system (21) exhibits a unique asymptotically stable equilibrium point;
(2) for $\beta_e = \beta_e^1$, the nullclines collide in a saddle-node point; at this stage, system (21) admits exactly two equilibria, being one stable and the other unstable (and, in particular, non-hyperbolic);
(3) for $\beta_e^2 > \beta_e > \beta_e^1$, we have three equilibria: the down and up states are asymptotically stable and the saddle state is a saddle point;
(4) for $\beta_e = \beta_e^2$, the same scenario as for $\beta_e = \beta_e^1$ takes place;
(5) for $\beta_e > \beta_e^2$, the phase portrait comprises again a unique stable equilibrium.

In Figures 7-10, we represent the transition in the number of equilibria, as the parameter β_e varies.

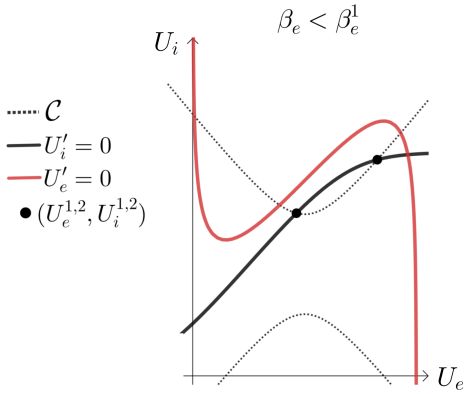

FIGURE 7. Representation of the β_e-system (21) with a unique equilibrium point which is asymptotically stable. This takes place for $\beta < \beta_e^1$, with $\beta_e^1 \approx 0.938$.

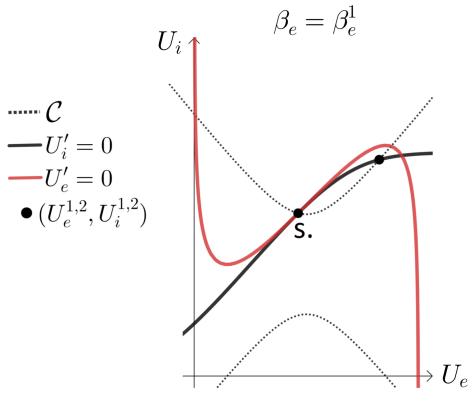

FIGURE 8. Tangent contact between the nullclines (of order ≥ 1) leading to the emergence of a new equilibrium, for $\beta = \beta_e^1$ bifurcation value; *s.* stands for *saddle-node point.*

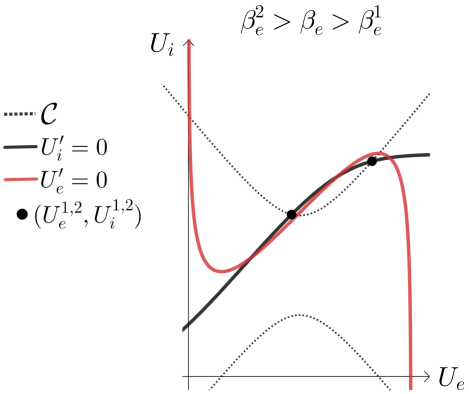

FIGURE 9. Three equilibrium points, for $\beta_e^2 > \beta > \beta_e^1$. This is highest number of equilibria possible for the β_e-system (21).

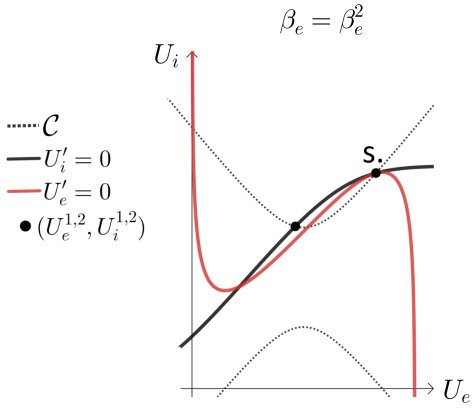

FIGURE 10. Second tangent contact between the nullclines and two equilibria present, for $\beta = \beta_e^2$ bifurcation value, with $\beta_e^2 \approx 1.177$.

VI.2. **Pitchfork bifurcation.** One feature that has not been mentioned before, albeit important for what follows, is that the U_e and U_i-nullclines of system (6) have rotational symmetry of π radians relatively to the points $(1/2, \varphi(1/2))$ and $(\psi(1/2), 1/2)$, respectively. Indeed, it can be easily verified that $U_e \mapsto \varphi(U_e + 1/2) - \varphi(1/2)$ is an odd function (same for $U_i \mapsto \psi(U_i + 1/2) - \psi(1/2)$). It should be remarked that this fact does not imply that the flow of the system detains the same feature, since the equations (6) do not display this symmetry.

A system undergoes a *pitchfork bifurcation* [29, 42, 51] (a codimension two bifurcation) when three equilibria, being two stable and one unstable, collide, for $\mu = \mu_1$ and $\rho = \rho_1$ bifurcation values, in a unique stable equilibrium point[6] (the reversed transition is also a pitchfork bifurcation).
This type of bifurcation is most common in systems exhibiting some symmetry [29] - in this case, the codimension is lowered to 1 and the transition is represented by

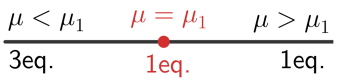

For our model, we can take advantage of both the symmetry and variation of the $U_{e,i}$-nullclines in order to deduce the transition. In particular, as a starting point, we may verify the existence of a contact of order ≥ 3 between the nullclines. This is an equilibrium, say (U_e^*, U_i^*), at which both curves agree up to order 2 (i.e. the polynomial approximations agree, at least, up to order 2).
Since we want to make use of the geometrical properties of the isoclines, it is convenient to take $(U_e^*, U_i^*) = (1/2, 1/2)$. On the other hand, according to the explanation above, the contact of order ≥ 3 at the center of the unit square $Q_1 =]0, 1[^2$ reads

$$\begin{cases} \varphi(1/2) = 1/2 \\ \psi(1/2) = 1/2 \\ \varphi'(1/2) = 1/\psi'(1/2) \\ \varphi''(1/2) = -\psi''(1/2)/\psi'(1/2)^3 \end{cases} \tag{22}$$

(recall the functions φ and ψ defined in section V). Further derivatives may eventually coincide for both φ and ψ at $(1/2, 1/2)$. We remark that the equilibrium point defined by condition (22) is not necessarily unique, since the nullclines may have a triple intersection, with E_s being the contact of order ≥ 3 (set, for example, $a_{ee} = 4.8$, $a_{ei} = 0.2$, $\beta_e = 2.3$, $a_{ie} = 20$, $a_{ii} = 1$ and $\beta_i = 9.5$).

[6] This is the definition that applies to our model.

Although kept for formalism, the last equation of (22) is actually redundant, since the equilibrium $(U_e^*, U_i^*) = (1/2, 1/2)$ is an inflection point for the curves φ and ψ. On the other hand, given the expressions defining both $U_i = \varphi(U_e)$ and $U_e = \psi(U_i)$, the first three conditions of (22) are recast into

$$\begin{cases} a_{ee} - 2\beta_e = a_{ei} \\ 2\beta_i + a_{ii} = a_{ie} \\ a_{ei}a_{ie} = (a_{ii} + 4)(a_{ee} - 4) \end{cases} . \tag{23}$$

For example, the set of constants

$$\{a_{ee} = 5, a_{ei} = 3, \beta_e = 1, a_{ie} = 3/2, a_{ii} = \beta_i = 1/2\} \tag{24}$$

is a solution of the equations in (23). In particular, provided the connection strengths are fixed according to the set (24), system (6) admits a contact of order ≥ 3 at $(1/2, 1/2)$ and numerical methods show that this is the unique equilibrium point of the system. Given the symmetry of the nullclines in a neighborhood of $(1/2, 1/2)$, perturbing this equilibrium with a proper parameter promotes the emergence of two new equilibria.

It remains to identify the connection strengths that work properly as bifurcation parameters, in order to observe a pitchfork bifurcation on system (6).
We assert that, if the a_{jk} and β_j are set according to (24), a perturbation on the constant $a_{ee} = 5$ creates the transition. Indeed, this constant regulates the maximum slope of the U_e-nullcline, since

$$\varphi'(1/2) = (a_{ee} - 4)/3.$$

If, after the perturbation, the equilibrium $(U_e^*, U_i^*) = (1/2, 1/2)$ persists and the maximum slope of the U_e-nullcline increases, a triple intersection between the nullclines occurs. The persistence of (U_e^*, U_i^*) may be achieved by translating $\beta_e = 1$ as we do below.
Under this description, the perturbed system, with parameter ϵ, follows:

$$\begin{cases} U_e' = -U_e + F((5 + \epsilon)U_e - 3U_i - 1 - \epsilon/2) \\ U_i' = -U_i + F(3U_e/2 - U_i/2 - 1/2) \end{cases} . \tag{25}$$

We add $-\epsilon/2$ to $\beta_e = 1$ to keep the equilibrium at $(U_e^*, U_i^*) = (1/2, 1/2)$. In particular, this setting does not alter the value of $\varphi'(1/2)$ (this number does not depend on β_e).

For $\epsilon = 0$, we have $\varphi'(1/2) = 1/3$, while $\epsilon > 0$ sufficiently small yields $\varphi'(1/2) = (1 + \epsilon)/3 > 1/3$. Since both $\psi(1/2)$ and $\psi'(1/2)$ do not depend on ϵ and $\varphi'(1/2)$ is monotonically increasing with ϵ, the nullclines have the behaviour of Figures 11 and 12.

We observe that although we have fixed, in advance, the connection strengths as in set (24) to describe the above geometrical method, an analogous procedure would apply to another set satisfying (23).

Example VI.2.1. According to the construction above, the ϵ-system

$$\begin{cases} U_e' = -U_e + F((5+\epsilon)U_e - 3U_i - 1 - \epsilon/2) \\ U_i' = -U_i + F(3U_e/2 - U_i/2 - 1/2) \end{cases}$$

has a pitchfork bifurcation at $\epsilon = 0$. More specifically:

(1) for $\epsilon = 0$, there is exactly one equilibrium which is asymptotically stable;
(2) for $\epsilon > 0$ (sufficiently small), there are three equilibria, two asymptotically stable and one unstable. In particular the emerging equilibria are equidistant from $(1/2, 1/2)$, by symmetry of the nullclines.

The transition diagram follows

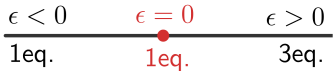

Another system exhibiting a pitchfork bifurcation, at $\epsilon = 0$ is given by

$$\begin{cases} U_e' = -U_e + F((5+\epsilon)U_e - (3+\epsilon)U_i - 1) \\ U_i' = -U_i + F(3U_e/2 - U_i/2 - 1/2) \end{cases} . \tag{26}$$

In fact, it can be verified that this system reveals the same modifications as the previous one, in the sense that the equilibrium $(1/2, 1/2)$ is invariant under the transition from $\epsilon = 0$ to $\epsilon > 0$ and the maximum slope of the curve $U_e' = 0$ increases.

More generally, any system of the form

$$\begin{cases} U_e' = -U_e + F((5+g(\epsilon))U_e - (3+g(\epsilon))U_i - 1) \\ U_i' = -U_i + F(3U_e/2 - U_i/2 - 1/2) \end{cases}$$

with $g(\epsilon)$ a differentiable positive function, for small $\epsilon > 0$, satisfying $g(0) = 0$ (thus $g'(0) \geq 0$), has as well a pitchfork bifurcation at $\epsilon = 0$. In particular, system (26) corresponds to $g(\epsilon) = \epsilon$.
This generalization is pertinent because, under a small perturbation of ϵ (in the positive direction), the (equal) deviation of the emerging equilibria (up and down states) from the equilibrium $(1/2, 1/2)$ is measured by $g'(0)$. More specifically, the higher the value of $g'(0)$, the more impaired (resp. enhanced) are the eletrical activities in the down (resp. up) state. The fact that the perturbation happens relatively to the a_{ej} gives significance to the role of the excitatory inputs in the eletrical convergence of the circuit.

In Figures 11 and 12 we show how the pitchfork bifurcation is generated as we vary the parameter ϵ from zero to a positive number, relatively to system (26).

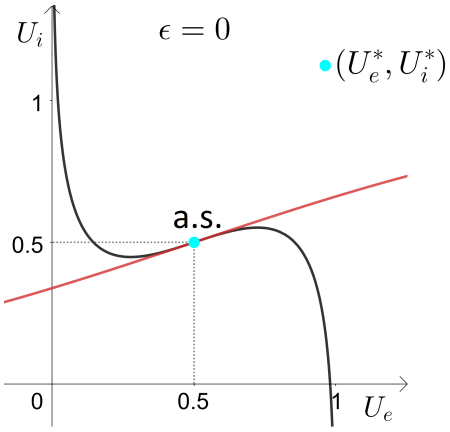

FIGURE 11. Configuration of the nullclines of system (26), for $\epsilon = 0$ (unperturbed system). The asymptotically stable (a.s.) equilibrium point $(U_e^*, U_i^*) = (1/2, 1/2)$ is the unique equilibrium of the system and, at the same time, a contact of order ≥ 3 between the nullclines.

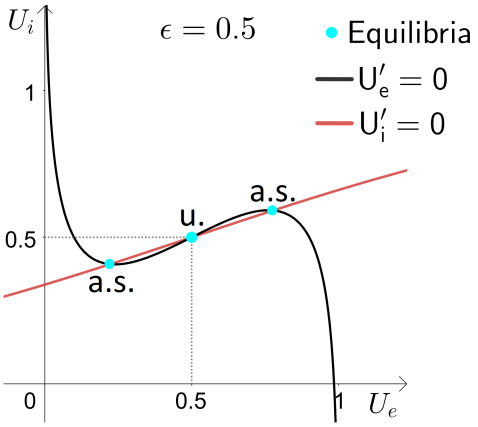

FIGURE 12. Depiction of the nullclines of the perturbed system, for $\epsilon = 0.5$, having a triple intersection. The equilibrium $(1/2, 1/2)$ persists after the perturbation and becomes unstable (u.), while the emerging equilibria (up and down states) are asymptotically stable (a.s.) and equidistant to $(1/2, 1/2)$.

VI.3. **Hopf bifurcation.** The previous bifurcations concerned local transitions involving equilibrium points. We look now for a more sofisticated transition, namely one having a periodic orbit as its hallmark. Periodic orbits, when present in biological models (see, for example, [18]), usually carry certain interpretations. The second part of this study will actually target that type of dynamics.

As described in [29], a *Hopf bifurcation* [14, 27, 29, 42] (codimension one bifurcation) occurs when a limit cycle (i.e. a periodic orbit that is the α or ω-limit set of points in a neighborhood) appears as a bifurcation parameter forces an equilibrium to change stability. In the nonlinear context, the coordinates of this equilibrium usually vary with the parameter as well. By the Implicit Function Theorem, it is however possible to verify that this equilibrium is locally unique for each sufficiently close value of the parameter to the bifurcation value.

(H1) Non-hyperbolicity and transversality conditions:
Let $(U_e^*(\mu), U_i^*(\mu))$ be the equilibrium of the μ-system (6) (in fact, the coordinates of this equilibrium may depend on μ), for a parameter $\mu \in \{a_{jk}, \beta_j\}$ to be chosen later, such that the eigenvalues $\lambda_{1,2}(\mu)$ of the linearization matrix $J(U_e^*(\mu), U_i^*(\mu))$ read

$$\lambda_{1,2}(\mu) := \alpha(\mu) \pm \omega(\mu) i,$$

with

$$\underbrace{\alpha(\mu^*) = 0,\ \omega(\mu^*) > 0}_{\text{Non-hyperbolicity conditions}}, \qquad \underbrace{\alpha'(\mu^*) \neq 0}_{\text{Transversality condition}},$$

for some $\mu = \mu^*$ bifurcation value.

(H2) Nondegeneracy condition:
The *first Lyapunov coefficient* [29] (which we will compute on a specific example) is non-zero. This coefficient regards the cubic terms of the expansion of the vector field in (6).

Under the genericity conditions (H1-2), the μ-system (6) reduces (up to translation) to the normal form

$$\begin{cases} x' = \eta x - y + \text{sgn}(\gamma)(x^2 + y^2)x \\ y' = x + \eta y + \text{sgn}(\gamma)(x^2 + y^2)y \end{cases}, \tag{27}$$

for some $\eta \equiv \eta(\mu)$ and $\text{sgn}(\gamma) = \pm 1$, provided γ is the first Lyapunov coefficient. The fact that γ is non-zero (and thus $\text{sgn}(\gamma)$ is well-defined) is a consequence of the nondegeneracy condition (H2). Furthermore, the signs of η and γ determine the stability of the limit cycle and the direction of the bifurcation.

To see that, we rewrite the equation (27) in polar coordinates (r, θ):

$$\begin{cases} r' = r(\eta + \text{sgn}(\gamma) r^2) \\ \theta' = 1 \end{cases},$$

from which it is easy to see that the origin is always an equilibrium point and that a limit cycle exists only when $\eta/\text{sgn}(\gamma) < 0$. In this case, for each η, the radius of this limit cycle is $\sqrt{-\eta/\text{sgn}(\gamma)}$, thus increasing with the value of η (this constant is related with the real and imaginary parts of the linearization eigenvalues). In the table below, we bring together the different cases regarding the stability of the equilibrium and the limit cycle (when it exists):

	$\gamma > 0$	$\gamma < 0$
$\eta < 0$	Unstable limit cycle Stable origin	No limit cycle Stable origin
$\eta = 0$	No limit cycle Unstable origin	No limit cycle Stable origin
$\eta > 0$	No limit cycle Unstable origin	Stable limit cycle Unstable origin

TABLE 1. Stability of the origin and the limit cycle of (27) under the different signs of $\gamma \neq 0$ and $\eta \in \mathbb{R}$.

The features corresponding to $\gamma > 0$ are implied in a *subcritical* Hopf bifurcation in η, while those corresponding to $\gamma < 0$ are implied in a *supercritical* bifurcation in η.
This classification must, in fact, encompass the parameter that is taken into account. Recall that $\eta = \eta(\mu)$, so that if, for example, $\eta > 0$ for $\mu < 0$ and $\gamma < 0$, the Hopf bifurcation becomes subcritical in μ.

Recall the Jacobian matrix $J(U_e^*, U_i^*)$ in (15) and the condition (16), both in section V. An equilibrium point (U_e^*, U_i^*) is, in particular, such that the matrix $J(U_e^*, U_i^*)$ has a pair of pure imaginary eigenvalues if and only if

$$\begin{aligned} &\text{tr}\, J(U_e^*, U_i^*) = -2 + a_{ee} p(U_e^*) - a_{ii} p(U_i^*) = 0 \\ &\det J(U_e^*, U_i^*) = -\text{tr}\, J(U_e^*, U_i^*) + \det \mathcal{A} p(U_e^*) p(U_i^*) - 1 > 0. \end{aligned} \tag{28}$$

For simplicity, we define $]0, 1/4] \ni p(U_e^*) =: q_1^*$ and $]0, 1/4] \ni p(U_i^*) =: q_2^*$, so that the above conditions regarding the trace and determinant of $J(U_e^*, U_i^*)$ make the point (q_1^*, q_2^*) lie in the intersection of the line $\mathcal{C}$ and the half-plane $\mathcal{S}$, respectively, defined by:

$$\begin{aligned} \mathcal{C}: &\quad \mathcal{C}(q_1, q_2) := -2 + a_{ee} q_1 - a_{ii} q_2 = 0 \\ \mathcal{S}: &\quad -\mathcal{C}(q_1, q_2) + \det \mathcal{A} q_1 q_2 - 1 > 0, \end{aligned}$$

with $(q_1, q_2) \in]0, 1/4]^2$.
Given the domain of the variables $q_{1,2}$, in the intersection $\mathcal{C} \cap \mathcal{S}$, we must have $\det \mathcal{A} q_1 q_2 > 1$, implying that $\det \mathcal{A} > 16$.
Thus we hereafter assume that the constants $\{a_{jk}\}$ satisfy

(H3) $\qquad \det \mathcal{A} = a_{ie}a_{ei} - a_{ee}a_{ii} > 16.$

With this assumption, the matrix $J(U_e^*, U_i^*)$ has a pair of imaginary eigenvalues if and only if the point (U_e^*, U_i^*) is of the form

$$(U_e^*, U_i^*) = \left(\frac{1 \pm \sqrt{1 - 4q_1^*}}{2}, \frac{1 \pm \sqrt{1 - 4q_2^*}}{2} \right), \tag{29}$$

for some $(q_1^*, q_2^*) \in \mathcal{C} \cap \mathcal{S}$. After some simple computations, one deduces that this intersection is actually the half-line

$$\left\{ (q_1, q_2) \in]0, 1/4]^2 : q_1 > \frac{1}{a_{ee}} \left(1 + \sqrt{\frac{a_{ei}a_{ie}}{\det \mathcal{A}}} \right), q_1 = \frac{2 + a_{ii}q_2}{a_{ee}} \right\}.$$

Example VI.3.1. Setting $a_{ee} = 12$, $a_{ei} = a_{ie} = 10$ and $a_{ii} = 5$, we find $\det \mathcal{A} = 40 > 16$. The half-line $\mathcal{C} \cap \mathcal{S}$ is, in this case, given by

$$\left\{ (q_1, q_2) \in]0, 1/4]^2 : q_1 > \frac{1}{12} \left(1 + \frac{\sqrt{10}}{2} \right), q_1 = \frac{2 + 5q_2}{12} \right\},$$

allowing us to take for instance $(q_1^*, q_2^*) = (0.25, 0.2) \in \mathcal{C} \cap \mathcal{S}$. According to (29), this point in the $q_1 q_2$ plane yields two admissible points (U_e^*, U_i^*) satisying (28):

$$(U_e^*, U_i^*) = \left(\frac{1}{2}, \frac{1 - \sqrt{1/5}}{2} \right) \text{ and } (U_e^*, U_i^*) = \left(\frac{1}{2}, \frac{1 + \sqrt{1/5}}{2} \right),$$

both in $]0, 1[^2$. For no particular reason, we choose the first point to apply the following procedure.

So let

$$(U_e^*, U_i^*) = \left(1/2, (1 - \sqrt{1/5})/2 \right). \tag{30}$$

We consider the system

$$\begin{cases} U_e' = -U_e + F(12U_e - 10U_i - \beta_e) \\ U_i' = -U_i + F(10U_e - 5U_i - \beta_i) \end{cases}, \tag{31}$$

in a way that the external inputs $\beta_{e,i}$ are such that the point (U_e^*, U_i^*) is an equilibrium. In this case, one easily obtains

$$\beta_e = 1 + \sqrt{5}, \qquad \beta_i = \frac{5 + \sqrt{5}}{2} - F^{-1} \left(\frac{1 - \sqrt{1/5}}{2} \right).$$

The linearization of (31), around (U_e^*, U_i^*), is given by ($p(x) = x - x^2$)

$$J(U_e^*, U_i^*) = \begin{pmatrix} -1 + 12p(U_e^*) & -10p(U_e^*) \\ 10p(U_i^*) & -1 - 5p(U_i^*) \end{pmatrix} = \begin{pmatrix} 2 & -5/2 \\ 2 & -2 \end{pmatrix},$$

whose eigenvalues are

$$\lambda_1 = i, \qquad \lambda_2 = -i$$

(which are pure imaginary, as expected by construction). The constants $a_{ee} = 12$, $a_{ei} = a_{ie} = 10$ and $a_{ii} = 5$ ensure the presence of a Hopf equilibrium point (a point that satisfies the non-hyperbolicity condition in (H1)) in our model, but we still need to identify those that might work as parameters for the desired Hopf bifurcation, according to the transversality condition in (H1) and the nondegeneracy of (H2).

Let us consider the a_{ee}-system

$$\text{(32)} \qquad \begin{cases} U_e' = -U_e + F(a_{ee}U_e - 10U_i - \beta_e) = h_1(U_e, U_i; a_{ee}) \\ U_i' = -U_i + F(10U_e - 5U_i - \beta_i) = h_2(U_e, U_i) \end{cases}.$$

Again, the external inputs $\beta_{e,i}$ are chosen in a way that (U_e^*, U_i^*) is an equilibrium, for $a_{ee} = 12$.
We hereafter denote by $(U_e^*(a_{ee}), U_i^*(a_{ee}))$ the equilibrium of (32), for each a_{ee} in a neighborhood of $a_{ee} = 12$. When $a_{ee} = 12$, we get the point in (30) and we keep the notation (U_e^*, U_i^*).

The eigenvalues of the linearization of the a_{ee}-system (32) are functions of the form $\lambda_{k=1,2}(a_{ee}) := \alpha(a_{ee}) + (-1)^{k+1}\omega(a_{ee})i$, provided

$$\text{(33)} \qquad \begin{aligned} \alpha(a_{ee}) &= \frac{-2 + a_{ee}p(U_e^*(a_{ee})) - 5p(U_i^*(a_{ee}))}{2} \\ \omega(a_{ee}) &= \frac{\sqrt{\rho(a_{ee})}}{2} \end{aligned}$$

for $|a_{ee} - 12| < \epsilon$, with $\epsilon > 0$ such that the function

$$\text{(34)} \qquad \begin{aligned} &\rho(a_{ee}) := -a_{ee}^2 p(U_e^*(a_{ee}))^2 + 400p(U_e^*(a_{ee}))p(U_i^*(a_{ee})) - \\ &10a_{ee}p(U_e^*(a_{ee}))p(U_i^*(a_{ee})) - 25p(U_i^*(a_{ee}))^2 \end{aligned}$$

is non-negative (this holds by the continuity of ρ and the equality $\rho(12) = 4$).

Our next step is to verify the transversality condition (H1) above for the eigenvalues $\lambda_{1,2}(a_{ee})$, relatively to $a_{ee} = 12$. The non-hyperbolicity is, by construction, satisfied.
We define the curve

$$\Gamma : \begin{array}{l} \{a_{ee} : |a_{ee} - 12| < \epsilon\} \longrightarrow Q_1 =]0,1[^2 \\ a_{ee} \longmapsto (U_e^*(a_{ee}), U_i^*(a_{ee})) \end{array},$$

which represents the trace position of the equilibrium point (U_e^*, U_i^*), as the parameter a_{ee} varies.

Recall the functions φ and ψ in section V, defining respectively the U_e and U_i nullclines and which, for convenience, we rewrite here

$$U_i = \varphi(U_e; a_{ee}) = \frac{1}{a_{ei}} \left[\ln \left(\frac{1}{U_e} - 1 \right) + a_{ee} U_e - \beta_e \right]$$

and

$$U_e = \psi(U_i) = \frac{1}{a_{ie}} \left[\ln \left(\frac{U_i}{1 - U_i} \right) + a_{ii} U_i + \beta_i \right].$$

Bearing in mind the definition of the function Γ above, we regard both U_e and U_i as functions of a_{ee}. Differentiating implicitly, with respect to the parameter a_{ee}, the curves $U_i = \varphi(U_e; a_{ee})$ and $U_e = \psi(U_i)$, yields

$$\begin{cases} \dfrac{1}{a_{ei}} \left[\left(-\dfrac{1}{p(U_e)} + a_{ee} \right) U_e' + U_e \right] = U_i' \\ \\ \dfrac{1}{a_{ie}} \left(\dfrac{1}{p(U_i)} + a_{ii} \right) U_i' = U_e' \end{cases}.$$

Making the substitutions $a_{ee} = 12$, $a_{ei} = a_{ie} = 10$, $a_{ii} = 5$ and $U_e = U_e^*$, $U_i = U_i^*$, the last equations are recast into

$$\begin{cases} \dfrac{1}{10} \left(8U_e' + \dfrac{1}{2} \right) = U_i' \\ \\ U_e' = U_i' \end{cases},$$

whose solution gives $U_e' = U_i' = 1/4$. In particular, the derivative of Γ at $a_{ee} = 12$ is $\Gamma'(12) = (1/4, 1/4)$.

Returning to the expression of the eigenvalues $\lambda_{k \in \{1,2\}}(a_{ee})$, we see that, in fact, the transversality condition holds:

$$\left. \frac{d\alpha}{da_{ee}} \right|_{a_{ee}=12} \approx -0.1545 < 0. \tag{35}$$

The transversality condition permits us to infer about the stability of the equilibria $(U_e^*(a_{ee}), U_i^*(a_{ee}))$ on both sides of $a_{ee} = 12$ (but sufficiently close to this value). Indeed, given (35), one deduces:

(1) when $a_{ee} > 12$, we have $\alpha(a_{ee}) < 0$ and thus the equilibrium point $(U_e^*(a_{ee}), U_i^*(a_{ee}))$ is asymptotically stable;
(2) if $a_{ee} < 12$, then $\alpha(a_{ee}) > 0$, implying that the equilibrium $(U_e^*(a_{ee}), U_i^*(a_{ee}))$ is unstable.

We are now interested in checking the non-degeneracy condition (H2) for system (32). To do this, we need to compute the parameter γ in the reduced equation (27). We will follow the procedure described in

[29]. After translating the equibrium (U_e^*, U_i^*) to the origin and making a linear invertible change of coordinates to put the linear part in the form of (27), the main idea consists in obtaining the Taylor expansion of order 3 of the vector field (32) around the equilibrium.

Recall that $J(U_e^*(a_{ee}), U_i^*(a_{ee}))$ denotes the Jacobian of the vector field $(h_1(U_e, U_i; a_{ee}), h_2(U_e, U_i))$.
For each a_{ee} sufficiently close to $a_{ee} = 12$, let $v_1(a_{ee})$ (respectively, $w_1(a_{ee})$) denotes the eigenvector of the matrix $J(U_e^*(a_{ee}), U_i^*(a_{ee}))$ (respectively, $J(U_e^*(a_{ee}), U_i^*(a_{ee}))^T$) corresponding to the eigenvalue $\lambda_1(a_{ee})$ (respectively, $\lambda_2(a_{ee})$). The eigenvectors $v_1 := v_1(12)$ and $\overline{v_1} := \overline{v_1(12)}$ corresponding, respectively, to $\lambda_1 = i$ and $\lambda_2 = -i$ read

$$v_1 = \begin{pmatrix} (i+2)/3 \\ 2/3 \end{pmatrix}, \qquad \overline{v_1} = \begin{pmatrix} (2-i)/3 \\ 2/3 \end{pmatrix} \tag{36}$$

(overbar denotes complex conjugate). We note that v_1 and $\overline{v_1}$ are unitary vectors. We also compute the eigenvectors $w_1 := w_1(12)$ and $\overline{w_1} := \overline{w_1(12)}$ of the transposed matrix $J(U_e^*, U_i^*)^T$. Indeed, the vectors

$$w_1 = \begin{pmatrix} 2 \\ i-2 \end{pmatrix}, \qquad \overline{w_1} = \begin{pmatrix} 2 \\ -2-i \end{pmatrix} \tag{37}$$

correspond, respectively, to the eigenvalues $\lambda_1 = i$ and $\lambda_2 = -i$ of $J(U_e^*, U_i^*)^T$.

Calculations in [29] are done with reference to a normal form in coordinates $(z, \overline{z})$, where denoting by $\langle \cdot, \cdot \rangle$ the euclidean inner product, z is a complex variable defined by

$$z = \langle \overline{w_1(a_{ee})}, (U_e, U_i) \rangle. \tag{38}$$

After translating the equilibrium (U_e^*, U_i^*) to the origin, system (32) is converted, in the $(z, \bar{z})$ coordinated, to

$$z' = \lambda_1(a_{ee}) z + g(z, \overline{z}, a_{ee}), \tag{39}$$

where $g = O(|z|^2)$ is the smooth function

$$g(z, \overline{z}, a_{ee}) = \langle \overline{w_1(a_{ee})}, G(z v_1(a_{ee}) + \overline{z}\,\overline{v_1(a_{ee})}, a_{ee}) \rangle, \tag{40}$$

where $G(\mathcal{U}, a_{ee})$ is a smooth vector function whose components are the Taylor expansions in $\mathcal{U} = (\mathcal{U}_e, , \mathcal{U}_i) := (U_e - U_e^*, U_i - U_i^*)$, with at least quadratic terms, of the translated vector field in (32). The utility of the expression for $g(z, \overline{z}, a_{ee})$ in (40) will be more clear in a further step.

At $a_{ee} = 12$, the translated system (32) admits the following expansion around the origin:

$$\mathcal{U}' = J(U_e^*, U_i^*)\mathcal{U} + \underbrace{\frac{1}{2} B(\mathcal{U}, \mathcal{U}) + \frac{1}{6} C(\mathcal{U}, \mathcal{U}, \mathcal{U}) + O(||\mathcal{U}||^4)}_{G(\mathcal{U}, 12)}, \tag{41}$$

where B and C are multilinear functions on the planar vectors $\mathcal{U} = (\mathcal{U}_e, \mathcal{U}_i)$, $\mathcal{V} = (\mathcal{V}_e, \mathcal{V}_i)$ and $\mathcal{W} = (\mathcal{W}_e, \mathcal{W}_i)$ defined, respectively, by

$$B(\mathcal{U}, \mathcal{V}) := \begin{pmatrix} k_{20} & k_{02} & k_{11} \\ l_{20} & l_{02} & l_{11} \end{pmatrix} \begin{pmatrix} \mathcal{U}_e\mathcal{V}_e \\ \mathcal{U}_i\mathcal{V}_i \\ \mathcal{U}\mathcal{V}_{\sigma_{ei}} \end{pmatrix} \tag{42}$$

and

$$C(\mathcal{U}, \mathcal{V}, \mathcal{W}) := \begin{pmatrix} k_{30} & k_{03} & k_{21} & k_{12} \\ l_{30} & l_{03} & l_{21} & l_{12} \end{pmatrix} \begin{pmatrix} \mathcal{U}_e\mathcal{V}_e\mathcal{W}_e \\ \mathcal{U}_i\mathcal{V}_i\mathcal{W}_i \\ \mathcal{U}\mathcal{V}\mathcal{W}_{\sigma_{eei}} \\ \mathcal{U}\mathcal{V}\mathcal{W}_{\sigma_{eii}} \end{pmatrix}. \tag{43}$$

The constants k_{nm} and l_{mn}, with $m, n \in \{0, 1, 2, 3\}$, are the partial derivatives of $h_{1,2}$ at (U_e^*, U_i^*) equilibrium point, which takes place for $a_{ee} = 12$. More specifically, these constants are defined by

$$k_{nm} = \left.\frac{\partial^{n+m} h_1}{\partial^n U_e \partial^m U_i}\right|_{(U_e^*, U_i^*)} \qquad \text{and} \qquad l_{nm} = \left.\frac{\partial^{n+m} h_2}{\partial^n U_e \partial^m U_i}\right|_{(U_e^*, U_i^*)}.$$

On the other hand, the entries of the form $\mathcal{U}\mathcal{V}_{\sigma_{ab}}$ and $\mathcal{U}\mathcal{V}\mathcal{W}_{\sigma_{abc}}$ represent the following respective expansions:

$$\mathcal{U}\mathcal{V}_{\sigma_{ab}} = \sum_{\sigma \in S^2(a,b)} \mathcal{U}_{\sigma(a)}\mathcal{V}_{\sigma(b)}$$

and

$$\mathcal{U}\mathcal{V}\mathcal{W}_{\sigma_{abc}} = \sum_{\sigma \in S^3(a,b,c)} \mathcal{U}_{\sigma(a)}\mathcal{V}_{\sigma(b)}\mathcal{W}_{\sigma(c)},$$

where $S^2(a, b)$ (resp. $S^3(a, b, c)$) denotes the set of permutations of order 2 (resp. 3) on $\{a, b\}$ (resp. $\{a, b, c\}$).

Under the definitions above, the constants k_{nm} and l_{nm} assume the values:

$$\begin{array}{ll} k_{20} = a_{ee}^2 q(U_e^*) = 0 & k_{02} = a_{ei}^2 q(U_e^*) = 0 \\ k_{11} = -a_{ee}a_{ei} q(U_e^*) = 0 & l_{20} = a_{ie}^2 q(U_i^*) = 4\sqrt{5} \\ l_{02} = a_{ii}^2 q(U_i^*) = \sqrt{5} & l_{11} = -a_{ie}a_{ii} q(U_i^*) = -2\sqrt{5} \end{array}$$

and

$$\begin{array}{ll} k_{30} = a_{ee}^3 r(U_e^*) = -216 & k_{03} = -a_{ei}^3 r(U_e^*) = 125 \\ k_{21} = -a_{ee}^2 a_{ei} r(U_e^*) = 180 & k_{12} = a_{ee}a_{ei}^2 r(U_e^*) = -150 \\ l_{30} = a_{ie}^3 r(U_i^*) = -40 & l_{03} = -a_{ii}^3 r(U_i^*) = 5 \\ l_{21} = -a_{ie}^2 a_{ii} r(U_i^*) = 20 & l_{12} = a_{ie}a_{ii}^2 r(U_i^*) = -10 \end{array}$$

with q and r being, respectively, the polynomials

$$q(x) = 2x^3 - 3x^2 + x \qquad \text{and} \qquad r(x) = -6x^4 + 12x^3 - 7x^2 + x$$

(these expressions are obtained from writing the higher order derivatives of $F(x) = 1/(1 + \exp(-x))$ in function of $F(x)$ itself).

The next step is to use the Taylor expansion (41) for the direct computation of the coefficient γ.
Recalling the eigenvectors of both $J(U_e^*, U_i^*)$ and its transpose, obtained in (36) and (37), we compute

$$\langle \overline{w_1}, v_1 \rangle = 4i/3.$$

Thus

$$\overline{w_1} = \begin{pmatrix} 3i/2 \\ 3/4 - 3i/2 \end{pmatrix},$$

is the rescaled form of $\overline{w_1}$ that leads to the normalization of $\langle \overline{w_1}, v_1 \rangle$.

Let

$$g_{nm} = \left. \frac{\partial^{n+m}}{\partial z^n \partial \overline{z}^m} \right|_{z=0},$$

provided $a_{ee} = 12$. Recovering the single equation in (39), the function $g(z, \overline{z}, 12)$ admits a Taylor expansion whose quadratic and cubic coefficients g_{20}, g_{11} and g_{21} are given, respectively, by the formulas:

$$g_{20} = \langle \overline{w_1}, B(v_1, v_1) \rangle, \quad g_{11} = \langle \overline{w_1}, B(v_1, \overline{v_1}) \rangle, \quad g_{21} = \langle \overline{w_1}, C(v_1, v_1, \overline{v_1}) \rangle.$$

Computing such coefficients, one obtains

$$\begin{aligned} &g_{20} = -4\sqrt{5}/3 + 2\sqrt{5}/3i, \quad g_{11} = 2\sqrt{5}/3 + 4\sqrt{5}/3i, \\ &g_{21} = -100/9 - 20/9i. \end{aligned}$$

Finally, the first Lyapunov coefficient γ reads

$$\gamma = \frac{1}{2} \mathrm{Re} \left(i g_{20} g_{11} + g_{21} \right),$$

being equal to $-20/9$, thus negative.

In conclusion, there is a unique and stable limit cycle for $a_{ee} < 12$ (subcritical Hopf bifurcation). Furthermore:

(1) For $a_{ee} < 12$, the equilibrium $(U_e^*(a_{ee}), U_i^*(a_{ee}))$ is unstable and the limit cycle is stable;
(2) For $a_{ee} \geq 12$, the equilibrium $(U_e^*(a_{ee}), U_i^*(a_{ee}))$ is asymptotically stable.

In Figure 13, we represent the numerical iteration (using the software *Mathematica*) of an orbit starting close to the equilibrium point $(U_e^*(11.8), U_i^*(11.8))$, but converging to a limit cycle. Thus, it is suggested that the orbit is repelled from the point $(U_e^*(11.8), U_i^*(11.8))$, while being attracted by a periodic orbit. In particular, we observe that this happens for $a_{ee} < 12$, as analytically deduced above.
On the other hand, Figure 14 represents the asymptotic convergence of the system to the equilibrium $(U_e^*(12.2), U_i^*(12.2))$, scenario that takes place for $a_{ee} > 12$, as expected.

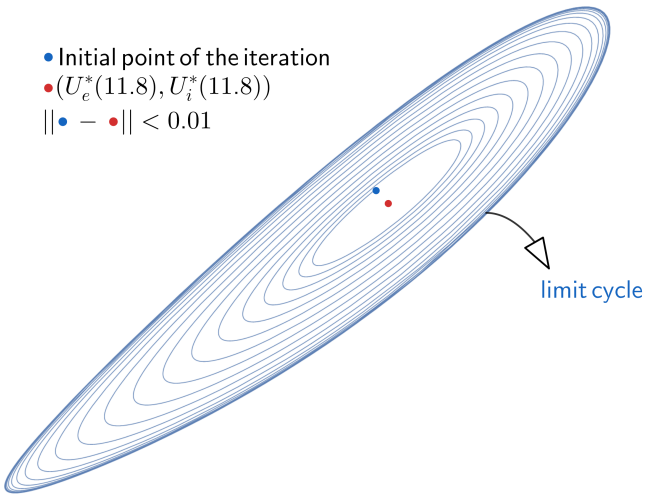

FIGURE 13. Stable limit cycle of system (32), for $a_{ee} = 11.8$, as the ω-limit set of a point (the blue one) in a small neighborhood of $(U_e^*(11.8), U_i^*(11.8))$ (red point). This limit cycle arises via subcritical Hopf bifurcation.

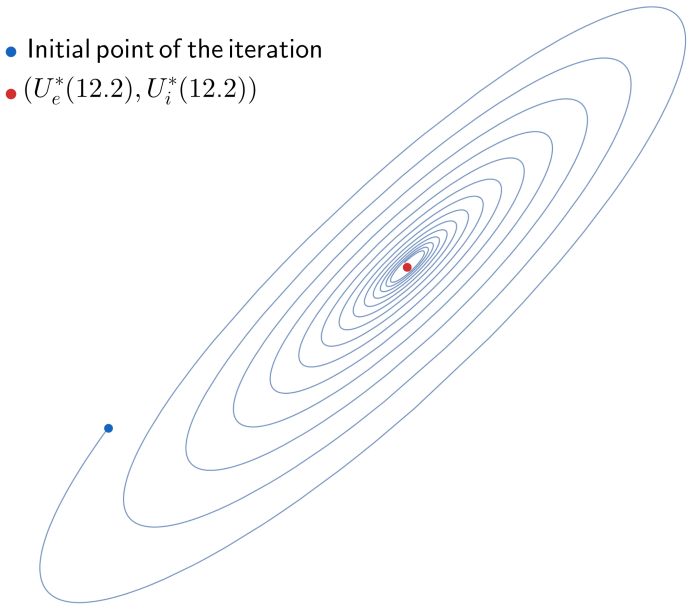

FIGURE 14. Asymptotically stable equilibrium point (stable focus, red point) of system (32), for $a_{ee} = 12.2$, as the ω-limit set of the point $(U_e, U_i) = (0.49, 0.27)$ (blue point).

Apart from checking the existence of oscillations, it is also important to deduce some of its properties, for example, the amplitude and oscillatory frequency. In general, if $\alpha(\mu) \pm i\omega(\mu)$ are the eigenvalues of

the linearization near the bifurcation point, the amplitude is approximately $\sqrt{\alpha(\mu)/\omega(\mu)}$ and the frequency is close to $\omega(\mu)/2\pi$.
In case of system (32), in a small left-neighborhood of $a_{ee} < 12$, the amplitude of the periodic solutions, say $\mathrm{Amp}(a_{ee})$, depends on a_{ee} and using the expression of the real and imaginary parts of the eigenvalues in (33), we find the formula

$$\mathrm{Amp}(a_{ee}) \approx \sqrt{\frac{-2 + a_{ee}p(U_e^*(a_{ee})) - 5p(U_i^*(a_{ee}))}{\sqrt{\rho(a_{ee})}}}.$$

On the other hand, the frequency of the oscillations, $\mathrm{Freq}(a_{ee})$, is given approximately by

$$\mathrm{Freq}(a_{ee}) \approx \frac{1}{4\pi}\sqrt{\rho(a_{ee})},$$

in the same range of a_{ee}. Since $\rho(a_{ee})$ cannot be computed analytically, we use the linear approximmation of $\mathrm{Freq}(a_{ee})$, around $a_{ee} = 12$, given by

$$\mathrm{Freq}(a_{ee})^{\times 10^3}(\mathrm{Hz}) \approx \frac{1}{2\pi} + \frac{\rho'(12)}{16\pi}(a_{ee} - 12) \tag{44}$$

where $\rho'(12)$ can be computed directly using differentiation, in order of a_{ee}, of the function in (34); in this case, one obtains $\rho'(12) \approx 4.71$.
Using that expansion, we record some values of the frequency of the oscillations, for a_{ee} sufficiently close to $a_{ee} = 12$:

a_{ee}	$\mathrm{Freq}(a_{ee})$
11.99	158 Hz
11.95	154 Hz
11.91	151 Hz

TABLE 2. Collection of the oscillatory frequency, for some values of $a_{ee} < 12$, using the approximation in (44).

Numerically (using the *Matcont* package from *Matlab*), we show in Figure 15 how the period of the oscillatory dynamics of system (32) varies with each value of $a_{ee} \in]11.73, 12[$ (values for which the oscillations are sustained). We observe that, as a_{ee} decreases, the period of the generated oscillations increase asymptotically (that is, the angular velocity of the system declines). In particular, this monotonic behaviour is, for example, one of the interisting findings of Wilson et al. in [53], when analysing the oscillatory dynamics of the model in function of a stimulus intensity. Furthermore, the asymptotic behavior of the curve may associate to the approach of the limit cycle to a saddle point, then giving rise to a homoclinic orbit (see Figure 16).
We recall that a homoclinic orbit is an orbit whose ω and α-limit sets are both equal to an equilibrium point, the point that connects the orbit to itself. Symbolically, for every point p in the homoclinic orbit,

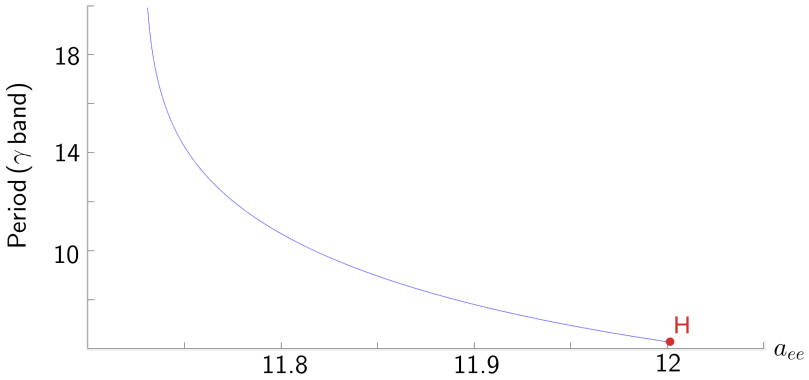

FIGURE 15. Curve giving the period of the oscillations, for each value of $a_{ee} \in]11.73, 12[$. The letter H indicates the Hopf bifurcation point. The period of the oscillations tends to infinity near $a_{ee} = 11.73$.

we have $\alpha(p) = \omega(p) = q$, where q is an equilibrium of the system. Homoclinic orbits are *structurally unstable* [29].

In fact, as depicted in Figure 16, as a_{ee} decreases from the bifurcation value $a_{ee} = 12$, the periodic orbit approaches a saddle-point, predicting a future homoclinic connection.

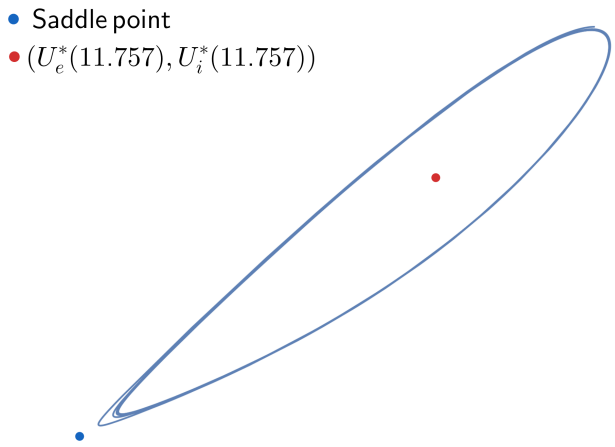

FIGURE 16. Approximation of the limit cycle to a saddle point (blue point) - the angular velocity of the system tends to slow during this dynamics. When the limit cycle meets the saddle point, we find a homoclinic orbit [13, 29].

VI.4. **Bogdanov-Takens bifurcation.** For a *Bogdanov-Takens bifurcation* [29, 42] (codimension two bifurcation) to occur, apart from a double-zero eigenvalue in the linearization, some nondegeneracy conditions must be verified, as what happened for the Hopf bifurcation. We will not pursue this goal here, however, we note that this bifurcation occurs generically in two-parameter families of vector fields. Further evidence is that the bifurcation point occurs where a line of saddle-node bifurcations is met, in a two-parameter space, by a line of Hopf bifurcations. The periodic solution created at the Hopf bifurcation is destroyed at a homoclinic connection.

In [29], Kuznetsov provides a Theorem (Theorem 8.4) that gives sufficient conditions for the existence of a smooth invertible change of coordinates under which a two-parameter system of differential equations is reduced to a normal form exhibiting that bifurcation. In particular, a two-parameter bifurcation diagram is represented, showing the many dynamics occuring as the parameters change.

VII. Bifurcation diagrams

In what follows, we complement the results obtained above (specially in subsection VI.3) with a numerical approach using *bifurcation diagrams*. The software Matcont on MATLAB will support all the analysis.

To illustrate the method, we give special attention to the a_{ee}-system (32). The first diagram below (Figure 17) gives a general overview of how bifurcation points (namely Hopf points and limit points) arise from the variation of the parameter a_{ee}. Some relevant observations result from the direct visualization of that diagram:

- The Hopf point H1 lies close to the limit point LP2. This suggests that a small perturbation on the remaining constants of (32) may promote the coalescence of those points, then (possibly) giving rise to a Bogdanov-Takens bifurcation (BT). As enlightened in subsection VI.4, among other genericity conditions, a double-zero eigenvalue at the linearized vector field is necessary for the generation of that bifurcation. In particular, equilibrium-cycle collision, via *homoclinic bifurcation* [29, 42], would be a consequence.
- The Hopf points H1 and H2 correspond, respectively, to supercritical and subcritical Hopf bifurcations. The software yields the first Lyapunov coefficients for these bifurcations, being approximately equal to $\gamma = -17.23$ and $\gamma = -2.22$, respectively. The collision of a subcritical Hopf point with a supercritical one corresponds to a new bifurcation termed *Generalized Hopf bifurcation* [29]: it is characterized by a vanishing first Lyapunov exponent and includes, among other dynamics, the connection between two distinct branches of periodic orbits.

To be more specific about the dynamics predicted in the above topics, we must extend the diagram of Figure 17 in a way that a new bifurcation parameter is introduced. In particular, we set β_i as the new parameter.
Fixing different values for β_i, we see that both the position and shape of the resulting branches change (see Figure 18). Indeed, higher values of β_i shrink the interval of a_{ee} on which three equilibria take place. On the other hand, when β_i varies from 4.58 to 4.2, the first Hopf bifurcation point H disappears, probably through the coalescence of H1 and LP2 in Figure 17. The scheme of Figure 18 also exhibits a sequence of *neutral saddle* equilibrium points (denoted NS) and the linearization of the system, when evaluated at those points, admits symmetric eigenvalues on the real axis. Such equilibria likely emerge from a Bogdanov-Takens (BT) bifurcation, at a point of double-zero eigenvalue (the eigenvalues move symmetrically from the imaginary to the real axis). Moreover,

the Hopf points $H_{1,\dots,5}$ in Figure 18 are such that the first Lyapunov coefficient γ increases (from negative values) as β_i admits lower values. We then predict the existence of a value for β_i for which γ vanishes.
Lastly, the diagram of Figure 19 completes/confirms our expectations by showing, on the $a_{ee}\beta_i$-plane, the codimension-two bifurcations along the equilibrium trace position. This curve contains two Bogdanov-Takens points (BT1 and BT2) and one Generalized Hopf bifurcation point (GH1). The coordinates of these last points are also identified.

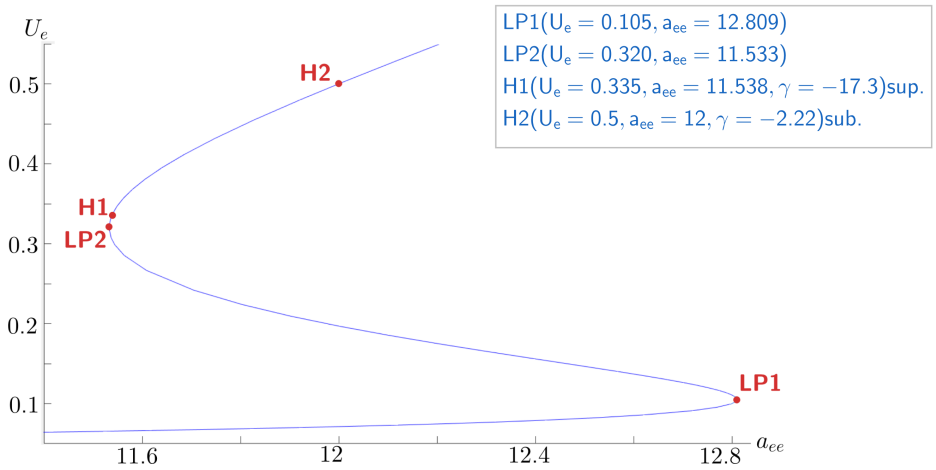

FIGURE 17. Bifurcation on the parameter a_{ee} of system (32). Hopf bifurcation points are indicated by H1 and H2 (H2 is that studied in Example VI.3.1); saddle-node points as LP1 and LP2 (limit points). The constant γ refers to the first Lyapunov coefficient of the resulting Hopf bifurcation and *sup.* and *sub.* are shorts for *supercritical* and *subcritical*, respectively.

VII.1. **Hysteresis.** From a theoretical point of view, the presence of multiple equilibria represents the possibility of certain levels of neuron's activity to be shifted under a sufficient perturbation.
A direct observation of diagram 17 reveals some *jumps* of the equilibria between branches of the bifurcation curve, as the parameter a_{ee} moves forward or backwards. In Figure 20, this effect is suggested by the green (a_{ee} moves backwards) and orange arrows (a_{ee} moves forward). Such phenomenon is known as the *hysteresis* [29, 53] and whose presence is typical in a *cusp bifurcation* [29].
In our example, a unique loop is represented. However, depending on the number of equilibria, more than one loop can be obtained in our model (possibly using other parameters), as properly suggested by

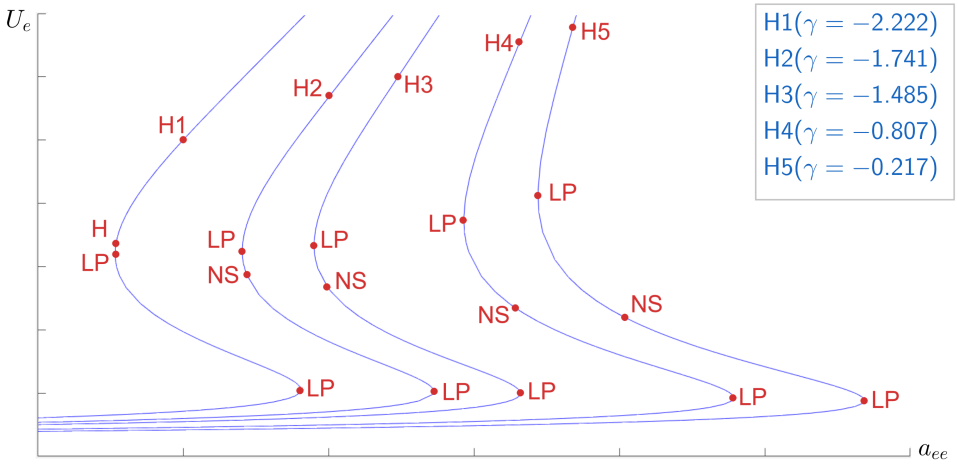

FIGURE 18. Bifurcation curves on the parameter a_{ee} for several values of β_i: from left to right, β_i takes the values of the set $\{4.58, 4.2, 4, 3.6, 3.4\}$, in the descending direction. The points labelled NS refer to *neutral saddle equilibria*, that is, equilibrium points whose eigenvalues are real and symmetric. These points follow the collision of H1 and LP2 from Figure 17, via Bogdanov-Takens bifurcation.

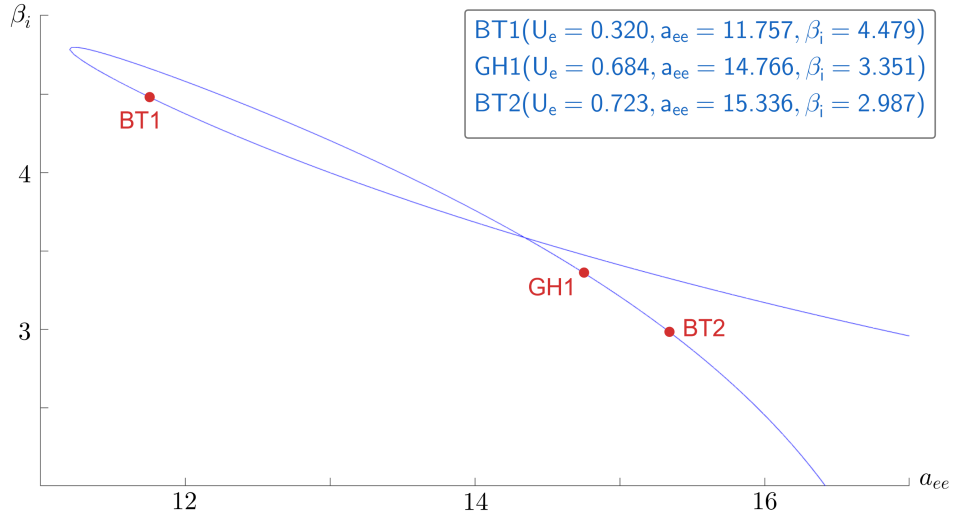

FIGURE 19. Trace position of the equilibrium (U_e^*, U_i^*), in function of the parameters a_{ee} and β_i in system (32): BT1 and BT2 correspond to Bogdanov-Takens points and GH1 to a Generalized Hopf bifurcation point.

Wilson et al. in [53]. The same authors also give physiological interpretation for these loops.

We present below a brief description of what really happens as the parameter a_{ee} changes in each direction during the hysteresis phenomenon:

- As a_{ee} increases from lower values, solutions are attracted to the down-state equilibrium, along a branch of the bifurcation curve; once a point of saddle-node bifurcation is met on the curve, the system switches its asymptotic behaviour to the up-state (this is represented by the orange arrows in Figure 20);
- As a_{ee} decreases from higher values, solutions are attracted to the up-state until it initiates an oscillatory dynamics at a Hopf point, where the up-state changes stability; once the oscillations cease, the solutions are attracted to the unique stable equilibrium point in the phase portrait, the down-state, around which it will remain for further lower values of a_{ee} (this is represented by the green arrows in Figure 20).

Thus, Hopf points are only encountered when the bifurcation parameter a_{ee} decreases.
In Figure 20, the amplitude of the oscillatory dynamics emerging from the Hopf points H1 and H2 is suggested (vertical blue segments). In particular, we observe that, as a_{ee} decreases from $a_{ee} = 12$, the amplitude of the successive limit cycles increase until a homoclinic connection is met, at $a_{ee} \approx 11.73$, as predicted in the subsection VI.3.

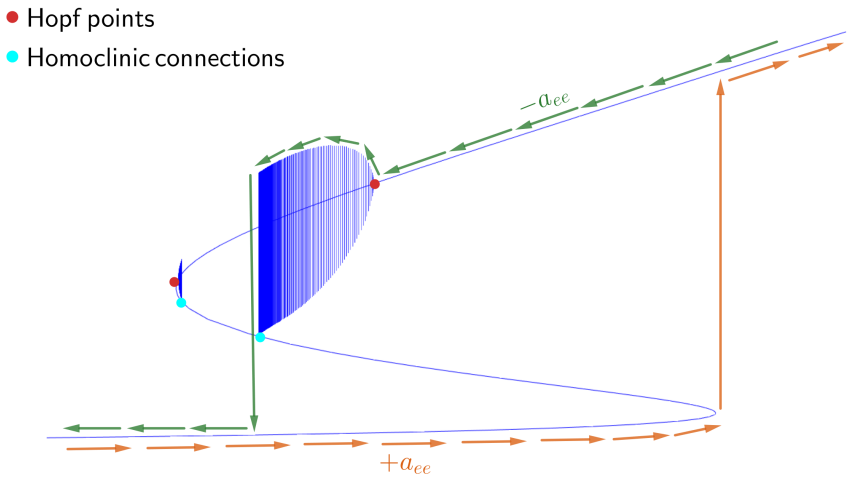

FIGURE 20. Hysteresis phenomenon occuring in system (32), along the curve of Figure 17. The amplitude of the oscillatory dynamics emerging from the Hopf points (in function of a_{ee}) is also suggested (vertical blue segments).

VIII. Emotional Regulation in the context of Psychiatry

In the main context of this work, we do not aim to give a detailed description of how emotion regulation and related mechanisms are processed in the brain. In what follows, we provide a brief explanation of the most important topics regarding the subject, all of them based in previous evidence. In particular, we neglect the experimental environment of this evidence (for example we do not distinguish between animal and human studies).

- According to the American Psychiatric Association (DSM-5) [1], a mental disorder must include a deficit in one of the following domains: cognition, self-regulation and behavior;
- Self-regulation (or emotional regulation) comprises the individual's ability to select certain emotions, process that is also defined by the temporal context and the way the emotions are experienced [19]. In particular, this description suggests that the ability is highly dependent on the environmental experiences and the genetic load, both interacting mutually to shape the way we engage with the exterior;
- Top-down control from cortical regions over subcortical ones has been implicated in the etiology of emotional regulation failure [8, 21];
- As observed by Cisler et al. in [7], emotion regulation and fear are interrelated in the sense that the former can augment or diminish the latter, in dependence of the employed strategy;
- Fear conditioning is a phenomenon of fear acquisition which consists in the association of a neutral stimulus (the to-be conditioned stimulus, CS) with an aversive one (unconditioned stimulus, US), in a way that a conditioned fear response (CR) is created relatively to the former (i.e. the CS alone generates an aversive response). The repeated presentation of the CS, absent of the US, ultimately contributes to the extinction of the fear response, phenomenon termed *fear extinction*. This extinction phenomenon usually occurs under well-defined conditions. In fact, extinction memories are context-dependent, meaning that their expression is more effective in the extinction environmental conditions. Once the conditioned stimulus (CS) is encountered outside the extinction context, the fear response is likely to return, phenomenon known as *fear renewal* [26]. There is an amount of evidence that supports the idea that the connections from the hippocampus to both the medial prefrontal cortex (mPFC for short) and the basolateral amygdala (BLA for short) mediate such phenomenon of fear renewal [40, 41]. Reciprocally, the robust synaptic transmission from the amygdala to the hippocampus has been proposed to be involved in

encoding of both positive and negative emotional arousal [15], then leading to the consolidation of long-term memories;

- Apart from the renewal mechanism, the triad cortex-amygdala-hippocampus (see Figure 21 for anatomical details) and respective mutual connections have as well a specific role in both the consolidation and extinction of fear memories [16, 41, 44]. In this latter phenomenon, the strengthening and depotentiation of synapses have been reported [41]. Furthermore, as observed by Jin et al. in [26] the fear extinction memory does not erase the conditioning memory; instead, a new extinction memory, apt to compete with the fear memory, is created in order to control behavioral reactions [4]. In the long term, the recall of the fear extinction memory has been attributed to the activation of the mPFC and hippocampus in concert [37]. As a matter of fact, the study of the interaction between the prefrontal cortex and the hippocampus is of scientific interest (see, for example, [17]). Additionally, extinction of fear memories requires plasticity inside the mPFC [35];
- Inside the mPFC, two main subregions lie in the origin of the cortical outputs to the amygdala: the prelimbic (PL) and infralimbic (IL) portions [9, 16, 34]. While the first promotes the excitation of the amygdala, during fear expression, the second is involved in mechanisms of fear extinction, in which the excitation of intercalated cells inhibits the amygdala's output [34]. These pathways are depicted in the scheme of Figure 22. A notable result from Corcoran et al. in [9] states that the prelimbic region mediates the expression of fear, but not the formation of aversive memories.

  Conversely, subcortical signals to both the PL and IL originate, among other regions, from the amygdala. In particular, the basolateral amygdala (BLA) is the subarea that mostly innervates the mPFC [24], via glutamatergic afferents, and promotes a cortical response that affects the outcome of fear and extinction learning [5, 49].

VIII.1. **Rhythmic activity of fear mechanisms.** The synchronization of the eletrical activity in the brain leads to the creation of propagated voltage oscillations, which are known as *brain waves* [6]. Such periodic dynamics fall within specific frequency bands - see Table 3 - and are directed to certain physiological functions.
For example, in Figure 15 of a previous section, we observe that the rythmic motion lies in > 30 Hz band for most of the $a_{ee} < 12$ values, which would correspond to the γ range of frequency. More generally, the regulation of γ-oscillations in the Wilson-Cowan model is a recent

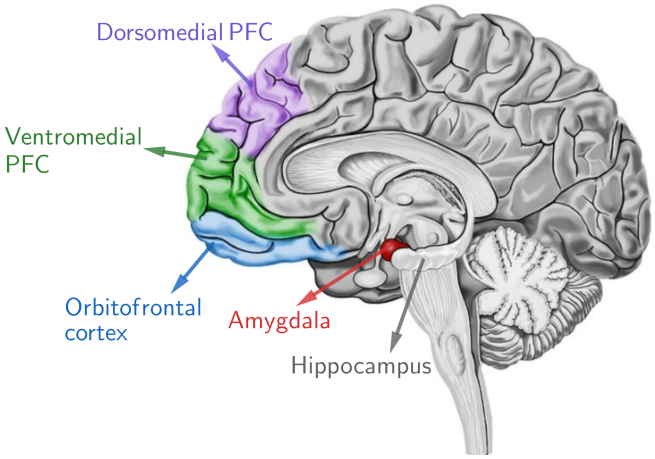

FIGURE 21. Anatomical location of the amygdala, the hippocampus and the subdivisions of the prefrontal cortex (PFC), including the ventromedial PFC, the dorsomedial PFC and the orbitofrontal cortex. The layout of this Figure is based on Figure 3 of [8] (with permission).

object of study. For example, Li et al. study in [30] how the self-connections of the model (which, in our case, would correspond to the constants $a_{ee,ii}$) cooperate to promote the emergence of γ-oscillations and how the oscillatory frequency is regulated.

Wave type	Range of frequency
Delta (δ)	1-4 Hz
Theta (θ)	4-10 Hz
Alpha (α)	8-12 Hz
Beta (β)	12-30 Hz
Gamma (γ)	>30 Hz

TABLE 3. Ranges of frequency of the miscellaneous brain waves.

When compared with higher bands of frequency, slower waves enable the communication between distant areas of the brain.
Previous studies showed that synchronized activity at θ frequency between the amygdala and hippocampus has been implied in the expression of fear conditioning [48]. On other hand, Watanabe et al. demonstrated in [52] that, during the extinction of fear memories, γ-oscillations are not only generated inside mPFC (or more specifically, between the IL and PL) but is also enhanced in the course of the extinction. The correlation of these waves with cognitive functions is well known [32].

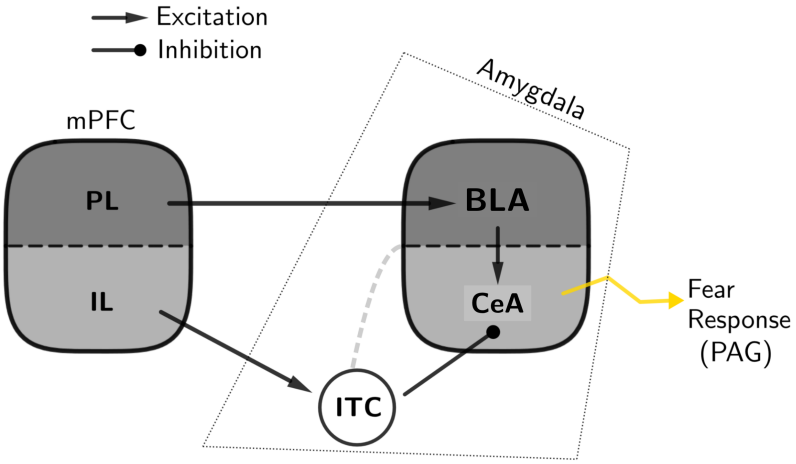

FIGURE 22. Outputs of the infralimbic and prelimbic cortical areas to the amygdala. As suggested, the prelimbic region sends excitatory signals directly to the basolateral amygdala (BLA), which, in turn, excites the central nucleus (CeA) in order to produce a fear response in the phenomenon of fear conditioning. This fear response relies on the intervention, among other regions, of the periaqueductal gray area (PAG). On the other hand, the infralimbic area sends excitatory signals to the intercalated cells of the amygdala (ITC) - anatomically positioned between the BLA and CeA - which, by inhibiting the output from the central nucleus, prevents the expression of fear.

IX. Modelling the mPFC-amygdala-hippocampus triad

Nonlinear modelling of neuronal activity, when combined with bifurcation theory, describes the dynamics of a neural aggregate in function of some pre-defined parameters (connection strengths, for example). The research in this field has taken important steps. For example, Rădulescu et al. [46] perform a numerical bifurcation analysis on a complex circuit involving several areas of human's brain, the cortico-striatal-thalamo-cortical pathway [43]. Incidentally, this circuit is highly implied in the etiology of obsessive-compulsive disorder (OCD) [47], psychopathology that we take care in a further topic, given its particular traits in what concerns failure of emotional regulation.

In what follows, we apply the Wilson-Cowan approach to a circuit between the medial prefrontal cortex (mPFC), the amygdala and the hippocampus, in an attempt to describe how local changes in the connections between these units are apt to propel the dynamics into distinct configurations. In particular, we will be mainly concerned with the oscillatory dynamics of the resulting modified system, under certain conditions, emulating the ideas of the subsection VIII.1.
Since each connection strength must be identified with some proper role regarding emotional regulation and related mechanisms (including fear conditioning and extinction), the effects of our simulations may serve either as a confirmation or a contrast for the results reported in the literature.

IX.1. **The model.** Consider the triad below (the arrows represent arbitrary connections), formed by the three targeted areas in our study: the mPFC (medial prefrontal cortex), the amygdala and the hippocampus.

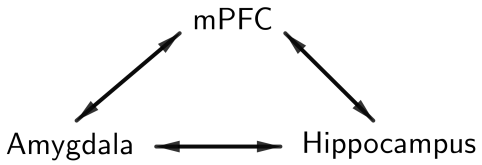

Attributing one variable to each node of this triad, we propose the following modified Wilson-Cowan system:

$$\begin{cases} C' = -C + F(e_{cc}C + e_{ca}A + e_{ch}H - \beta_c) \\ A' = -A + F(\mu_1 C + \mu_2 H - \beta_a) \\ H' = -H + F(e_{hc}C + e_{ha}A - \beta_h) \end{cases}, \tag{45}$$

where the variables C, A and H denote, respectively, the (average) activities of the mPFC, the amygdala and the hippocampus, and F is the function in (7). The constants e_{jk} and i_{jk} are, respectively, the excitatory and the inhibitory connections, while β_j are external inputs (for

our study, these inputs will only serve to set the proper environment for the simulations).
For convenience, both $\mu_{1,2}$ are defined to be $\mu_1 := e_{ac} - i_{ac}$ and $\mu_2 := e_{ah} - i_{ah}$. In Figure 23, we represent the neuronal circuit that is in conformity with the proposed system (45).

In fact, reciprocal connections between any pair of the triad mPFC-amygdala-hippocampus are considered, as it was suggested in the description of the section VIII. In particular, the constants e_{ac} and i_{ac} refer, respectively, to the pre and infralimbic cortical innervations to the amygdala, so that we identify them with the abbreviations PL and IL, as observed in Figure 23.
Furthermore, the constant e_{cc} is the only self-connection in the circuit and the inhibitory pathway i_{ah}, being based on the main result of [31], is aimed to make the circuit less excitable.

As it can be easily noticed, some implicit steps regarding fear conditioning and extinction mechanisms are not taken into account in this framework: for example, instead of integrating the role of the intercalated cells in the inhibition of the amygdala's output, a unique inhibitory connection originating from the mPFC is considered (the infralimbic connection i_{ac}).
We also note that, unlike our initial model, in which we considered two different neuronal populations with opposite effects (either excitatory or inhibitory), in this case, the same population (relative to the same brain region) may have simultaneously both effects relatively to another population. It is the case of the mPFC relatively to the amygdala.

Although, in the analysis that follows, we will mostly be concerned with the oscillatory dynamics of system (45), we note that it may admit a number of equilibria which is significantly variable. In fact, this number can go from a unique equilibrium point to a set of nine equilibria, each of which being such that the first two coordinates, say (C^*, A^*), satisfy

$$\begin{cases} F(e_{cc}C^* + e_{ca}A^* + e_{ch}F(e_{hc}C^* + e_{ha}A^* - \beta_h) - \beta_c) = C^* \\ F(\mu_1 C^* + \mu_2 F(e_{hc}C^* + e_{ha}A^* - \beta_h) - \beta_a) = A^* \end{cases},$$

then uniquely determining the last coordinate H^*, given by

$$H^* = F(e_{hc}C^* + e_{ha}A^* - \beta_h).$$

For our study, it will however be convenient to restrict the number of equilibria, reflecting a simpler asymptotic behavior from the whole system.

IX.2. **Periodic solutions.** In what follows, we look for the conditions concerning the connections e_{jk} and i_{jk} under which system (45) verifies

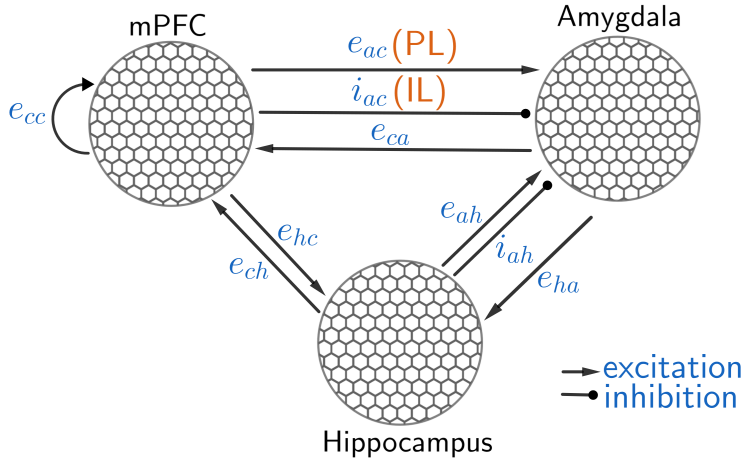

FIGURE 23. Representation of the triad mPFC-amygdala-hippocampus and respective connections, according to the configuration of the system (45). In particular, we refer to the connections e_{ac} and i_{ac} as the *pre* (PL) and *infralimbic connection* (IL), respectively.

the assumptions of the Hopf bifurcation, in the three-dimensional case [29].

Let (C^*, A^*, H^*) be an arbitrary equilibrium point of system (45). System (45) admits the following linearization matrix J around the equilibrium (C^*, A^*, H^*):

$$J(C^*, A^*, H^*) = \begin{pmatrix} e_{cc}p(C^*) - 1 & e_{ca}p(C^*) & e_{ch}p(C^*) \\ \mu_1 p(A^*) & -1 & \mu_2 p(A^*) \\ e_{hc}p(H^*) & e_{ha}p(H^*) & -1 \end{pmatrix}. \tag{46}$$

We set

$$q_J(\lambda) = a_0 + a_1\lambda + a_2\lambda^2 - \lambda^3$$

as the characteristic polynomial of the above matrix $J(C^*, A^*, H^*)$, provided $a_0 = \det J(C^*, A^*, H^*)$, $a_2 = \operatorname{tr} J(C^*, A^*, H^*)$ and

$$a_1 = e_{ca}\mu_1 p(C^*)p(A^*) + 2e_{cc}p(C^*) + e_{ch}e_{hc}p(C^*)p(H^*) + \mu_2 e_{ha}p(A^*)p(H^*) - 3.$$

We first obtain conditions for the constants e_{jk} and i_{jk} under which $\lambda = \alpha + \omega i$ is a root of $q_J(\lambda)$, with $\alpha \in \mathbb{R}$ and $\omega \neq 0$. Taking real and imaginary parts of $q_J(\alpha + \omega i)$, one finds

$$\begin{cases} a_0 + a_1\alpha + a_2\alpha^2 + (3\alpha - a_2)\omega^2 - \alpha^3 = 0 \\ (a_1 + 2a_2\alpha - 3\alpha^2)\omega + \omega^3 = 0 \end{cases}. \tag{47}$$

The solution $\omega \neq 0$ of the second equation in (47) is

$$\omega^2 = -(a_1 + 2a_2\alpha - 3\alpha^2).$$

At an arbitrary Hopf point, we have $\alpha = 0$ and (47) becomes

$$\begin{cases} a_0 - a_2\omega^2 = 0 \\ \omega^2 = -a_1 \end{cases},$$

so the non-hyperbolicity condition for a Hopf bifurcation at (C^*, A^*, H^*) is simply

$$a_0 = -a_1 a_2 \qquad \wedge \qquad a_1 < 0.$$

Let $\mu \in \{e_{cc}, e_{ca}, e_{ch}, \mu_1, \mu_2, e_{hc}, e_{ha}\}$ be a bifurcation parameter of system (45) and $\lambda = \alpha(\mu) + \omega(\mu)i$ an eigenvalue of the Jacobian $J(C^*(\mu), A^*(\mu), H^*(\mu))$. In particular, if $\mu = \mu^*$ is a Hopf bifurcation value, we have $\alpha(\mu^*) = 0$ and $\omega(\mu^*) \neq 0$, with the equilibrium $(C^*(\mu^*), A^*(\mu^*), H^*(\mu^*))$ being simply the previously considered point (C^*, A^*, H^*).
We consider the following hypothesis:

(H1) Non-hyperbolicity condition:
The condition $\alpha(\mu^*) = 0$ and $\omega(\mu^*) \neq 0$ corresponds to

$$\begin{cases} a_1(\mu^*) < 0 \\ a_0(\mu^*) = -a_2(\mu^*)a_1(\mu^*) \end{cases}.$$

(H2) Transversality condition:
Writing $a_j' := \left.\dfrac{da_j}{d\mu}\right|_{\mu=\mu^*}$ (in fact, a_j can be regarded as functions of μ, with the definitions above applied to $(C^*(\mu), A^*(\mu), H^*(\mu))$ equilibrium point) and $\omega' := \left.\dfrac{d\omega}{d\mu}\right|_{\mu=\mu^*}$, it follows from (47) that

$$\begin{cases} 2\omega\omega' = -a_1' - 2a_2\alpha' \\ a_0' + a_1\alpha' + (3\alpha' - a_2')\omega^2 - 2a_2\omega\omega' = 0 \end{cases},$$

at $\mu = \mu^*$, and hence the condition $\left.\dfrac{d\alpha}{d\mu}\right|_{\mu=\mu^*} \neq 0$ corresponds to

$$\left.\frac{d\alpha}{d\mu}\right|_{\mu=\mu^*} = \left.\frac{a_0' + a_1a_2' + a_1'a_2}{2(a_1 - a_2^2)}\right|_{\mu=\mu^*} \neq 0,$$

provided $a_1(\mu^*) \neq a_2^2(\mu^*)$.

(H3) Nondegeneracy condition:
The first Lyapunov coefficient of the restricted equation to the center manifold of the μ^*-system (45) is nonzero (see [29] for more details). The existence of this manifold is ensured by the non-hyperbolicity condition above.

We additionally assume that

(H4) Existence of a stable manifold:
At $\mu = \mu^*$, a stable manifold exists if the third eigenvalue of the matrix $J(C^*, A^*, H^*)$ is negative. In particular, this last condition takes place if

$$\operatorname{tr} J(C^*, A^*, H^*) = a_2(\mu^*) < 0.$$

Under (H1-4), the μ-system (45) is locally topologically equivalent to the normal form

$$\begin{cases} z' = (\eta + i)z \pm z\,|z|^2 \\ v' = -v \end{cases}, \tag{48}$$

with $\eta \equiv \eta(\mu)$. We observe that, in this last system, the variables z and v are uncoupled, with z giving the dynamics on the parameter-dependent center manifold, for small $|\mu - \mu^*|$, and v giving the direction of the stable manifold.

IX.3. **Simulation.** In the further numerical simulation, different connection strengths will be set for the parameter μ. Once μ is chosen, the remaining constants on system (45) will be set according to the following assumptions:
(A1) All the connection strengths $\{e_{jk}, i_{jk}\}$ lie in the interval $[0, 10]$ (this way, we impose a limitation of these constants);
(A2) $\mu_2 > 0$ and the interconnections between the amygdala and the hippocampus are stronger than those between the hippocampus and the cortex: $e_{ah}, e_{ha} > e_{hc}, e_{ch}$;
(A3) The connection strength e_{ah} (resp. e_{ch}) is lower than e_{ha} (resp. e_{hc});
(A4) $|\mu_1| = e_{ca}$.

In fact, (A1-4) are assumptions about the dendritic density inside the mPFC-amygdala-hippocampus triad and the significance of intersecting roles of certain connection strenghts, in a way that the unperturbed framework will be more compatible with the phenomenon of fear extinction (for example, we assume that the connection e_{ah} - resp. e_{ch} - has a more relevant role in the formation/recovery of fear memories, when compared with the pathway e_{ha} - resp. e_{hc} -, so that it is accepted that $e_{ah} < e_{ha}$ - resp. $e_{ch} < e_{hc}$); on the other hand, it is assumed that the strength of the connection e_{ca} determines the magnitude of the sum of the pre and infralimbic outputs, so that $|\mu_1| = e_{ca}$.

Example IX.3.1. Consider the set of connection strengths

$$E := \{e_{ch} = 3, e_{ah} = 6, i_{ah} = 2, e_{hc} = 5, e_{ha} = 7\}, \tag{49}$$

whose values clearly satisfy (A1-4).
For now, the constants e_{cc} and $\mu_1 = e_{ac} - i_{ac} < 0$ are left as parameters.

In particular, for our purposes, we set $e_{ac} = 0$, so that $\mu_1 = -i_{ac}$. Two reasons stand for the choice of those parameters:

(1) Our study will be based fundamentally on the effects of the infralimbic output i_{ac} on the dynamics of the whole triad;
(2) The self-connection e_{cc}, being functionally separated from the miscellaneous connections, is adequate for the pairing with i_{ac}, as a bifurcation parameter.

Substituting the above fixed connection strengths in system (45) and bearing in mind the assumption (A4) above, we obtain the following equations

$$\left\{ \begin{array}{l} C' = -C + F(e_{cc}C + i_{ac}A + 3H - \beta_c) \\ A' = -A + F(-i_{ac}C + 4H - \beta_a) \\ H' = -H + F(5C + 7A - \beta_h) \end{array} \right. . \tag{50}$$

The constants $\beta_{c,a,h}$ are chosen so that

$$(C^*, A^*, H^*) = (0.8, 0.2, 0.5)$$

is an equilibrium of (50) at $e_{cc} = e_{cc}^*$ and $i_{ac} = i_{ac}^*$, values for which the matrix $J(0.8, 0.2, 0.5)$ has a pair of imaginary eigenvalues.
We observe above that $C^* > A^*$, i.e. we are assuming that the cortical activity exceeds the amygdalar activity, as expected in a phenomenon of fear extinction (recall the stipulated hypothesis that the unperturbed framework agrees with the conditions of the fear extinction phenomenon).

According to our previous construction, the Hopf bifurcation curve at $(C^*, A^*, H^*) = (0.8, 0.2, 0.5)$ is defined by the condition

$$\left\{ \begin{array}{l} \mathcal{C} : a_0 + a_1 a_2 = \det J(0.8, 0.2, 0.5) + a_1 \mathrm{tr}\, J(0.8, 0.2, 0.5) = 0 \\ \mathcal{S} : a_1 < 0 \end{array} \right. , \tag{51}$$

with

$$a_1 = -1.28 + 0.32 e_{cc} - 0.0256 i_{ac}^2$$

and

$$J(0.8, 0.2, 0.5) = \begin{pmatrix} 0.16e_{cc} - 1 & 0.16i_{ac} & 0.48 \\ -0.16i_{ac} & -1 & 0.64 \\ 1.25 & 1.75 & -1 \end{pmatrix}, \tag{52}$$

both depending on the pre-defined parameters i_{ac} and e_{cc}.
Only one of the branches of the curve $\mathcal{C}$ in (51) intersects the half-plane $\mathcal{S}$. In particular, that branch can be expressed explicitely as $e_{cc} = \zeta(i_{ac})$ (i.e. as a function of the parameter i_{ac}). The intersection $\mathcal{C} \cap \mathcal{S}$ is represented in Figure 24. This intersection is such that the parameter e_{cc} ranges, approximately, between 5.81 and 12.5, while i_{ac} lies above 4.752. The set $\mathcal{S} \cap \mathcal{C}$ then represents the possible bifurcation values for a Hopf bifurcation to occur in the (e_{cc}, i_{ac})-system (50); the

star notation for those points is used from now on.

For each $i^*_{ac} > 4.752$, the Jacobian matrix in (52) has eigenvalues

$$\begin{array}{l} \lambda_{1,2} = \pm\sqrt{1.28 - 0.32\zeta(i^*_{ac}) + 0.0256(i^*_{ac})^2}\, i, \\ \lambda_3 = -3 + 0.16\zeta(i^*_{ac}) \end{array} . \tag{53}$$

In particular, $\lambda_3 \in \mathbb{R}$ is always negative for any $i^*_{ac} > 4.752$.
We observe that the assumptions (H1) and (H4) in subsection IX.2 are indeed verified, in this specific case (the first by construction and the second by condition (53)). The transversality condition (H2), as well as the non-degeneracy condition (H3), although more complex to deduce analytically (we could use the Implicit Function Theorem for the effect), hold in our simulations.

In Figure 24, we also represent the set of bifurcation values $(e^*_{cc}, i^*_{ac}) \in \mathcal{C} \cap \mathcal{S}$, say T, that will serve our further simulations. This set is defined by

$$T := \{(e^*_{cc}, i^*_{ac}) \in \mathcal{C} \cap \mathcal{S} : i^*_{ac} = 5.5 + h/2, h \in \{0, 1, ..., 9\}\}\,. \tag{54}$$

Thus, the set T comprises some Hopf bifurcation values of the (e_{cc}, i_{ac})-system (50) separated, in the i_{ac}-direction, by a step of size $1/2$. Moreover, T is well-defined, since each component of a pair $(e^*_{cc}, i^*_{ac}) \in T$ is in conformity with the proposed assumption (A1) above (which can be easily verified deducing the expression for the function ζ).
Let T^1 and T^2 be, respectively, the set of first and second components of the elements of T.

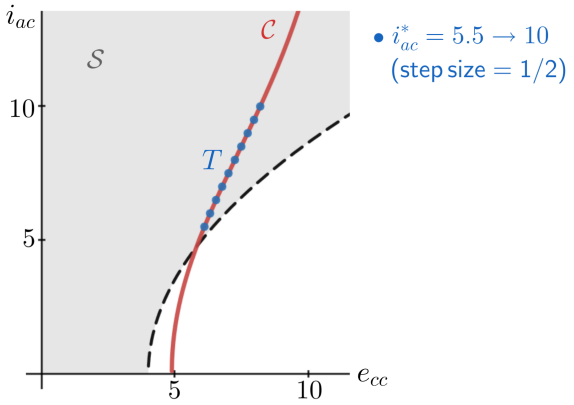

FIGURE 24. Hopf bifurcation curve at $(C^*, A^*, H^*) = (0.8, 0.2, 0.5)$, being the intersection of the curve $\mathcal{C}$ with the half-plane $\mathcal{S}$. The blue points are the simulation points in the set $T \subseteq \mathcal{C} \cap \mathcal{S}$.

For every admissible pair $(e^*_{cc}, i^*_{ac}) \in T$, the point $(C^*, A^*, H^*) = (0.8, 0.2, 0.5)$ is the unique equilibrium of the (e^*_{cc}, i^*_{ac})-system (50) and it is asymptotically stable.

IX.3.1. *Bifurcation of periodic solutions.* In order to infer about the impact of perturbing certain connection strengths on the oscillatory activity, we consider the following system, for some pair $(e^*_{cc}, i^*_{ac}) = (\zeta(i^*_{ac}), i^*_{ac}) \in T$,

$$\begin{cases} C' = -C + F((e^*_{cc} + \epsilon_1)C + i^*_{ac}A + (3+\epsilon_2)H - \beta^*_c) \\ A' = -A + F(-i^*_{ac}C + (4+\epsilon_3)H - \beta^*_a) \\ H' = -H + F((5+\epsilon_4)C + (7+\epsilon_5)A - \beta^*_h) \end{cases}, \tag{55}$$

provided

$$\begin{aligned} \beta^*_c &= 0.8e^*_{cc} + 0.2i^*_{ac} + 1.5 - F^{-1}(0.8), \\ \beta^*_a &= -0.8i^*_{ac} + 2 - F^{-1}(0.2), \\ \beta^*_h &= 5.4 - F^{-1}(0.5). \end{aligned} \tag{56}$$

We observe that $(C^*, A^*, H^*) = (0.8, 0.2, 0.5)$ is an equilibrium when all the ϵ_j vanish.

When displaced from zero, each ϵ_j is designed to perturb the corresponding connection strength of the (e^*_{cc}, i^*_{ac})-system (50) (ϵ_1 perturbs $e_{cc} = e^*_{cc}$, ϵ_2 perturbs $e_{ch} = 3$, and so forth). This perturbation will be performed individually, in the sense that if we take ϵ_j to be a bifurcation parameter of system (55), for some j, then all the remaining ϵ_k, with $k \neq j$, are set to be zero.
More specifically, we want that perturbation to be such that an oscillatory dynamics in the (e^*_{cc}, i^*_{ac})-system (50), which arise via Hopf bifurcation, exists. As a consequence of this, the ϵ_j do not necessarily have all a common sign. In fact, depending on whether the Hopf bifurcation is supercritical or subcritical on each connection strength of (50), we may either take $\epsilon_j > 0$ or $\epsilon_j < 0$, respectively. For example, fixing some $(e^*_{cc}, i^*_{ac}) \in T$, the e_{ch}-system

$$\begin{cases} C' = -C + F(e^*_{cc}C + i^*_{ac}A + e_{ch}H - \beta^*_c) \\ A' = -A + F(-i^*_{ac}C + 4H - \beta^*_a) \\ H' = -H + F(5C + 7A - \beta^*_h) \end{cases}$$

admits a supercritical Hopf bifurcation at $e_{ch} = 3$, so that ϵ_2 in system (55) must be positive in order to guarantee the existence of periodic solutions in a neighborhood of $e_{ch} = 3$.

The analysis that will follow is based on two main goals:

(1) For each $(e^*_{cc}, i^*_{ac}) \in T$, we investigate the impact of perturbing (in the direction that promotes the desired dynamics) each connection strength of

$$\{e_{cc} = e^*_{cc}, e_{ch} = 3, \mu_2 = 4, e_{hc} = 5, e_{ha} = 7\}$$

on the period/amplitude of the oscillations (goal 1);

(2) In our simulations, the oscillations disappear with the progressive reduction of the amplitude and the asymptotic behaviour of the system switches to the convergence to some equilibrium point. For further discussion, we will be interested in both the extension of this oscillatory motion and the coordinates of the post-oscillatory equilibrium (goal 2). We use the star notation for those values of ϵ_i until which the oscillations are sustained.

Once the results of these goals are achieved, they will lack a suitable contextualization in the light of the main subject of this text, which is the communication between neuronal areas. The following topic suggests how we may regard the results in order to create the proper environment for discussion.

IX.3.2. *How the oscillatory dynamics and surrounding behaviours will be interpreted in this context?* Miscellaneous mechanisms can underlie the generation of brain waves. As noted by Buskila et al. in [6], changes in neuronal excitability is one of those mechanisms, specially when they result from alterations in the extracellular concentrations of ions. By *neuronal excitability* it is meant the neuron's susceptibility to generate action potentials, preferentially in response to a small stimulus.
As the connectivity between two neuronal populations is enhanced, the response of the targeted cluster to the eletrical stimulus coming from other population is improved as well. In this sense, it is reasonable to assume here that perturbations on the functional connection strength between two neural populations is conducive to the generation of a rhythmic eletrical activity. Conversely, neural oscillations facilitate synaptic plasticity and interregional communication, as observed by Totty et al. in [50]. Thus, while a (small) perturbation on a connection strength triggers an oscillatory activity, this dynamics extends the level of connectivity, in a way that a stronger/weaker connection is obtained (see the scheme of Figure 25). In particular, the activity of the connected clusters may suffer variations after this process.

In order to integrate the above ideas in our modified model, we consider the scheme of Figure 26 which mainly depicts the enhancement (the weakening would be totally analogous) of a given connection strength (denoted by a) and the dynamics that are observed during the progress. Three steps of this evolution are considered:

(1) In step A, two brain regions (brain region I, BR1, and brain region II, BR2) interact with a certain level of connectivity (this connection corresponds to a parameter of the model), in a way that the neuronal model is locally convergent to a resting state

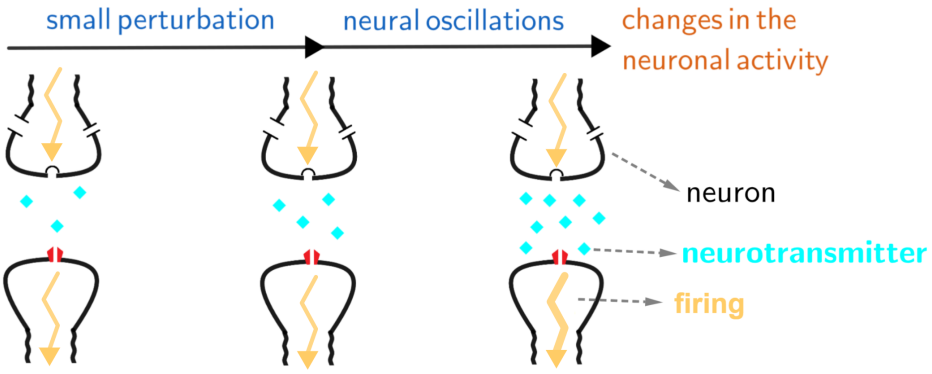

FIGURE 25. Scheme proposing a mechanism of interregional strenghtening: a small perturbation promotes a low-grade enhancement of the connectivity between neurons; this effect, in turn, facilitates the generation of rhythmic activities, which lead to a optimal strengthening of that connectivity (also reflecting changes in the neuronal firing, represented by yellow arrows whose thickness alludes to the rate of spiking). It should be noted that the scheme does not exhibit other mechanisms of neuronal strengthening, apart from the increase of neurotransmitters in the synapse. Another example concerns the quantity of membrane receptors (see [28]).

of activity (corresponding to an asymptotically stable equilibrium point). In particular, at this resting state, the activity of the brain region I is denoted $V_A(\text{BR1})$, while the activity of the brain region II is denoted $V_A(\text{BR2})$. Furhermore, in our model, the strength of the connection corresponds, at this stage, to a Hopf bifurcation value;

(2) In step B, after a perturbation on a connection strength between those regions is performed (we can suppose that it is enhanced), the brain region II becomes more suscetible to the stimuli from region I (and vice-versa) and an oscillatory dynamics is initiated: the eletrical activities of the brain regions I and II oscillate under well-defined amplitude and oscillatory frequency (i.e., the amplitude/frequency do not vary in long-term for each value of the perturbed connection). In the phase portrait of the neuronal model, this scenario corresponds to the emergence of a stable limit cycle (only stable closed orbits are physically observable). During this oscillatory stage, the branch of the equilibrium point is unstable, i.e. the system locally favors the convergence to rhythmic activities, rather than a resting state. Only this way may we give meaning to the presence of oscillations;

(3) The periodic solutions are sustained until the connection achieves its optimal strengthening/weakening, point from which the original asymptotic behaviour of step A is recovered. Since the past oscillatory dynamics altered the interregional communication, it is expected that the new resting state encodes different levels of neural activity, when in comparison with that of step A (in our diagram, the activity of the brain region I increased, while the activity of the brain region II decreased, i.e. $V_C(BR1) > V_A(BR1)$ and $V_C(BR2) < V_A(BR2)$). This last situation is depicted in the step C.

Recalling the construction from subsection IX.2 and the setups in Example IX.3.1, the steps A, B and C are quali/quantitatively read as follows:

(1) The equilibrium point of step A is the point $(C^*, A^*, H^*) = (0.8, 0.2, 0.5)$ and the connection strength a between the neuronal regions, being unperturbed, satisfies $\epsilon_i = 0$ in system (55);
(2) The oscillatory dynamics of step B emerges via Hopf bifurcation, as some ϵ_i is displaced from zero - for further discussion, we will be concerned with the main features of those periodic solutions (amplitude, frequency, etc.);
(3) The oscillations are sustained until $\epsilon_i = \epsilon_i^*$ and the levels of activity encoded by the resting state in the step C are, at this point, unknown but to be identified in the presence of the simulation diagrams. It will turn out that this resting state is actually a new Hopf point of the equilibrium branch.

In our simulations, the assumptions regarding the equilibrium/limit cycle stability (as in Figure 26) apply.

In conclusion, the above approach explains some mechanisms of neuronal plasticity in function of the encountered dynamics in the circuit. In practice, only the inverse relation is performed, that is, one perturbs a connection strength in order to observe the dynamical impact. We enunciate below some additional conditions and ideas to follow while establishing the bridge between the modified model and the environmental contextualization, at the same time, describing some weakenesses of our framework:

- The frequency of the oscillations, as a function of the admissible values (those that sustain the rhythmic effect) of a certain connection strength must be a well-behaved function (in this case, a funtion which does not vary between distant ranges of frequency). In our simulations, this property is observed. Furthermore, for interpretative effects, it is not viable to implicate a numerical oscillatory frequency, for some level of connectivity,

in a mechanism that takes place *in vivo* (this is due to the equal time scales attributed to the variables). Instead, we may refer to transitions between ranges of frequency;

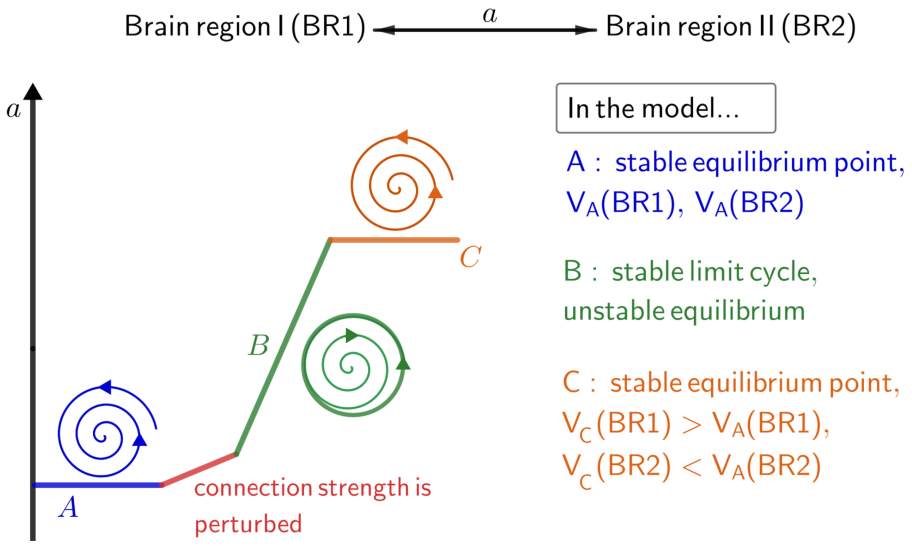

FIGURE 26. Enhancement of the connectivity between two brain regions, the brain region I (BR1) and the brain region II (BR2). This process is split into three main stages, numerated A, B and C. Each stage represents a specific dynamics in the phase portrait of the modified model. Furthermore, we use the abbreviations V for the activities of the brain regions in each stage.

- In order to integrate the dependence of the interregional strengthening/weakening relatively to the passage of time (as a consequence of the oscillatory activity), we assume that each connection strength is, in fact, a function of time, but occuring in a time scale that is much smaller than that inherent to the neuronal communication. Since, in the course of fear conditioning/extinction, we mostly care about long-term strengthening, the above assumption yields a suitable approximation to the desired perspective. Formally this translates into adopting the system (which is an extension of (55))

$$\begin{cases} C' = -C + F((e^*_{cc} + \epsilon_1)C + i^*_{ac}A + (e_{ch} + \epsilon_2)H - \beta^*_c) \\ A' = -A + F(-i^*_{ac}C + (\mu_2 + \epsilon_3)H - \beta^*_a) \\ H' = -H + F((e_{hc} + \epsilon_4)C + (e_{ha} + \epsilon_5)A - \beta^*_h) \\ \tau_i \epsilon_i' = g(\epsilon_i, C, A, H) \end{cases},$$

for sufficiently high τ_i (the constants $\beta^*_{c,a,h}$ were defined in (56)) and some continuous function g.

As in previous sections, the diagrams supporting the simulations were obtained using the software Matcont on MATLAB. Some of the obtained curves may contain irrelevant information in our biological context (for example, some connection strengths may change sign during the bifurcation analysis). We will mantain this information for a mathematical description.

IX.3.3. *Simulation diagrams.*

$$\star \textbf{ Constant } e_{cc} = e^*_{cc}$$

We first investigate what happens as we perturb $e_{cc} = e^*_{cc} = \zeta(i^*_{ac})$ in system (50), for each $i^*_{ac} \in T^2$. Recall that ϵ_1 is defined to be magnitude of the pertubation on e^*_{cc} (the remaining ϵ_j, with $j \neq 1$, are set to be zero), as suggested in system (55). In this case, $\epsilon_1 = 0$ is a Hopf bifurcation value and stable oscillations exist for $\epsilon_1 > 0$, the bifurcation being then supercritical.

In the simulations of Figure 28, i^*_{ac} takes the values in the set

$$T^*_2 := \{5.5, 6.5, 7.5, 8.5, 9.5\} \subseteq T_2$$

and each row of diagrams corresponds to one of these values, in the same ascending order (i.e. the first row corresponds to $i^*_{ac} = 5.5$, the second to $i^*_{ac} = 6.5$ and so forth).
Each diagram represents the equilibrium trace position, relatively to the variable C (left diagram) or the variable A (right diagram), in a neighborhood of $\epsilon_1 = 0$, with ϵ_1 the bifurcation parameter of the system (55): this dependence is written $(C^*(\epsilon_1), A^*(\epsilon_1), H^*(\epsilon_1))$. In particular, $\epsilon_1 = 0$ is (by our previous construction) a Hopf bifurcation value of that system - it corresponds to the Hopf point $H_1(\epsilon_1 = 0, C = 0.8, A = 0.2, H = 0.5)$ in the diagrams - and a stable oscillatory dynamics (s.l.c. in the diagrams) emerges from the equilibrium $(C^*, A^*, H^*) = (0.8, 0.2, 0.5)$ via Hopf bifurcation for $\epsilon_1 > 0$. The amplitude and extension of the oscillations are as well identified in the diagrams.

For each $i^*_{ac} \in T^*_2$ and as ϵ_1 increases from zero, the produced oscillations (originally emerging from the Hopf point H_1) cease in a new Hopf point[7], in a way that the equilibrium $(C^*(\epsilon_1), A^*(\epsilon_1), H^*(\epsilon_1))$ switches stability, becoming asymptotically stable (a.s. in the diagrams). We record in Table 4 the coordinates of the new Hopf points $(H_{i\in\{2,\dots,11\}})$[8], as follows:

$$H_{i,i+1}(\epsilon_1 = \epsilon^*_1, C = C^*(\epsilon^*_1), A = A^*(\epsilon^*_1), H = H^*(\epsilon^*_1)), \;\; i \geq 2$$

(the branch of limit cycles is defined in the interval $\epsilon_1 \in]0, \epsilon^*_1[$).
In conclusion:

- For $\epsilon_1 \leq 0$, but sufficiently close to zero, the equilibrium point $(C^*(\epsilon_1), A^*(\epsilon_1), H^*(\epsilon_1))$ is asymptotically stable (a.s.);

[7]This point is associated to a subcritical Hopf bifurcation.

[8]For each $i \geq 2$, the Hopf points H_i and H_{i+1} only differ on the dependent variable of the respective diagram. Since in Table 4 we collect the coordinates, relative to all variables, of each H_i, we do not make distinction between Hopf points of the form H_i and H_{i+1}, $i \geq 2$.

- For $\epsilon_1 > 0$ between the two Hopf points H_1 and $H_{i>1}$, the equilibrium $(C^*(\epsilon_1), A^*(\epsilon_1), H^*(\epsilon_1))$ is unstable (u.), while the limit cycle is stable (s.l.c.);
- For further values of $\epsilon_1 > 0$ (outside the gap between H_1 and $H_{i>1}$), the equilibrium point $(C^*(\epsilon_1), A^*(\epsilon_1), H^*(\epsilon_1))$ recovers its asymptotic stability.

i^*_{ac}	$H_{i,i+1}$	ϵ_1^*	$C^*(\epsilon_1^*)$	$A^*(\epsilon_1^*)$	$H^*(\epsilon_1^*)$
5.5	$H_{2,3}$	0.654	0.803	0.150	0.417
6.5	$H_{4,5}$	0.809	0.807	0.142	0.408
7.5	$H_{6,7}$	1.032	0.813	0.129	0.394
8.5	$H_{8,9}$	1.293	0.819	0.116	0.379
9.5	$H_{10,11}$	1.570	0.825	0.103	0.365

TABLE 4. Coordinates (relative to all variables) of the second Hopf points in Figure 28, for each $i^*_{ac} \in T_2^*$.

In Figure 27, each blue curve associates to a specific $i^*_{ac} \in T_2$ and displays the variation of the period of the oscillations as $\epsilon_1 > 0$ increases, while suggesting how *extent* the oscillatory dynamics is. In particular, the descending sequence of curves is obtained as the infralimbic pathway i^*_{ac} goes increasingly from 5.5 to 10, with a step size equal to 1/2.

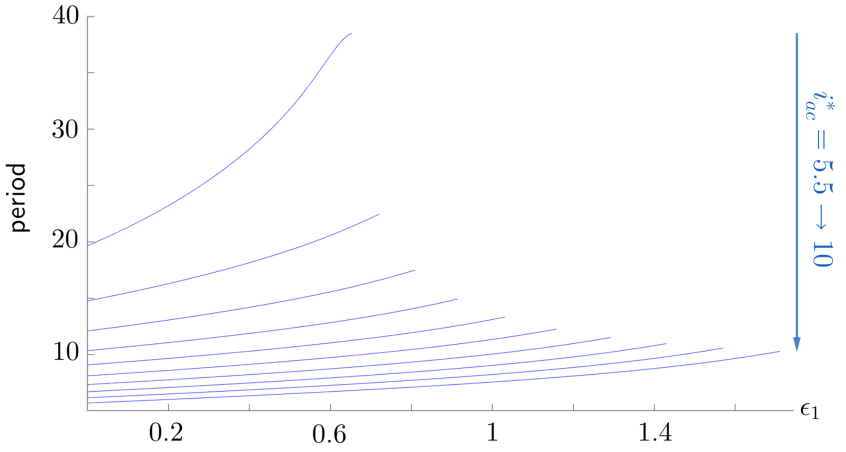

FIGURE 27. Period of the oscillations of system (55) in function of $\epsilon_1 > 0$. Each blue curve represents a specific value of $i^*_{ac} \in T_2$, according to the indicated direction.

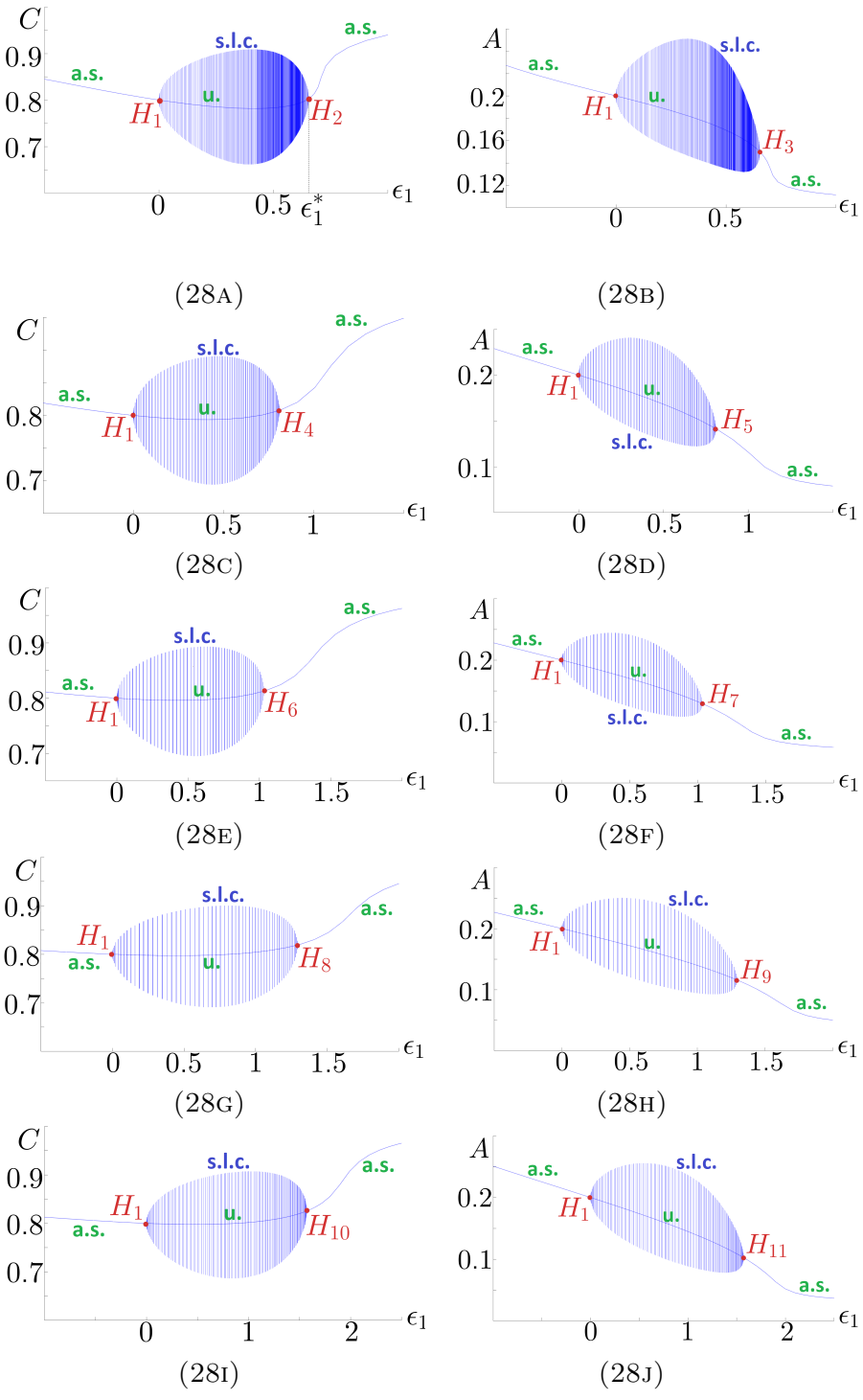

FIGURE 28. Asymptotic behavior of the ϵ_1-system (55), for each $i_{ac}^* \in T_2^*$, relatively to the variables C and A. The coordinates (with respect to all variables) of H_i, are identified in Table 4. The blue curves are functions of ϵ_1, describing the variation of the first two coordinates of the equilibrium point $(C^*(\epsilon_1), A^*(\epsilon_1), H^*(\epsilon_1))$. This equilibrium is unstable (u.) between H_1 and H_i and asymptotically stable (a.s.) outside that gap. Vertical segments are the diameters of the successive stable limit cycles (s.l.c.).

⋆ Constant $e_{ch} = 3$

Perturbing $e_{ch} = 3$ in system (50) is, in this case, equivalent to taking ϵ_2 as a parameter in system (55) (while $\epsilon_j = 0$, for $j \neq 2$). The results are very similar to those for $e_{cc} = e^*_{cc}$. For example, $\epsilon_2 = 0$ is a Hopf bifurcation value, a stable limit cycle arises for $\epsilon_2 > 0$ and we have a supercritical Hopf bifurcation.

The diagrams of Figure 30 have the same background as those in the previous analysis for $e_{cc} = e^*_{cc}$, also showing similar results, so that an analogous description applies.
In particular, the coordinates $(\epsilon^*_2, C^*(\epsilon^*_2), A^*(\epsilon^*_2), H^*(\epsilon^*_2))$ of the Hopf points $H_{i>1}$ are identified in the Table 5.

i^*_{ac}	$H_{i,i+1}$	ϵ^*_2	$C^*(\epsilon^*_2)$	$A^*(\epsilon^*_2)$	$H^*(\epsilon^*_2)$
5.5	$H_{2,3}$	1.285	0.807	0.148	0.418
6.5	$H_{4,5}$	1.766	0.815	0.134	0.404
7.5	$H_{6,7}$	2.447	0.825	0.117	0.388
8.5	$H_{8,9}$	3.237	0.834	0.100	0.372
9.5	$H_{10,11}$	4.078	0.844	0.086	0.359

TABLE 5. Coordinates of the second Hopf points in Figure 30, for each $i^*_{ac} \in T^*_2$.

In Figure 29, we represent, for each $i^*_{ac} \in T_2$, the extension of the oscillatory motion and the variation in their frequency as $\epsilon_2 > 0$ increases. The descending order of the blue curves coincides with the ascending value of $h = 0, ..., 9$ in $i^*_{ac} = 5.5 + h/2$ (analogously to Figure 27).

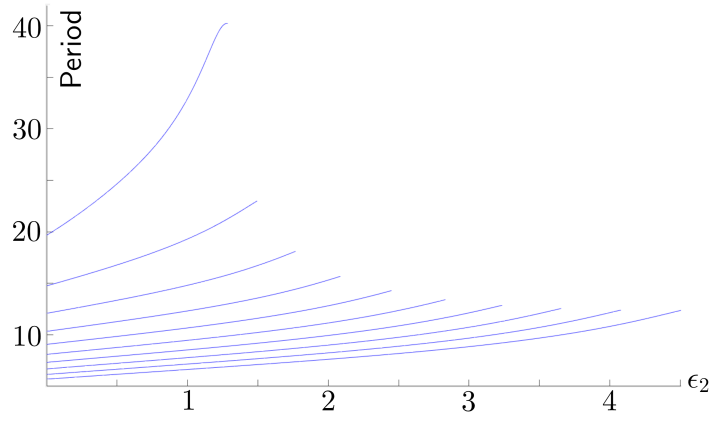

FIGURE 29. Period of the oscillations of system (55) in function of $\epsilon_2 > 0$. Each blue curve represents a specific value of $i^*_{ac} \in T_2$.

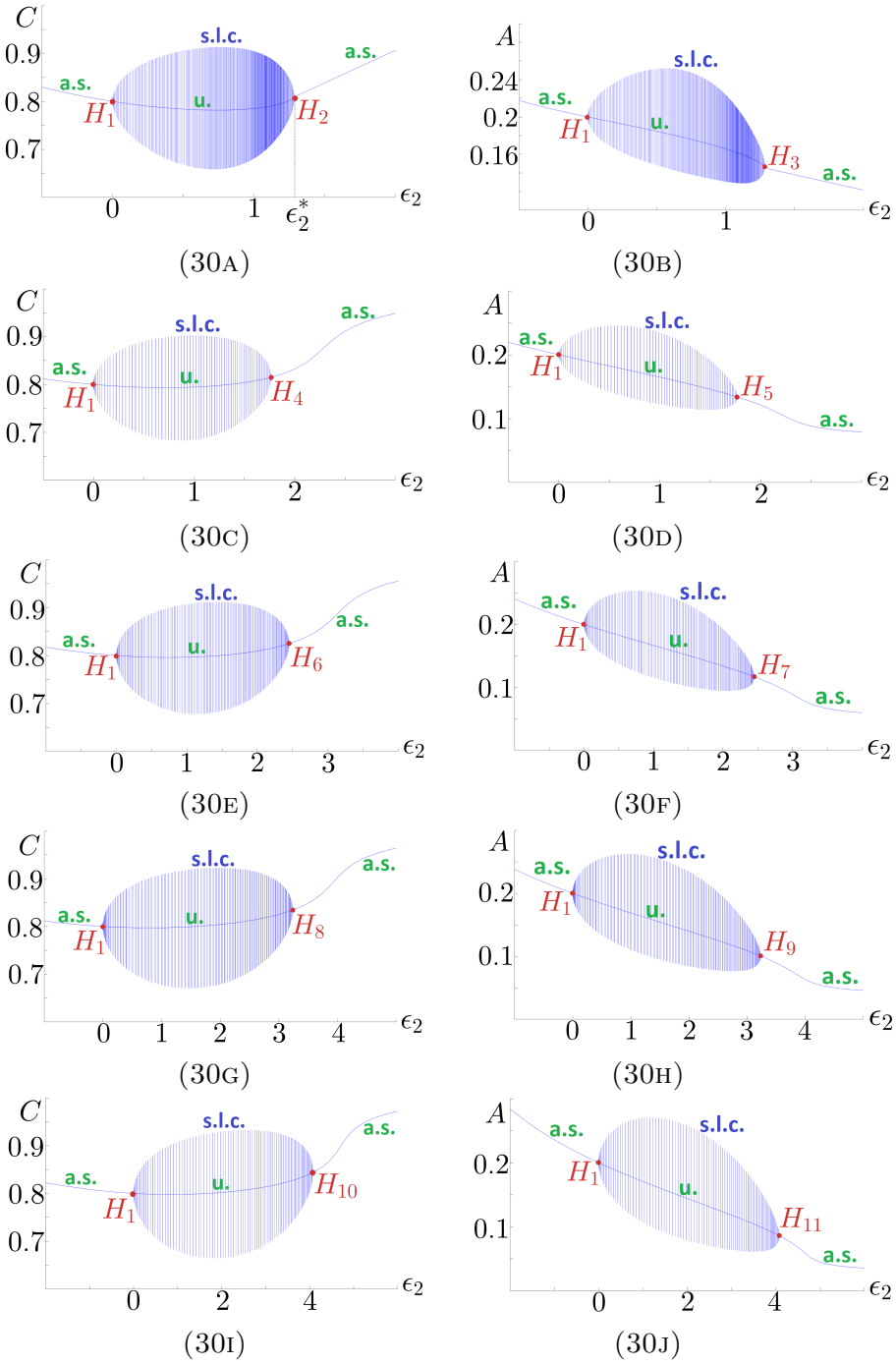

FIGURE 30. Asymptotic behavior of the ϵ_2-system (55), for each $i_{ac}^* \in T_2^*$, relatively to the variables C and A. The coordinates of the Hopf points $H_{i,i+1}$, with $i \geq 2$, are identified in Table 5.

⋆ Constant $\mu_2 = 4$

System (55) undergoes a Hopf bifurcation at $\epsilon_3 = 0$, with a stable limit cycle emerging for $\epsilon_3 < 0$ and thus we are in the presence of a subcritical Hopf bifurcation.

In the following, we skip a detailed description of Figures 31 and 32 below, as they follow the same pattern from the previous simulations.

i^*_{ac}	$H_{i,i+1}$	ϵ^*_3	$C^*(\epsilon^*_3)$	$A^*(\epsilon^*_3)$	$H^*(\epsilon^*_3)$
5.5	$H_{2,3}$	-2.794	0.286	0.454	0.312
6.5	$H_{4,5}$	-4.006	0.318	0.437	0.320
7.5	$H_{6,7}$	-5.309	0.329	0.430	0.323
8.5	$H_{8,9}$	-6.856	0.326	0.432	0.321
9.5	$H_{10,11}$	-8.708	0.314	0.437	0.316

TABLE 6. Coordinates of the second Hopf points in Figure 32, for each $i^*_{ac} \in T^*_2$.

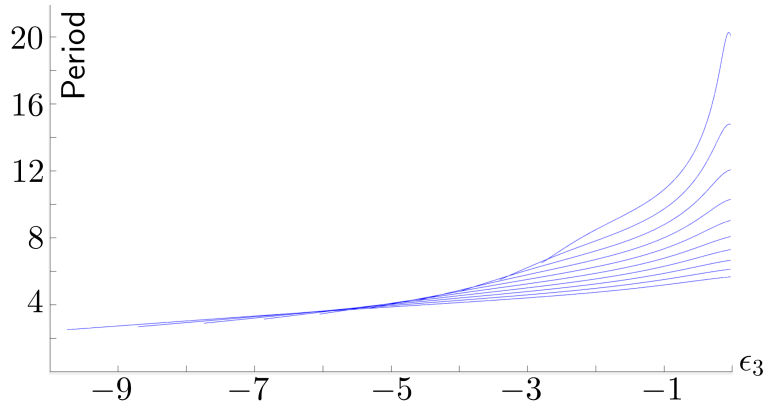

FIGURE 31. Period of the oscillations of system (55) in function of $\epsilon_3 < 0$. Each blue curve represents a specific value of $i^*_{ac} \in T_2$.

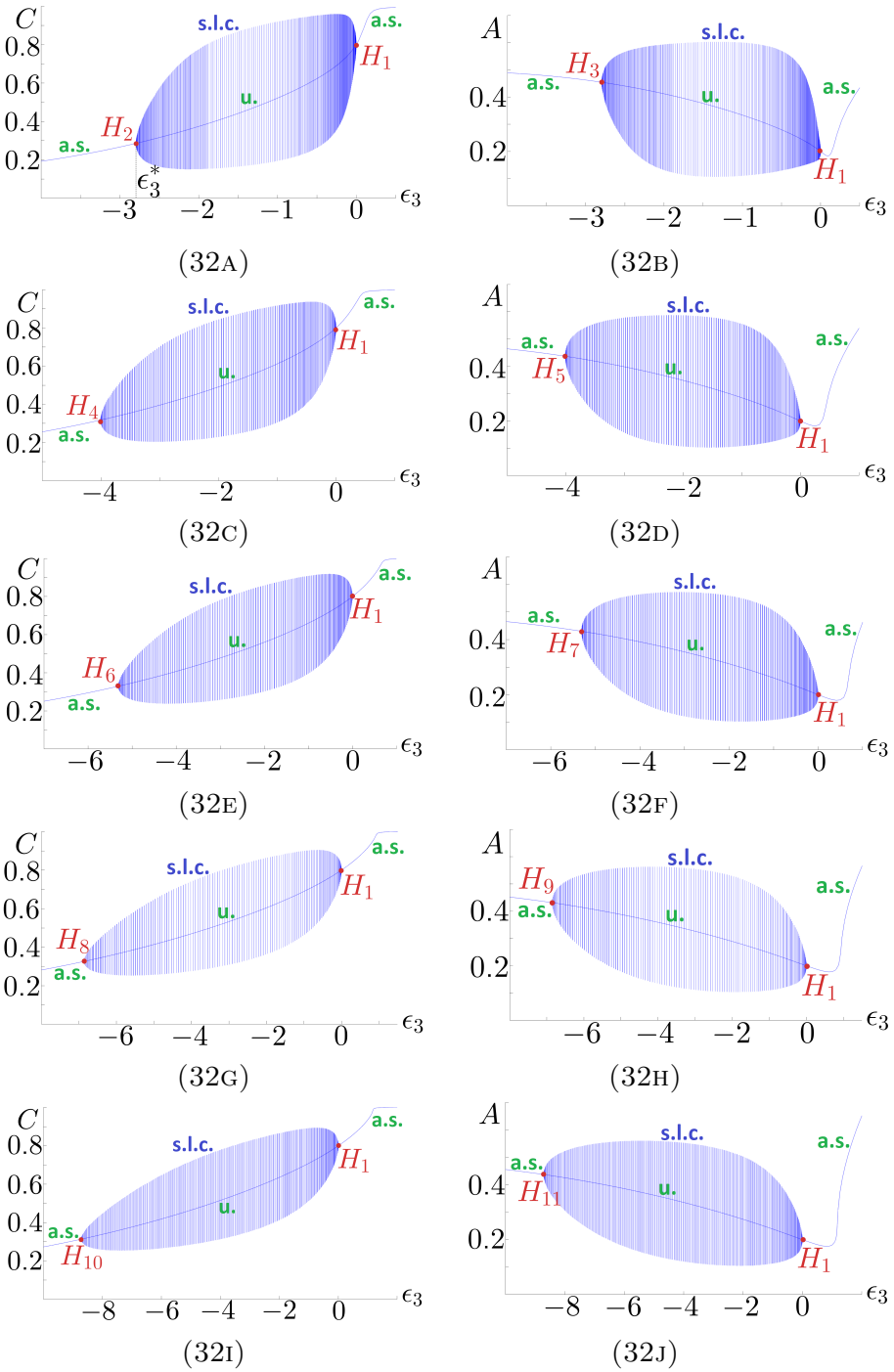

FIGURE 32. Asymptotic behavior of the ϵ_3-system (55), for each $i^*_{ac} \in T^*_2$, relatively to the variables C and A. The coordinates of the Hopf points $H_{i,i+1}$, with $i \geq 2$, are identified in Table 6.

⋆ **Constant** $e_{hc} = 5$

When ϵ_4 is taken as a parameter in system (55), a Hopf bifurcation occurs at $\epsilon_4 = 0$ and a stable limit cycle emerges in a neighborhood $\epsilon_4 < 0$, implying that the bifurcation is subcritical.

i^*_{ac}	$H_{i,i+1}$	ϵ^*_4	$C^*(\epsilon^*_4)$	$A^*(\epsilon^*_4)$	$H^*(\epsilon^*_4)$
5.5	$H_{2,3}$	-5.542	0.261	0.546	0.152
6.5	$H_{4,5}$	-6.940	0.314	0.541	0.098
7.5	$H_{6,7}$	-7.852	0.367	0.523	0.058
8.5	$H_{8,9}$	-9.033	0.414	0.502	0.028
9.5	$H_{10,11}$	-12.917	0.453	0.482	0.004

TABLE 7. Coordinates of the second Hopf points in Figure 34, for each $i^*_{ac} \in T^*_2$.

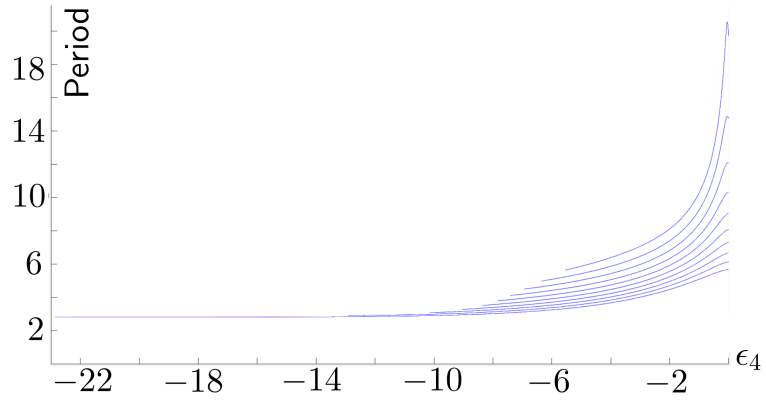

FIGURE 33. Period of the oscillations of system (55) in function of $\epsilon_4 < 0$ ($\epsilon_j = 0$, for $j \neq 4$). Each blue curve represents a specific value of $i^*_{ac} \in T_2$.

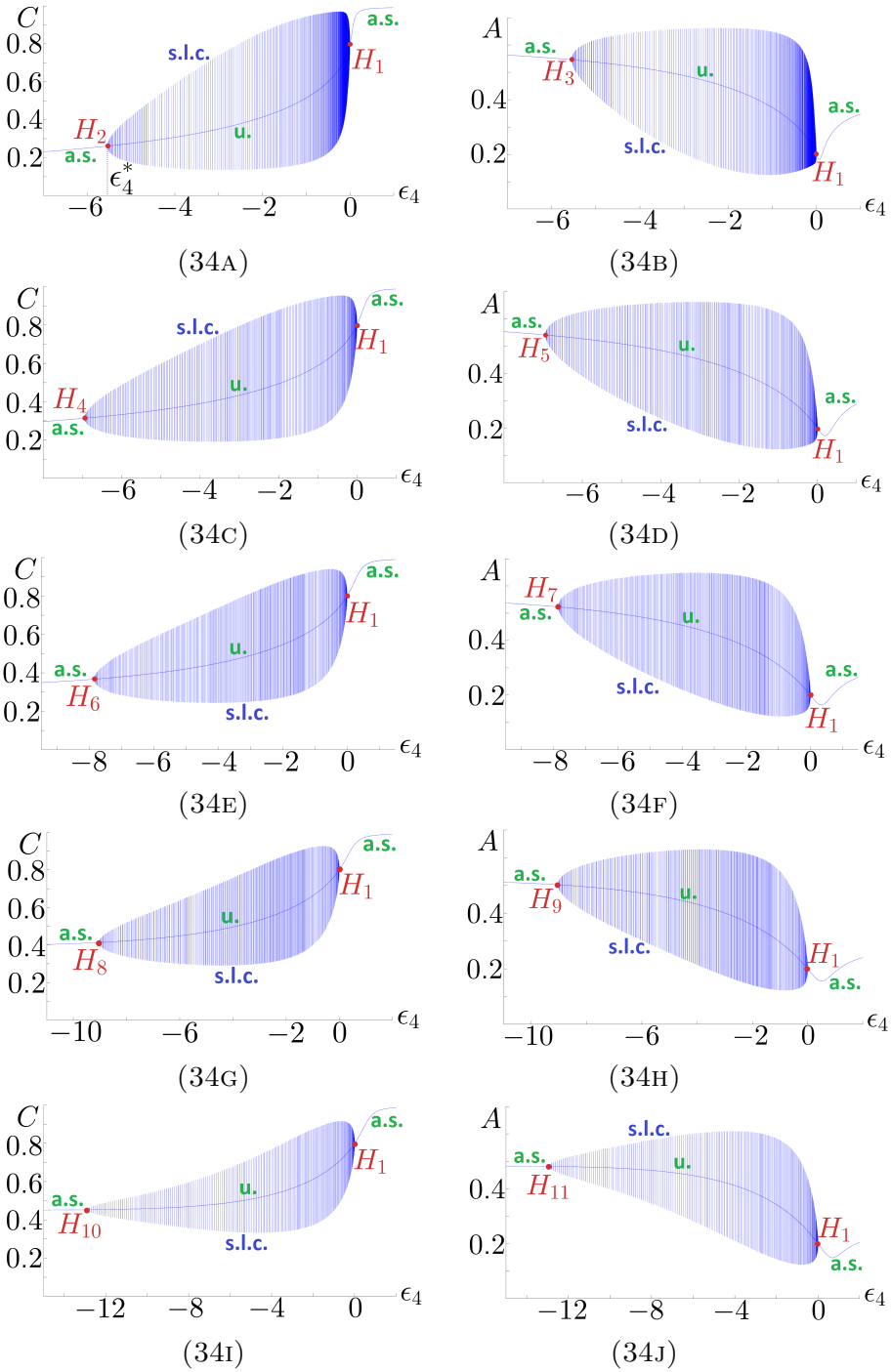

FIGURE 34. Asymptotic behavior of the ϵ_4-system (55), for each $i^*_{ac} \in T^*_2$, relatively to the variables C and A. The coordinates of the Hopf points $H_{i,i+1}$, with $i \geq 2$, are identified in Table 7.

$\star$ **Constant** $e_{ha} = 7$

System (55) admits a Hopf bifurcation at $\epsilon_5 = 0$, with a stable limit cycle arising in a neighborhood $\epsilon_5 < 0$. The Hopf bifurcation is then subcritical.

i^*_{ac}	$H_{i,i+1}$	ϵ^*_5	$C^*(\epsilon^*_5)$	$A^*(\epsilon^*_5)$	$H^*(\epsilon^*_5)$
5.5	$H_{2,3}$	-2.121	0.358	0.483	0.223
6.5	$H_{4,5}$	-2.665	0.462	0.429	0.227
7.5	$H_{6,7}$	-2.872	0.549	0.376	0.249
8.5	$H_{8,9}$	-2.829	0.617	0.331	0.282
9.5	$H_{10,11}$	-2.601	0.670	0.294	0.320

TABLE 8. Coordinates of the second Hopf points in Figure 36, for each $i^*_{ac} \in T^*_2$.

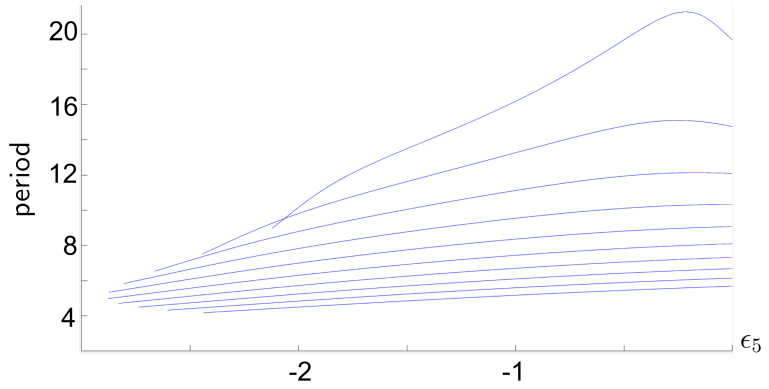

FIGURE 35. Period of the oscillations of system (55) in function of $\epsilon_5 < 0$ ($\epsilon_j = 0$, for $j \neq 5$). Each blue curve represents a specific value of $i^*_{ac} \in T_2$.

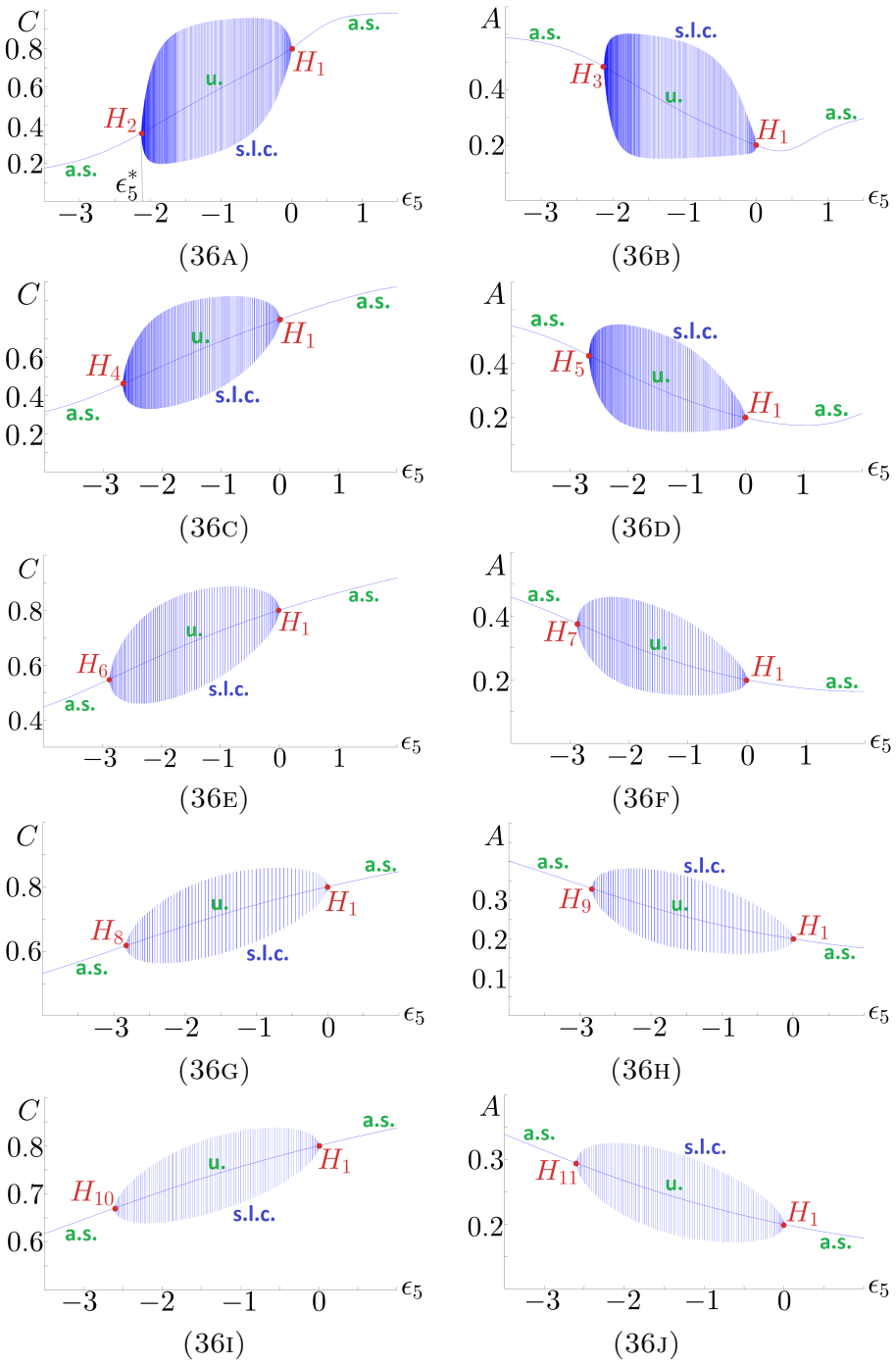

FIGURE 36. Asymptotic behavior of the ϵ_5-system (55), for each $i^*_{ac} \in T^*_2$, relatively to the variables C and A. The coordinates of the Hopf points $H_{i,i+1}$, with $i \geq 2$, are identified in Table 8.

X. Results

Recall system (55), which perturbs each of the connection strengths in system (50). In particular, provided $\epsilon_j = 0$ in (55), the point $(C^*, A^*, H^*) = (0.8, 0.2, 0.5)$ is an equilibrium and the Jacobian matrix has a pair of pure imaginary eigenvalues, when evaluated at that equilibrium.
In our simulations, every perturbation was performed and considered individually and the privileged direction of perturbation was that promoting an oscillatory dynamics. Considering one and only one ϵ_i as a parameter of system (55), with the remaining set to zero, the underlying Hopf bifurcation occurs at $\epsilon_i = 0$ and is either supercritical or subcritical on that parameter, as summarized in the table below.

Parameter	Type of Hopf bifurcation
ϵ_1, ϵ_2	Supercritical
$\epsilon_3, \epsilon_4, \epsilon_5$	Subcritical

Table 9. Classification of the Hopf bifurcation for each perturbed connection strength.

We now analyse, in detail, the observed results of the simulations, for each perturbed connection strength. As previously indicated, these results will fundamentally be based on the following aspects:

(1) The interval $]0, \epsilon_i^*[$ (or $]\epsilon_i^*, 0[$) that represent the extension of the oscillatory dynamics. According to the topic IX.3.2, that information transmits, on one hand, the sensibility of the system to the generation of oscillations and, on the other, the level of interregional strength that resulted from the oscillations;
(2) The period and the amplitude of the oscillations, which give insight about the sensibility of the system to the variation of certain connection strengths, as well as the transitions between ranges of frequency;
(3) The coordinates of the second Hopf points H_i, with $i \geq 2$, which tells how much the post-oscillatory eletrical activities varied relatively to the pre-oscillatory ones.

We note that, while the extension and frequency variation of the oscillatory dynamics were tested for $i_{ac}^* \in T_2$, for convenience, the amplitude of the rhythmic effect and coordinates of the second Hopf points were deduced for more restricted values of i_{ac}^*, namely $i_{ac}^* \in T_2^*$. Once one of these features is invoked, it is implicit the values of i_{ac}^* that are considered.

⋆ Constant $e_{cc} = e^*_{cc}$

Let $i^*_{ac} \in T_2$. By Table 9, periodic solutions arise for $\epsilon_1 > 0$, when perturbing the constant $e_{cc} = e^*_{cc} = \zeta(i^*_{ac})$ in system (50). This oscillatory dynamics is such that:

(1) **Interval** $]0, \epsilon^*_1[$**:** the value of ϵ^*_1 increases with $i^*_{ac} \in T_2$. At the second Hopf bifurcation, the equilibrium satisfies

$$C^*(\epsilon^*_1) > C^* = 0.8, A^*(\epsilon^*_1) < A^* = 0.2$$

and

$$C^*(\epsilon^*_1) - C^* < A^* - A^*(\epsilon^*_1),$$

for each $i^*_{ac} \in T^*_2$. Hence there is an increased cortical activity and a decreased amygdalar firing, effect that is more marked in the latter case and is reinforced with the augmentation of $i^*_{ac} \in T^*_2$;

(2) **Period and amplitude of the oscillations:** for each $i^*_{ac} \in T_2$, the period of the oscillations are increasing functions of $\epsilon_1 \in]0, \epsilon^*_1[$. In particular, this variation is more profound for lower values of $i^*_{ac} \in T_2$ (extending to $i^*_{ac} = 4.9$, the period of the oscillations range approximately from 46 to 75, these values corresponding to different bands of frequency, according to Table 3 in subsection VIII.1). On the other hand, the amplitude of the rhythmic activity is well regulated, in the sense that the periodic solutions do not jump between opposite states of activity, namely up and down states. In particular, this effect is enhanced as $i^*_{ac} \in T^*_2$ increases.

⋆ Constant $e_{ch} = 3$

The effects of perturbing $e_{ch} = 3$ in system (50), achieved by taking positive values of ϵ_2 in (55), are very similar to those previously observed for $e_{cc} = e^*_{cc}$, so that we skip a detailed description. The only major difference to be underlined is the fact that

$$\epsilon^*_1(i^*_{ac}) < \epsilon^*_2(i^*_{ac}), \qquad \forall i^*_{ac} \in T_2$$

($\epsilon^*_i(i^*_{ac})$ means ϵ^*_i *in function of* i^*_{ac}), the oscillatory dynamics ceasing with the convergence to a resting state which is even more displaced, in the same direction, from the initial levels of activity (in particular, the amygdalar activity is more inhibited and the cortical activity is more enhanced, when in comparison with the perturbation of $e_{cc} = e^*_{cc}$).

⋆ Constant $\mu_2 = 4$

Let $i^*_{ac} \in T_2$. Periodic solutions arise for $\epsilon_3 < 0$, when perturbing the constant $\mu_2 = 4$ in system (50). This oscillatory dynamics is such that:

(1) **Interval** $]\epsilon^*_3, 0[$**:** the value of ϵ^*_3 decreases, in the negative side, with $i^*_{ac} \in T_2$; there is also a great sensibility to these oscillations, in the sense that large perturbations of $\mu_2 = 4$ are able to sustain the rhythmic effect. Once terminated, the stable oscillations give place to a stable equilibrium satisfying

$$0.8 = C^* > C^*(\epsilon^*_3) < A^*(\epsilon^*_3) > A^* = 0.2$$

and

$$C^* - C^*(\epsilon^*_3) > A^*(\epsilon^*_3) - A^*,$$

meaning that the cortical activity decreases and the amygdalar firing increases, the first variation being more prominent. Those conditions do not show any change with the augmentation of $i^*_{ac} \in T^*_2$;

(2) **Period and amplitude of the oscillations:** perturbing $\mu_2 = 4$ to lower values results in a quick convergence to ultrafast oscillations[9] [25], especially when μ_2 changes sign, i.e. when the connection strength becomes inhibitory (loosing its meaning in the main neuronal circuit). The high amplitude of the periodic solutions is also evident for all values of $i^*_{ac} \in T^*_2$, with the rhythmic activity jumping between up and down states. These features bring a sense of uncontrollability to the oscillatory dynamics: a little perturbation on $\mu_2 = 4$ makes the system escape from a sufficiently small neighborhood of the equilibrium point $(C^* = 0.8, A^* = 0.2, H^* = 0.5)$.

⋆ Constant $e_{hc} = 5$

Fixing $i^*_{ac} \in T_2$, we found that an oscillatory dynamics emerges for $e_{hc} < 5$ and satisfies $\epsilon^*_3(i^*_{ac}) < \epsilon^*_4(i^*_{ac})$, meaning that the oscillations are more sustained when perturbing $e_{ch} = 5$ than when perturbing $\mu_2 = 4$. In contrast, both the period and amplitude show a similar behaviour to that of perturbing $\mu_2 = 4$. Additionally, the post-oscillatory convergence of the system also favors the amygdalar activity in detriment of the cortical firing rate. However, unlike the case of μ_2, this last effect is slightly attenuated as $i^*_{ac} \in T^*_2$ increases.

[9] We consider as *ultrafast* those oscillations exceeding 200 Hz of frequency.

⋆ **Constant** $e_{ha} = 7$

In comparison with the miscellaneous connection strengths, the perturbation of $e_{ha} = 7$ shows the most distinct effects in what concerns the features of the generated oscillations, which take place for $e_{ha} < 7$. In fact, for $8 \geq i^*_{ac} \in T_2$, we have that ϵ^*_5 is an increasing function of i^*_{ac}, while for $8 \leq i^*_{ac} \in T_2$, that function is decreasing. This dichotomy was not observed in the remaining connections.
On the other hand, for all values of $i^*_{ac} \in T_2$, the period of the rhythmic activity converges to fast oscillations. Finally, the amplitude of the oscillatory dynamics decreases with $i^*_{ac} \in T^*_2$ and the post-oscillatory convergence of the system approaches gradually to the initial levels of activity, with

$$C^*(\epsilon^*_5) \approx C^* = 0.8, A^*(\epsilon^*_5) \approx A^* = 0.2,$$

for the highest values of $i_{ac} \in T^*_2$.

For convenience, we exhibit below some suggestive diagrams showing how much the post-oscillatory equilibrium $(C^*(\epsilon^*_i), A^*(\epsilon^*_i), H^*(\epsilon^*_i))$ is displaced, in the vertical direction, from the *initial levels of activity* (ILA for short, numerically given by $(C^* = 0.8, A^* = 0.2, H^* = 0.5)$), for each $i^*_{ac} \in T^*_2$. In particular, we assume that there is an *affine* continuity (continuity by poligonal segments) between consecutive values of i^*_{ac}, so that straight segments are used between the numerical points (this assumption will be broadly considered in the discussion of the results).

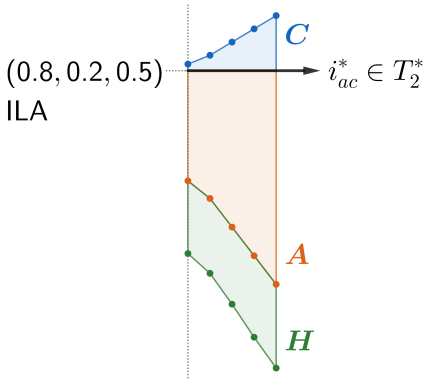

(37A) Constant $e_{cc} = e^*_{cc}$

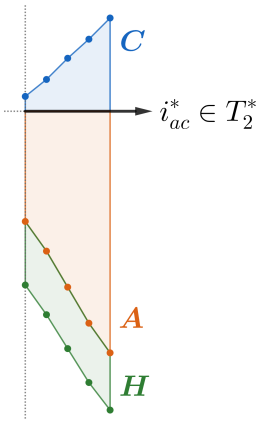

(37B) Constant $e_{ch} = 3$

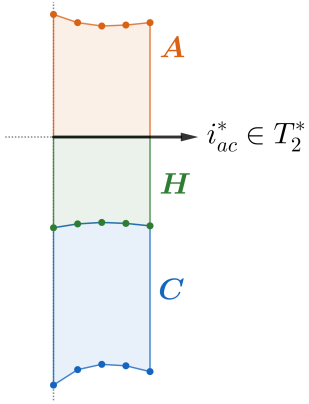

(37C) Constant $\mu_2 = 4$

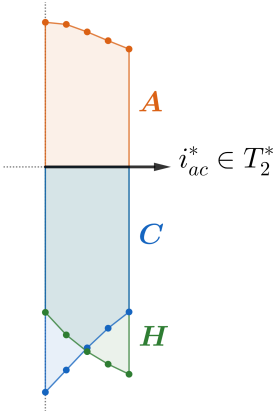

(37D) Constant $e_{hc} = 5$

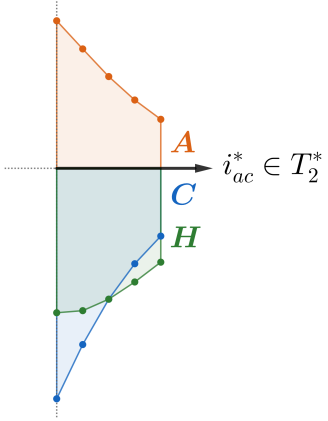

(37E) Constant $e_{ha} = 7$

FIGURE 37. Overview of the displacement, in the vertical direction, of the post-oscillatory neuronal activities (numerically given by $(C^*(\epsilon^*_i), A^*(\epsilon^*_i), H^*(\epsilon^*_i))$) from the initial levels of activity (ILA, given by $(C^*, A^*, H^*) = (0.8, 0.2, 0.5)$), for the different values of $i^*_{ac} \in T^*_2$ (the diagrams are not drawn on the same scale).

XI. Discussion

Setting some connection strength of interest as a parameter for the modified Wilson-Cowan model, we performed a perturbation apt to generate an oscillatory dynamics. The direction of this perturbation was that promoting a meaningful environment for interregional transformations, according to the assumptions of the topic IX.3.2. This transformations will further be classified as *positive*, *negative* or *neutral*, under our subjective reading of the results described previously.
As suggested by the diagrams of Figure 37, a suitable discussion of the results requires some assumptions about the continuity between the simulation points. In particular, we can assume that there is an *affine* continuity between those points.

The above results are conclusive in the following main aspect: applying small perturbations on each targeted connection strength (in the proper direction), the oscillatory dynamics created in a late phase of fear extinction (i.e. when the infralimbic cortical pathway is stregthened) consist of faster periodic solutions. Given the correlation between fast oscillations (especially in the γ-band) and cognitive performance [32], that observation possibly sheds light on the relevance of the cognitive abilities and the (long-term) inhibition of fear expression.
In parallel, a weaker infralimbic pathway (present in an early phase of fear extinction) is conducive to the generation of oscillations of lower frequency.

We observe that both the cortical self-connection and the hippocampal output to the cortex are exponentially strengthened as the oscillations get faster along the ascending phases of fear extinction (see Figure 38), effect that is more prominent in the latter connection. Since this process is accompanied by an enhancement of the top-down control (i.e. the amygdala is gradually inhibited by the mPFC[10]), we propose that the early stage of extinction is mediated by the subcortical operation in a slower rhythm (during the consolidation of memories, for example), promoting the strengthening of the $H \to C$ innervation, while in the late stage the cortical activity prevails in a faster rhythm (during mechanisms that encourage an adaptive behaviour, for example), promoting a dendritic strengthening in the cortex. The transition between the ascending phases of extinction are then accompained by the regulation of the oscillatory frequency, with the oscillations moving from the β to the γ band.
Given that, the impact of perturbing the hippocampus→cortex and the cortical self-connection is suggestively classified as *positive*, in the

[10]The drop of the amygdalar activity is actually more significant than the enhancement of the cortical activity.

sense that it functionally enhances the top-down control inherent to the extinction of fear memories. The prominence of one connection relatively to the other may predict a more relevant role in this phenomenon.

In contrast, our simulations suggest that ultrafast waves impair the top-down control, via weakening of the pathways cortex→hippocampus and hippocampus→amygdala. This fact, together with the promoted high amplitudes between extremal activities, makes us assert that those connections, when perturbed (to lower strengths), are conducive to a *negative* impact on the whole triad. In particular, we direct this observation to the significance of maintaining the $C \to H$ and $H \to A$ innervations with sufficient strengths in order to keep an healthy top-down control, during any stage of extinction. This requirement could have a role on the formation of extinction memories, for example.

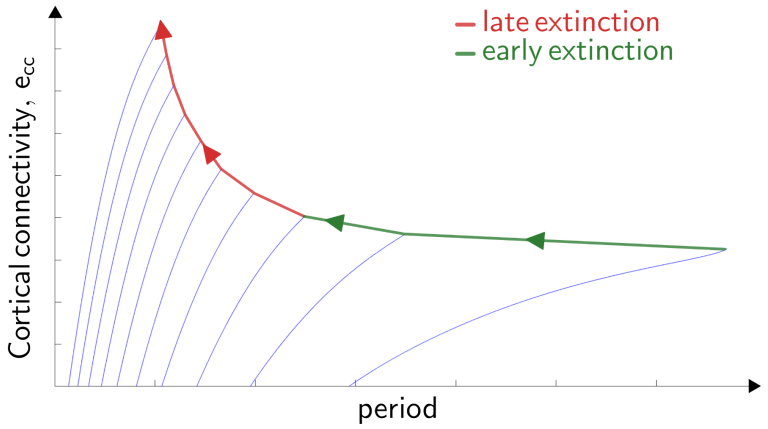

FIGURE 38. Exponential strengthening of the cortical connectivity along the fear extinction phenomenon, with each blue curve being the inverse of the respective from Figure 27. More specifically, as one travels through the ascending phases of extinction, the oscillatory dynamics gets gradually faster and promotes a rapid growth of the cortical connectivity (the connectivity is recovered from each step of extinction); a continuity (by straight lines) between the endpoints of the curves is considered. This continuity approach is supposed to be interpreted together with that of Figure 37.

Lastly, the amygdala→hippocampus innervation reveals distinct results from those commented above. In fact, while in an early phase of extinction, the same argument used for $C \to H$ and $H \to A$ applies, when moving to a late phase, perturbing the connection $A \to H$ does not show significant impacts on the initial amygdalar and cortical activities, suggesting that the triad becomes less sensible to the perturbation.

This fact is reinforced by the smaller amplitudes and the subtle weakening of the pathway in a late stage of extinction, when in comparison with the early one. Since the $A \to H$ innervation is involved in encoding of positive/negative emotions, we propose that, in a late phase of extinction, the triad gets less vulnerable to the negative stimuli urged by the fear memory. Suggestively, the impact is here classified as being *neutral*.
We summarize in the table below the classified effects of perturbing the many connection strengths:

Connection strength	Effect
$e_{cc} = e^*_{cc}$	Positive
$e_{ch} = 3$	Positive
$\mu_2 = 4$	Negative
$e_{hc} = 5$	Negative
$e_{ha} = 7$	Neutral

TABLE 10. (Subjective) effects of perturbing the different connection strengths on the initial conditions of the fear extinction phenomenon (conditions that are characterized by the unperturbed framework set in Example IX.3.1). The perturbations of the connections $e_{cc} = e^*_{cc}$ and $e_{ch} = 3$ (resp. $\mu_2 = 4$ and $e_{hc} = 5$) are classified as producing *positive* (resp. *negative*) effects. In contrast, perturbing $e_{ha} = 7$ does not show significant impacts.

In Figure 39, we make an attempt to describe possible mechanisms that, according to our simulations, are apt to optimize the conditions of fear extinction. They are:

- Both the cortical connectivity and the hippocampus→cortex are strengthened during the different stages of extinction; we suggest that the early phase of extinction, which is mediated by slower waves, is involved in the cognitive inhibition [10] and memory formation, both demanded during emotional training; in turn, the late phase of extinction, being mediated by faster waves, comands long-term adaptive behaviours linked to emotion regulation, telling the individual how to react under the negative stimuli from fear (executive function). We note that both the cognitive inhibition and adaptative behaviour are usually implicated in extra cortical areas beyond the mPFC, such as the dorsolateral prefrontal cortex (see [10]);
- For a successful extinction of fear memories, several connections are required to achieve sufficient levels of strength, namely the interconnections betwen the amygdala and the hippocampus, as well as the cortical projetion to the hippocampus; the

significance of this condition is higher in the early stages of extinction, during, for example, the synaptic remodelling responsible for the installation of new memories; we also propose that the recall of these memories [37], in a late stage of extintion, primarily results from the hippocampus→amygdala and cortex→hippocampus routes, the latter correlated with the activation of both the hippocampus and mPFC.

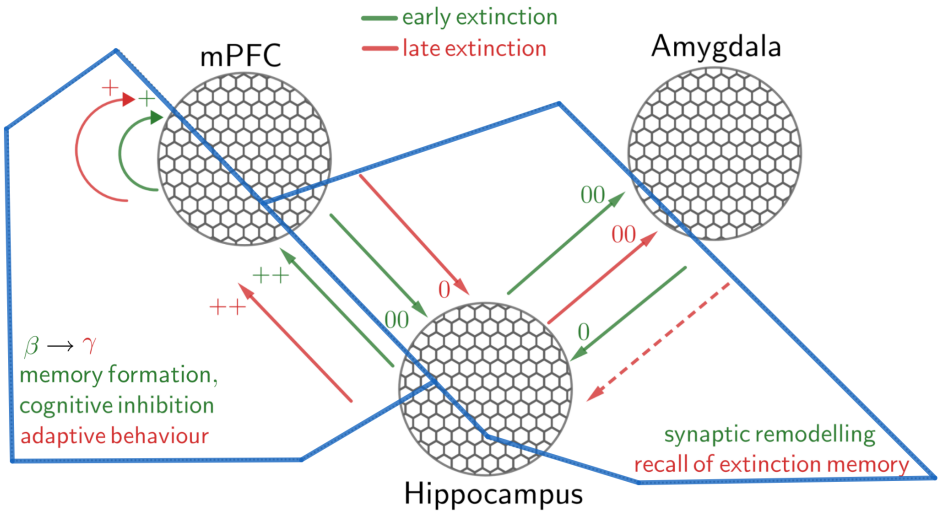

FIGURE 39. Mechanisms of extinction optimization: the letters γ and β allude for the type of oscillations related with the labelled pathway, in a certain phase of extinction; the signs + and ++ represent the strengthening of the corresponding pathways, with the double sign giving a relative significance of one route relative to other; the signs 0 and 00 determine the constancy requirement for the corresponding connection strength, with the double sign having the same reading as for +; the dashed arrow points to a less significance of the pathway (neutral effect) on the conditions of fear extinction.

XII. Future Directions

In this section, we describe some directions for future work.

- **Geometric Singular Perturbation**
  Natural phenomena evolve on several time scales. In our context, synaptic transmission between different brain regions is included in such phenomena. Using equations in different time scales to model the interaction between neurons can predict the role of one type neuron in the whole complex.
  Letting $\tau_{1,2} > 0$, we put

$$\begin{cases} \tau_1 U_e' = -U_e + F(a_{ee}U_e - a_{ei}U_i - \beta_e) \\ \tau_2 U_i' = -U_i + F(a_{ie}U_e - a_{ii}U_i - \beta_i) \end{cases}.$$

  The constants $\tau_{1,2}$ are usually interpreted as the average synaptic times for the corresponding populations [30].
  For example, when periodic solutions are present, one may attempt to ascertain how the oscillatory frequency and amplitude are modulated in function of those constants and ultimately if the oscillations are sustained under the perturbation of such constants.

  On the other hand, considering one of those time scales sufficiently small and using methods from Singular Perturbation Theory [23], a good approach consists of approximating the flow of the above system, namely in a neighborhood of the so-called *slow manifold*, defined by the U_e-nullcline.

XIII. Appendix

XIII.1. **A special case: Obsessive-compulsive disorder.** Among all the anxiety conditions, obsessive-compulsive disorder (OCD) [1, 45] must be one of those whose symptoms are more prominent when it comes to emotional imparment. In fact, this anxiety disorder involves the presence of obsessions and/or compulsions[11]. While the former lie in the pure emotional dysfunctionality of the condition, the latter is a behavioral response to this state.
Obsessions consists of thoughts, mental images and doubts that are intrusive, causing a sense of impending danger and subsequent disconfort (egodystonic symptom). Here, *intrusive* means the individual's inability to supress the thoughts, as if the brain was constantly projecting them in the mind. This attribute might, in part, be responsible for the resultant anxious state. A sequence of rituals then follows towards a relief of the induced fear state. Such rituals are known as the *compulsions*, and their execution is kept by reinforcement.
The line that separates these two facets of OCD is not always clear, since the compulsions may comprise mental executions as well. It is then important, namely in a therapeutical context, to establish a proper distinction between a pure obsessional version of the disease and the eventual tenuous separation of obsessions from compulsions.

The content of the obsessions varies from individual to individual. They usually involve situations that the person does not desire and whose possible negative consequences are overestimated, resulting in an anxious feeling.
Despite of the heterogeneity of the contexts that may trigger the intrusive thoughts, there are some patterns of obsessions that characterize most versions of OCD. Indeed, ruminations about contamination and doubts leading to checking behabiour (known as *pathological doubts*) are very common.
In particular, these stereotypes show the limitating effect of OCD symptoms, not only for the time spent on the execution of the compulsions, but also for the restricted mental availability caused by obsessions.

Unlike many other mental disorders, most suffering from OCD reveal some level of *insight*, meaning that they recognize the irrationality of both the obsessions and compulsions, while not having control on them.

In what concerns the epidemiology, OCD covers around 2 to 3% of the population and has usually an early onset, especially in young males.

[11]The dichotomy and/or, there emphasized, has to with the fact that some versions of OCD may primarily be formed by obsessions or compulsions.

The negative impact on the individual's psychosocial development is then inevitable, increasing the likelihood of developing comorbidities. For this reason, the early start of OCD is usually attributed to a bad prognosis.
Yet, one shall not take that *early start* very seriously, as young children may exhibit some traces of perfectionism or symmetry (for example, while playing), behaviour that usually makes part of the normal development.

The specific neurobiological causes of OCD, in turn, are still unknown. The most consensual studies point towards dysfunctionalities involving both prefrontal and subcortical areas, namely the orbitofrontal cortex, the anterior cingulate cortex and the striatum [33]. Incidentally, these areas strongly mediate the CTCS circuit [43], fact that leads to the association between the disorder and the circuit.
In particular, genetic variation leading to dysfunctional glutamate transmission in the CTCS has been implied in the etiology of OCD [47].

While the favorable insight should be a reason for a good prognosis, treatment for OCD is usually challenging in the context of psychiatry and psychotherapy. In fact, the standard treatment for the condition targets two main methods: cognitive-behavioral therapy and pharmacology. The former concerns a cognitive reformulation whose goal is to replace the dysfunctional beliefs that support obsessions by more adaptative perspectives. This way, the individual should be able to tune out irrelevant stimuli.
Additionally, in the cases where compulsions prevail, a specific method of exposing the individual to the obsessions and preventing the execution of the rituals (known as *exposure and response prevention*) is customary.
The integration of tools aimed to improve the regulation of emotions and the psychoeducation of those surrounding the individual are also crucial.

In what concerns the pharmacological intervention, first line treatment usually draws on antidepressants (SSRI's) that aim to augment the serotonergic transmission in the brain, specifically in those areas that might be more affected in the disease. The expected result comprises both the decrease in the anxiety levels and the antiobsessional state (meaning that the obsessions become less intrusive), effects that have been attributed to the downregulation of 5-HT1A autoreceptors and 5-HT2 postsynaptic receptors, as observed by Andrade et al. in [2]. Interestingly, this class of antidepressants have also been reported to increase the neuroplasticity [2] in the brain, thus making the psycotherapeutical approach more effective.

References

[1] American Psychiatric Association. *Diagnostic and Statistical Manual of Mental Disorders.* Fifth Edition, 2013.

[2] Andrade C. and Rao N. S. K. *How antidepressant drugs act: A primer on neuroplasticity as the eventual mediator of antidepressant efficacy.* Indian Journal of Psychiatry, Vol. 52, Issue 4, pp. 378-386, 2010.

[3] Borisyuk G. N., Borisyuk R. M., Khibnik A. I. and Roose D. *Dynamics and Bifurcations of Two Coupled Neural Oscillators with Different Connection Types.* Bulletin of Mathematical Biology, Vol. 57, Issue 6, pp. 809-840, 1995.

[4] Bouton M. E. and Bolles R. C. *Contextual Control of the Extinction of Conditioned Fear.* Learning and Motivation, Vol. 10, Issue 4, pp. 445-466, 1979.

[5] Burgos-Robles A., Kimchi E. Y., Izadmehr E. M., Porzenheim M. J., Ramos-Guasp W. A., Nieh E. H., Felix-Ortiz A. C., Namburi P., Leppla C. A., Presbrey K. N., Anandalingam K. K., Pagan-Rivera P. A., Anahtar M., Beyeler A. and Tye K. M. *Amygdala inputs to prefrontal cortex guide behavior amid conflicting cues of reward and punishment.* Nature Neuroscience, Vol. 20, Issue 6, pp. 824-835, 2017.

[6] Buskila Y., Bellot-Saez A. and Morley J. W. *Generating Brain Waves, the Power of Astrocytes.* Frontiers in Neuroscience, Vol. 13, Art. 1125, 2019.

[7] Cisler J. M., Olatunji B. O., Feldner M. T. and Forsyth J. P. *Emotion Regulation and the Anxiety Disorders: An Integrative Review.* Journal of Psychopathology and Behavioral Assessment, Vol. 32, Issue 1, pp. 68-82, 2010.

[8] Compare A., Zarbo C., Shonin E., Gordon W. V. and Marconi C. *Emotional Regulation and Depression: A Potential Mediator between Heart and Mind.* Cardiovascular Psychiatry and Neurology, Vol. 2014, Art. 324374, 2014.

[9] Corcoran K. A. and Quirk G. J. *Activity in Prelimbic Cortex Is Necessary for the Expression of Learned, But Not Innate, Fears.* The Journal of Neuroscience, Vol. 27, Issue 4, pp. 840-844, 2007.

[10] Dixon M. L. *Cognitive control, emotional value, and the lateral prefrontal cortex.* Frontiers in Psychology, Vol. 6, Art. 758, 2015.

[11] Eccles J. C., Fatt P. and Koketsu K. *Cholinergic and inhibitory synapses in a pathway from motor-axon collaterals to motoneurones.* Journal of Physiology, Vol. 126, Issue 3, pp. 524-562, 1954.

[12] Ermentrout B. *Neural networks as spatio-temporal pattern-forming systems.* Reports on Progress in Physics, Vol. 61, Issue 4, pp. 353-430, 1998.

[13] Ermentrout G. B. and Cowan J. D. *Temporal Oscillations in Neuronal Nets.* Journal of Mathematical Biology, Vol. 7, Issue 3, pp. 265-280, 1979.

[14] Ermentrout G. B. and Terman D. H. *Mathematical Foundations of Neuroscience.* Springer, 2010.

[15] Fastenrath M., Coynel D., Spalek K., Milnik A., Gschwind L., Roozendaal B., Papassotiropoulos A. and Quervain D. J. F. *Dynamic Modulation of Amygdala–Hippocampal Connectivity by Emotional Arousal.* The Journal of Neuroscience, Vol. 34, Issue 42, pp. 13935-13947, 2014.

[16] Giustino T. F. and Maren S. *The Role of the Medial Prefrontal Cortex in the Conditioning and Extinction of Fear.* Frontiers in Behavioral Neuroscience, Vol. 9, Art. 298, 2015.

[17] Godsil B. P., Kiss J. P., Spedding M. and Jay T. M. *The hippocampal–prefrontal pathway: The weak link in psychiatric disorders?* European Neuropsychopharmacology, Vol. 23, Issue 10, pp. 1165-1181, 2013.

[18] González-Olivares E., Tintinago-Ruiz P. C. and Rojas-Palma A. *A Leslie-Gower-type predator-prey model with sigmoid functional response.* International Journal of Computer Mathematics, Vol. 92, Issue 9, pp. 1895–1909, 2014.

[19] Gross J.J. *Antecedent- and Response-Focused Emotion Regulation: Divergent Consequences for Experience, Expression, and Physiology.* Journal of Personality and Social Psychology, Vol. 74, Issue 1, pp. 224–237, 1998.

[20] Harris J. D. *Analysis of a Spatially-Distributed Wilson-Cowan Model of Cortex.* University of Pittsburgh, 2017.

[21] Heatherton T. F. and Wagner D. D. *Cognitive neuroscience of self-regulation failure.* Trends in Cognitive Sciences, Vol. 15, Issue 3, pp. 132-139, 2011.

[22] Hebb D. O. *The Organization of Behaviour; a neuropsychological theory.* Wiley, 1949.

[23] Hek G. *Geometric singular perturbation theory in biological practice.* Journal of Mathematical Biology, Vol. 60, Issue 3, pp. 347-386, 2010.

[24] Hoover W. B. and Vertes R. P. *Anatomical analysis of afferent projections to the medial prefrontal cortex in the rat.* Brain Structure and Function, Vol. 212, Issue 2, pp. 149-179, 2007.

[25] Hughes J. R. *Gamma, fast, and ultrafast waves of the brain: Their relationships with epilepsy and behavior.* Epilepsy & Behaviour, Vol. 13, Issue 1, pp. 25-31, 2008.

[26] Jin J. and Maren S. *Fear renewal preferentially activates ventral hippocampal neurons projecting to both amygdala and prefrontal cortex in rats.* Scientific Reports, Vol. 5, Art. 8388, 2015.

[27] Kelley W. G. and Peterson A. C. *The Theory of Differential Equations, Classical and Qualitative.* Second Edition, Springer, 2010.

[28] Kumar A. *Long-term potentiation at CA3–CA1 hippocampal synapses with special emphasis on aging, disease, and stress.* Frontiers in Aging Neuroscience, Vol. 3, Art. 7, 2011.

[29] Kuznetsov Y. A. *Elements of Applied Bifurcation Theory.* Third Edition, Springer, 2004.

[30] Li X., Li Z., Yang W., Wu Z. and Wang J. *Bidirectionally Regulating Gamma Oscillations in Wilson-Cowan Model by Self-Feedback Loops: A Computational Study.* Frontiers in Systems Neuroscience, Vol. 16, Art. 723237, 2022.

[31] Lübkemann R., Eberhardt J., Röhl F., Janitzky K., Nullmeier S., Stork O., Schwegler H. and Linke R. *Identification and Characterization of GABAergic Projection Neurons from Ventral Hippocampus to Amygdala.* Brain Sciences, Vol. 5, Issue 3, pp. 299-317, 2015.

[32] Mably A. J. and Colgin L. L. *Gamma oscillations in cognitive disorders.* Current Opinion in Neurobiology, Vol. 52, pp. 182-187, 2018.

[33] Maia T. V., Cooney R. E. and Peterson B. S. *The Neural Bases of Obsessive-Compulsive Disorder in Children and Adults.* Development and Psychopathology, Vol. 20, Issue 4, pp. 1251-1283, 2008.

[34] Maren S. *Seeking a Spotless Mind: Extinction, Deconsolidation, and Erasure of Fear Memory.* Neuron, Vol. 70, Issue 5, pp. 830-845, 2011.

[35] Maroun M. *Medial Prefrontal Cortex: Multiple Roles in Fear and Extinction.* The Neuroscientist, Vol. 19, Issue 4, pp. 370-383, 2012.

[36] Menon A., Mehrotra K., Mohan C. K. and Ranka S. *Characterization of a Class of Sigmoid Functions with Applications to Neural Networks.* Neural Networks, Vol. 9, Issue 5, pp. 819-835, 1996.

[37] Milad M. R., Wright C. I., Orr S. P., Pitman R. K., Quirk G. J. and Rauch S. L. *Recall of Fear Extinction in Humans Activates the Ventromedial Prefrontal Cortex and Hippocampus in Concert.* Biological Psychiatry, Vol. 62, Issue 5, pp. 446-454, 2007.

[38] Murray J. D. *Mathematical Biology II: Spatial Models and Biomedical Applications.* Third Edition, Springer, 2003.

[39] Murthy V. N. *Synaptic plasticity: Step-wise strengthening.* Current Biology, Vol. 8, Issue 18, pp. R650-R653, 1998.

[40] Orsini C. A., Kim J. H., Knapska E. and Maren S. *Hippocampal and Prefrontal Projections to the Basal Amygdala Mediate Contextual Regulation of Fear after Extinction.* The Journal of Neuroscience, Vol. 31, Issue 47, pp. 17269-17277, 2011.

[41] Orsini C. A. and Maren S. *Neural and cellular mechanisms of fear and extinction memory formation.* Neuroscience and Biobehavioral Reviews, Vol. 36, Issue 7, pp. 1773-1802, 2012.

[42] Perko L. *Differential Equations and Dynamical Systems.* Third Edition, Springer, 2001.

[43] Peters S. K., Dunlop K. and Downar J. *Cortico-Striatal-Thalamic Loop Circuits of the Salience Network: A Central Pathway in Psychiatric Disease and Treatment.* Frontiers in Systems Neuroscience, Vol. 10, Art. 104, 2016.

[44] Quirk G. J., Russo G. K., Barron J. L. and Lebron K. *The Role of Ventromedial Prefrontal Cortex in the Recovery of Extinguished Fear.* The Journal of Neuroscience, Vol. 20, Issue 16, pp. 6225-6231, 2000.

[45] Rachman S., De Silva P. *Obsessive-compulsive disorder.* Fourth Edition, Oxford University Press, 2009.

[46] Rădulescu A., Herron J., Kennedy C. and Scimemi A. *Global and local excitation and inhibition shape the dynamics of the cortico-striatal-thalamo-cortical pathway.* Scientific Reports, Vol. 7, Art. 7608, 2017.

[47] Rajendram R., Kronenberg S., Burton C. L. and Arnold P. D. *Glutamate Genetics in Obsessive-Compulsive Disorder: A Review.* Journal of the Canadian Academy of Child and Adolescent Psychiatry, Vol. 26, Issue 3, pp. 205-213, 2017.

[48] Seidenbecher T., Laxmi T. R., Stork O. and Pape H. *Amygdalar and Hippocampal Theta Rhythm Synchronization During Fear Memory Retrieval.* Science, Vol. 301, Issue 5634, pp. 846-850, 2003.

[49] Senn V., Wolff S. B. E., Herry C., Grenier F., Ehrlich I., Gründemann J., Fadok J. P., Müller C., Letzkus J. J. and Lüthi A. *Long-Range Connectivity Defines Behavioral Specificity of Amygdala Neurons.* Neuron, Vol. 81, Issue 2, pp. 428-437, 2014.

[50] Totty M. S. and Maren S. *Neural Oscillations in Aversively Motivated Behavior.* Frontiers in Behavioral Neuroscience, Vol. 16, Art. 936036, 2022.

[51] Valls C. and Barreira L. *Ordinary Differential Equations: Qualitative Theory.* American Mathematical Society, 2012.

[52] Watanabe M., Uematsu A. and Johansen J. P. *Enhanced synchronization between prelimbic and infralimbic cortices during fear extinction learning.* Molecular Brain, Vol. 14, Art. 175, 2021.

[53] Wilson H. R. and Cowan J. D. *Excitatory and Inhibitory Interactions in Localized Populations of Model Neurons.* Biophysical Journal, Vol. 12, Issue 1, pp. 1-24, 1972.